

INVESTIGATION ON
SEISMIC WAVE FORMS

ARTHUR LAKES LIBRARY
COLORADO SCHOOL OF MINES
GOLDEN, COLORADO

by
J. H. Tien

ProQuest Number: 10796013

All rights reserved

INFORMATION TO ALL USERS

The quality of this reproduction is dependent upon the quality of the copy submitted.

In the unlikely event that the author did not send a complete manuscript and there are missing pages, these will be noted. Also, if material had to be removed, a note will indicate the deletion.



ProQuest 10796013

Published by ProQuest LLC (2019). Copyright of the Dissertation is held by the Author.

All rights reserved.

This work is protected against unauthorized copying under Title 17, United States Code
Microform Edition © ProQuest LLC.


ProQuest LLC.
789 East Eisenhower Parkway
P.O. Box 1346
Ann Arbor, MI 48106 – 1346

A Thesis submitted to the Faculty and the Board of Trustees of the Colorado School of Mines in partial fulfillment of the requirements for the degree of Doctor of Philosophy in Geophysics.

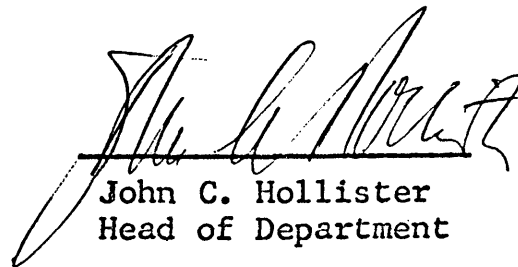
Signed: 
Jean Hsiung Tien

Golden, Colorado

Date: 19 April, 1972

Approved: 
Frank A. Hadsell
Thesis Advisor

ARTHUR LAKES LIBRARY
COLORADO SCHOOL OF MINES
GOLDEN, COLORADO


John C. Hollister
Head of Department

Golden, Colorado

Date: 19 April, 1972

ABSTRACT

Here it is necessary that the reader has in mind a clear distinction between elastic and seismic waves. The former is an idealization of the latter. Seismic waves exist in the earth while elastic waves are mathematical abstractions used to describe certain first order features of seismic waves. In this thesis seismic waves are described by computing corresponding elastic waves and then filtering these through linear filters designed to simulate real inelastic processes.

In any real medium the coherent energy characteristic of elastic waves propagating in a homogeneous medium is converted into incoherent energy, i.e., heat and scattered waves. This conversion process is called attenuation. This yields a decay of the observed wave amplitude in addition to the geometrical spreading. A consequence of this entropy growth, or attenuation, is dispersion.

Elastic propagation is studied analytically or numerically in terms of boundary value problems. The mechanisms

of attenuation are so numerous and complicated that it is very difficult to incorporate them into a meaningful but solvable boundary value problem. The problem here is to study the seismic wave forms without using the wave equations, generalized to include attenuation terms. In this thesis the approach, in which the attenuation is approximated by linear systems, is general for models of attenuation. The constraint for postulating a model is that the amplitude response of the model satisfies the Paley-Wiener condition. The phase response of a causal minimum-phase-shift system is derived from Hilbert transform. The impulse response of the attenuation system is obtained by inverse Fourier transforming the system function. Two models of attenuation (Voigt and constant Q) are used as examples of this approach.

Two types of elastic waves chosen for use as input to the attenuator are plane and spherical waves. The spherical waves were considered in an infinite medium and in a half-space. Cagniard's method is applied to the problem of spherical elastic waves in a half-space.

The attenuated seismic wave forms are obtained through the convolution of the elastic wave forms and the impulse

ARTHUR LAKES LIBRARY
COLORADO SCHOOL OF MINES
GOLDEN, COLORADO

response of the attenuation systems. The wave forms so obtained show changes characteristic of attenuation.

TABLE OF CONTENTS

	<u>Page</u>
ILLUSTRATIONS	viii
LIST OF SYMBOLS	x
ACKNOWLEDGMENTS	xiii
INTRODUCTION	1
ELASTIC WAVES	3
Introduction	3
Plane Compressional Wave in an infinite Elastic Medium	4
Spherical Compressional Waves in an infinite Elastic Medium	7
Spherical Wave in a Half-Space	12
ATTENUATION	36
Introduction	36
Mechanisms and Measurements of Attenuation Attenuation, Dispersion, and Frequency Dependence	44
Linear Attenuation Filter	47
Impulse Responses of Voigt and Constant Q Solids	52
SEISMIC WAVES	64
Plane Compressional Seismic Waves in an Infinite Medium	64
Spherical Compressional Seismic Waves in an Infinite Medium	65
Spherical Compressional Seismic Waves in a Half-Space	69

	<u>Page</u>
CONCLUSIONS AND RECOMMENDATIONS	92
BIBLIOGRAPHY	95
APPENDIX	100

22
23

ILLUSTRATIONS

<u>Figure</u>		<u>Page</u>
1	Spherical elastic wave in an infinite medium	11
2	Geometrical configuration of spherical elastic waves in a half-space	13
3	Contour of integration in Cagniard's formulation	20
4	Geometries of 5 receiver locations	25
5	Spherical elastic wave in a half-space--Rayleigh wave	26
6	Spherical elastic wave in a half-space--second surface wave	27
7	Spherical elastic wave in a half-space--total surface wave	28
8	Spherical elastic wave in a half-space--body wave	29
9	Spherical elastic wave in a half-space--total elastic wave	30
10-14	Spherical elastic waves in a half-space at location 1-5	31-35
15	Impulse response of attenuator--Voigt solid	58
16	Comparison of Voigt waves	59
17	Impulse response of attenuator--constant Q solid	63

<u>Figure</u>		<u>Page</u>
18	Spherical seismic wave in an infinite low-frequency-approximated Voigt solid	67
19	Spherical seismic wave in an infinite constant Q solid	68
20	Spherical seismic wave in a Voigt half-space--Rayleigh wave	72
21	Spherical seismic wave in a Voigt half-space--second surface wave	73
22	Spherical seismic wave in a Voigt half-space--total surface wave	74
23	Spherical seismic wave in a Voigt half-space--body wave	75
24	Spherical seismic wave in a Voigt half-space--total seismic wave	76
25-29	Spherical seismic waves in a Voigt half-space at location 1-5	77-81
30	Spherical seismic wave in a constant Q half-space--Rayleigh wave	82
31	Spherical seismic wave in a constant Q half-space--second surface wave	83
32	Spherical seismic wave in a constant Q half-space--total surface wave	84
33	Spherical seismic wave in a constant Q half-space--body wave	85
34	Spherical seismic wave in a constant Q half-space--total seismic wave	86
35-39	Spherical seismic waves in a constant Q half-space at location 1-5	87-91

LIST OF SYMBOLS

<u>Symbol</u>	<u>Definition</u>	<u>Page</u>
A	Transmission factor of compressional wave	15
$\alpha(\omega, x)$	Attenuation	44
*	Convolution	9
B	Transmission factor of shear wave	15
η	Moving branch cut in u-plane	19
δ	δ -function	5
δ'	Doublet function	6
δ^{-1}	Step function	6
δ^{-2}	Unit ramp	20
E	Contour of integration	19
$e(t, x)$	Elastic wave as input to attenuator	48
$F(t)$	Cagniard's source function	12
$F^I(t)$	$F^I(t) = \delta^{-1}(t) * F(t)$	19
$F^{II}(t)$	$F^{II}(t) = \delta^{-2}(t) * F(t)$	19
$\phi(\omega, x)$	Phase lag of a linear system	48
Φ	Dilatational potential	7
γ	Euler's constant	45

<u>Symbol</u>	<u>Definition</u>	<u>Page</u>
Γ	Contour of integration	19
g	$g^2 = V_p^2 / V_s^2$	105
$h(t, x)$	Impulse response of attenuator	48
$H(\omega, x)$	System function of attenuator	48
l	Displacement	4
\mathcal{L}^{-1}	Inverse Laplace transform	15
λ	Lamé's constant	4
\ln	Natural log	45
\tilde{l}_r	Radial component of displacement from an arbitrary pressure source	9
l_2	Vertical component of displacement	14
M	Receiver position in a half-space	12
μ	Lamé's constant	4
$p(t)$	Pressure	5
$P, \text{ \& } P'$	Contour of integration	19
$P \{ \}$	Cauchy principal value	51
π	Source position in a half-space	12
Ψ	Dilatational potential	14
Q	Quality factor	45
r	Radial coördinate	7
NF	Normalizing factor	11

<u>Symbol</u>	<u>Definition</u>	<u>Page</u>
r_0	Radius of source cavity	12
ρ	Density	4
S	Slowness of compressional wave	17
s	Slowness of shear wave	17
$s(t, x)$	Seismic wave as output of attenuator	48
$\mathcal{S}(\omega, x)$	Fourier transform of seismic wave	48
σ	Poisson's ratio	8
$\sigma(0, t)$	Stress at $x = 0$	5
t	Time	4
U	Vector potential	14
V_p	Compressional wave velocity	4
ω	Frequency	8
$w(t)$	Impulse response of source region	14
ω_c	Cut-off frequency	54
ω_0	Ricker's transition frequency	52
x	Spatial coördinate	4
\bar{X}_p	Cagniard's exponential coefficient	14
\bar{Y}_p	Cagniard's exponential coefficient	14
z	Spatial coördinate	14

ACKNOWLEDGMENTS

To Professor Frank A. Hadsell of the Colorado School of Mines I wish to express my deepest gratitude for acting as advisor on this research project. His encouragement, many invaluable discussions, and advice are sincerely appreciated.

I sincerely wish to thank Professor John C. Hollister for inducing me to do graduate work in Geophysics and serving on my doctoral committee, to Professor Alfred H. Balch, Professor F. Richard Yeatts, and Professor Edward G. Fisher for serving on my doctoral committee.

To the American Petroleum Institute and its Executive Committee on Exploration and Production Research goes my sincere appreciation for the generous research fellowship grant provided for past three years, and for the financial support and encouragement for a research project on elastic waves. This grant supported the development of part of the computer program library at Department of Geophysics, Colorado School of Mines, by Dr. Russell L. Gray and Dr.

T. K. Chao. Part of these computer programs are used to compute the elastic waves in this thesis. And I thank very much the developers.

INTRODUCTION

Elastic waves propagating in an isotropic homogeneous Hookean medium have been extensively studied for over a century. Analytical solutions generally involve plane, cylindrical, or spherical wave fronts and boundaries. Physical interpretations of these solutions are most commonly made in terms of asymptotic approximations. With the application of the digital computer to the boundary value problem, numerical methods have been used to study both elastic and seismic waves (Balch and Smolka, 1970).

A general theory of attenuation does not exist, nor does its development appear to be imminent; however several useful special theories exist (Jackson and Anderson, 1970; Kolsky, 1956; White, 1965). Plane Voigt waves have been described analytically by Ricker (1953), and Collins (1960). Plane and spherical Voigt waves have been described numerically through the finite difference method by Balch and Smolka (1970). In studying the constant Q model, Carpenter (1966) applied Futterman's (1962) formula for phase velocity and obtained the transient, attenuated seismic wave. O'Brien (1969) used

Carpenter's approach to explain the results of his experiments on compressional waves through rocks. Strick (1970) predicted a precursor or pedestal effect for pulses propagating in constant Q solids. The Voigt solid and the constant Q solid are the most extensively studied models; the Voigt solid because it yields a linear generalized wave equation and the constant Q solid because it seems to be a good model for earth materials for a large frequency range (White, 1965).

The boundary value problems of transient elastic wave theory are greatly complicated if one attempts to account for inelastic attenuation.

The approach used in this thesis does not concern the attenuation mechanisms. In this sense, this approach is phenomenological. Seismic wave forms are obtained by convolving the elastic wave forms with the impulse responses of linear filters which are used to approximate the effects of attenuation. Two models of attenuation and several types of elastic waves are used.

This work is organized in three sections: elastic waves, attenuation, and seismic waves.

ELASTIC WAVES

INTRODUCTION

In this study the elastic wave forms included are plane compressional waves in an infinite medium, spherical waves in an infinite medium, and spherical waves in a half-space.

The spherical wave in an infinite medium was studied by Sharpe (1942) and Blake (1951), amongst others Cagniard (1939), Pekeris (1940), and de Hoop (1960) have all treated the spherical wave in a half-space. Cagniard's method is referred to as the exact ray theory by Spencer (1965) because each term can be associated with one unique ray of the plane wave theory.

The following sections contain brief outlines of elastic wave theories used in this thesis and the computed wave forms. These wave forms will be used as input to the linear attenuators.

PLANE COMPRESSIONAL WAVE
IN AN INFINITE ELASTIC MEDIUM

The displacement field of the particles for the plane compressional wave in an isotropic, homogeneous, perfectly elastic infinite medium is described by wave equations of the following form:

$$\frac{\partial^2 \ell}{\partial x^2} = \frac{1}{V_p} \frac{\partial^2 \ell}{\partial t^2}$$

where ℓ is the displacement of the particles from their equilibrium position, x is the space coordinate, and V_p is the velocity of the compressional wave in the perfectly elastic medium.

The velocity of the compressional wave in the perfectly elastic medium is a constant and is equal to $\{(\lambda + 2\mu)/\rho\}^{\frac{1}{2}}$, where λ and μ are the Lamé's constants, and ρ is the density of the medium. Later, when attenuation is considered, it is seen that compressional seismic wave components of different frequencies travel at different velocities.

The boundary condition at $x = 0$ for the plane compressional wave equation is that the normal component of the

stress vector on the plane $x=0$ be equal to a specified function of time, i.e.,

$$\sigma(0, t) = p(t)$$

$p(t)$ is the applied pressure at $x=0$.

The infinite boundary condition, i.e., $x \rightarrow \infty$ is not rigorously formulated because it is realized that the plane compressional wave is an approximation of the spherical wave. Essentially the condition can be stated that there will be no source at infinity, i.e., there will be no wave radiated from infinity toward the finite domain.

The wave equation can be solved by the Laplace transform. Two types of pressure source are considered here, the unit impulse and the unit doublet in pressure.

For the unit impulse in pressure

$$\sigma(0, t) = 1 \cdot \delta(t)$$

and the solution has the following form:

$$l(x, t) = - \frac{1}{\rho V_p} \delta^{-1} \left(t - \frac{x}{V_p} \right)$$

where ρ is the density of the medium.

For the unit doublet in pressure

$$f(0, t) = 1 \cdot \delta'(t)$$

the solution is as follows:

$$l(x, t) = - \frac{1}{\rho V_p} \delta \left(t - \frac{x}{V_p} \right)$$

In the perfectly elastic medium, the impulsive pressure causes a step in displacement, and the doublet pressure causes an impulse in displacement. There will be no change of the wave form as the plane compressional waves propagate.

⊙
⊙

SPHERICAL COMPRESSIONAL WAVES
IN AN INFINITE ELASTIC MEDIUM

Elastic waves in an isotropic, homogeneous, perfectly elastic infinite medium from an arbitrary pressure in a hypothetical spherical cavity source has been studied by Sharpe (1942), and by Blake (1952). Sharpe considered the case of the Lamé's constant $\lambda = \mu$, and Blake the case of arbitrary values of λ and μ . An outline of the techniques used by Sharpe and Blake follows.

The wave equation for the spherically symmetric displacement potential is written for polar coordinates as:

$$\frac{\partial^2}{\partial r^2} (r \Phi) = \frac{1}{V_p^2} \frac{\partial^2}{\partial t^2} (r \Phi) ,$$

where r is the radial distance from the center of the spherical cavity, Φ is the displacement potential, i.e., the displacement $\vec{\ell} = \nabla \Phi$, and V_p is the velocity of compressional waves in the medium. The boundary condition is that at the surface of the spherical cavity source, the radial component of the stress is equal to the negative of the pressure in the source. This can be written

$$- \left[(\lambda + 2\mu) \frac{\partial l_r}{\partial r} + 2\lambda \frac{l_r}{r} \right]_{r=r_0} = p(t)$$

where l_r is the radial component of displacement, r_0 is the radius of cavity source, and $p(t)$ is the pressure inside the cavity. By superposing solutions to the wave equation and carrying out the resulting integral by contour integration, the displacement for $p(t) = p_0 \delta^{-1}(t)$ is obtained by Sharpe for $\lambda = \mu$ as:

$$l_r(\tau, r) = \delta^{-1}(\tau) p_0 \frac{r_0}{4\mu} \left\{ \left(\frac{r_0}{r}\right)^2 - \sqrt{\frac{3}{2}} \left(\frac{r_0}{r}\right)^2 e^{-\frac{\omega_0 \tau}{\sqrt{2}}} \sin[\omega_0 \tau + \tan^{-1} \sqrt{2}] + \sqrt{2} \left(\frac{r_0}{r}\right) e^{-\frac{\omega_0 \tau}{\sqrt{2}}} \sin \omega_0 \tau \right\}$$

where $\tau = t - \frac{r-r_0}{V_p}$, p_0 is the amplitude of the pressure on the surface of the source cavity, σ is Poisson's ratio for the medium and $\omega_0 = \frac{V_p}{r_0} \frac{(1-2\sigma)^{1/2}}{1-\sigma}$.

For the general case of λ and μ Blake derived:

$$\Phi(\tau, t) = \delta^{-1}(\tau) \rho_0 \frac{r_0^3 K}{\rho r V_p} \left\{ -1 + \left(\frac{4K}{4K-1} \right)^{\frac{1}{2}} e^{-\alpha_0 \tau} \cos \left[\omega_0 \tau - \tan^{-1} (4K-1)^{-\frac{1}{2}} \right] \right\},$$

where $K = \frac{1-\sigma}{2(1-2\sigma)}$, ρ represents density, and

$$\alpha_0 = \frac{V_p}{r_0} \frac{(1-2\sigma)^{1/2}}{1-\sigma}.$$

The displacement, or potential, due to an arbitrary pressure change is obtained by convolving the arbitrary pressure with the impulse response of the elastic wave propagating system. The impulse response of this system is the displacement, or its potential, resulting from a unit impulse in pressure in the source cavity. Hence the displacement resulting from an arbitrary pressure in the source is:

$$\begin{aligned} \tilde{l}_r &= \frac{1}{r_0} \frac{d}{dt} [l_r(t)] * p(t) \\ &= \frac{1}{r_0} \frac{d}{dt} \int_0^t p(\tau) l_r(t-\tau) d\tau \end{aligned}$$

Flinn & Dix (1962) derived an equivalent formula by the Laplace transform method.

The amplitude of the spherical wave decays along the propagation path even though the medium is perfectly elastic, i.e., lossless. This is because of a spherical wave front, which spreads in propagation. Hence this type of decay is referred to as geometrical spreading.

Figure 1 shows examples of elastic waves computed from algorithms derived from the above theory. Note that for the parameters selected there is no appreciable change in the wave forms in radial distance beyond 65 feet. In these figures NF represents the normalization factor and the unit of the abscissas is two-milliseconds. The zero time in the plot corresponds to the arrival time for each trace at its location. The horizontal line associated with each trace represents the zero amplitude for that trace.

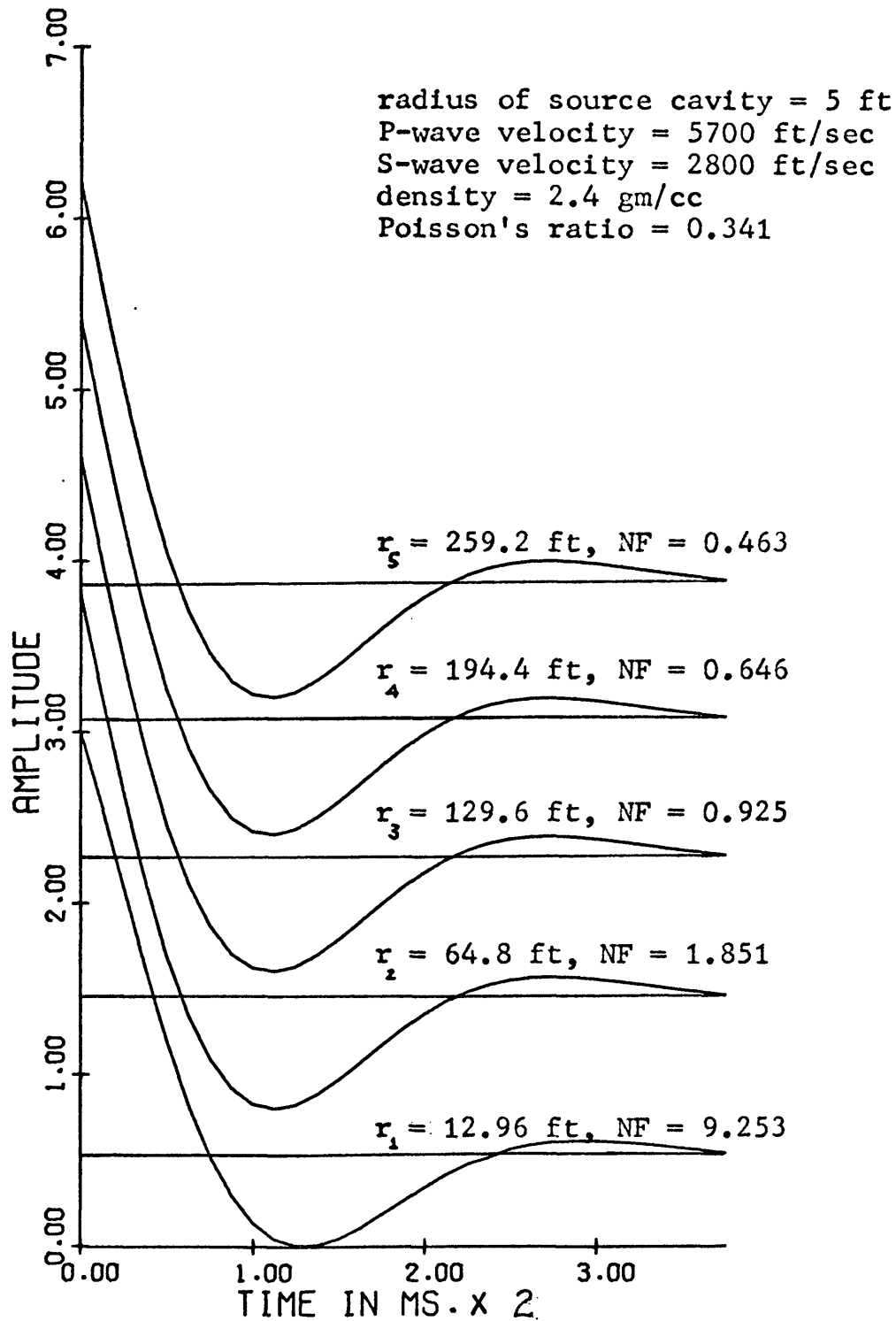


Figure 1. Spherical waves in an isotropic, homogeneous, infinite perfectly elastic medium: radial displacement from an impulsive pressure with parameters and configuration shown. NF represents the normalizing factor.

SPHERICAL WAVE IN A HALF-SPACE

The formal solution to the problem of spherical waves in an elastic half-space has been formulated by many investigators, including Cagniard (1939), Sobolev (1933), and Pekeris (1948). In this thesis Cagniard's formulation is used. The equations have been checked by comparing computed results with those obtained by other methods (Chao, 1970; Leitinger, 1970). The numerical calculations were made with a Digital Equipment Corporation PDP-10 computer using a teletype terminal.

The geometrical configuration for the problem is indicated in figure 2. The free surface is a plane, and the source, π , and the receiver, \mathcal{M} , can be at any depth in the elastic half-space. The medium is homogeneous, isotropic, and perfectly elastic with Lamé's constants λ and μ .

The source for the half-space problem is the same as the source for the infinite medium problem of the previous section. The notation $p(t) * w(t)$ is used in place of Cagniard's $F(t)$. The source function, $w(t)$, is $r \left[\frac{\partial \Phi}{\partial t} \right]_{r=r_0}$
 $\rho_0 = 1$

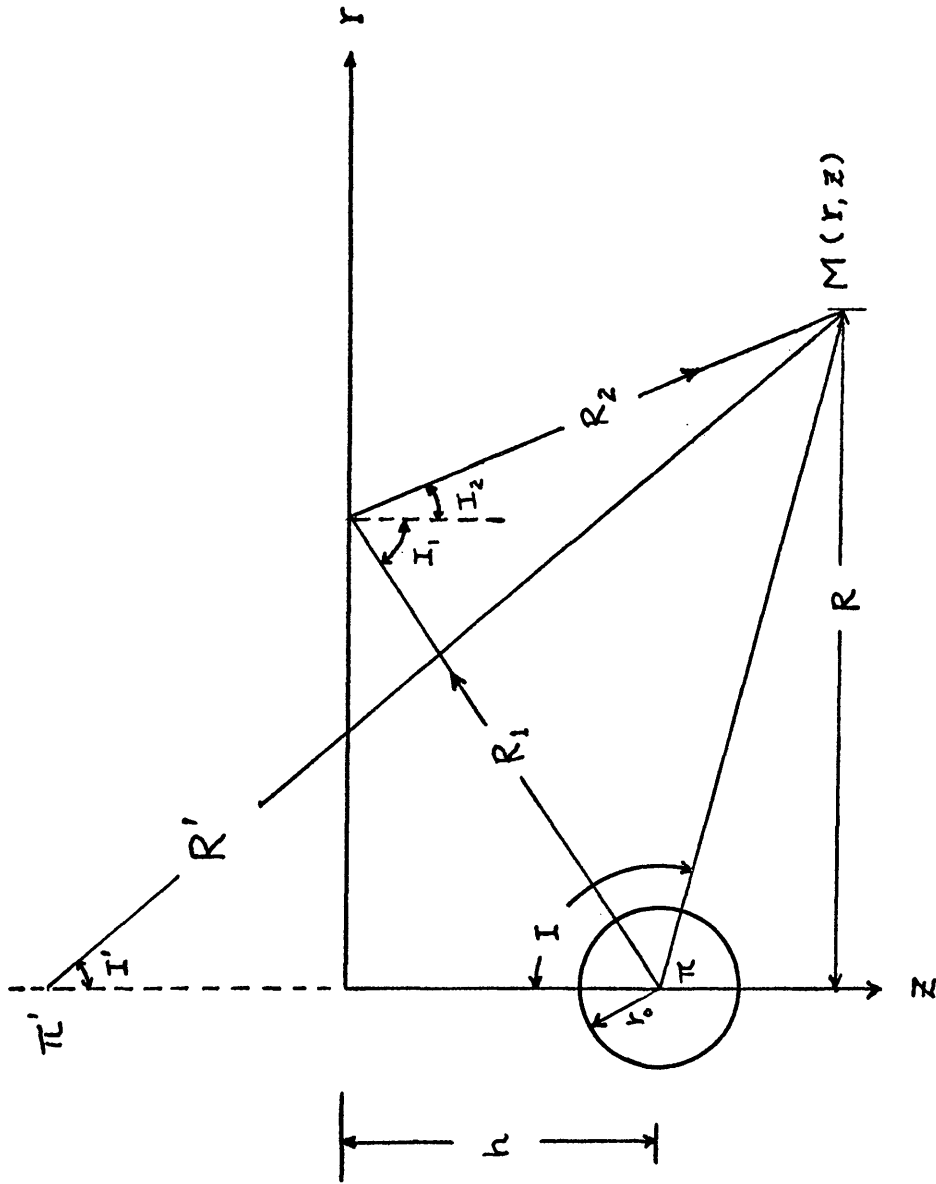


Figure 2. Geometrical configuration for the half-space problem in Cagniard's formulation. The source is at π , and receiver at M .

Note that in writing $w(t)$, r_0 is set equal to dimensionless unity.

The formal solution to the wave equation of the problem is in Cagniard's book and hence only an outline will be presented here.

The radial and the vertical components of displacements, l_r and l_z , are expressed in terms of the scalar and the vector potentials of displacements, ψ and Ω as follows:

$$l_r = \frac{\partial \psi}{\partial r} - \frac{\partial \Omega}{\partial z}$$

$$l_z = \frac{\partial \psi}{\partial z} + \frac{\partial \Omega}{\partial r} + \frac{\Omega}{r}$$

Let $p * w$ denote the source function, and \bar{X}_p , \bar{Y}_p denote Cagniard's exponential coefficients, or physically, the Laplace transform of the solution to this boundary value problem for a source function $p(t) * w(t) = \delta(t)$. If $p(t)$ and $w(t)$ are impulses so that $F(t) \equiv p * w = \delta(t)$ then \bar{X}_p and \bar{Y}_p are transforms of Green's functions. The Laplace transforms of the displacement potentials, the

solutions, and the source function are related according to:

$$\bar{\Psi} = \bar{X}_p \bar{F}$$

$$\bar{U} = \bar{Y}_p \bar{F}$$

where the bar over a quantity denotes the Laplace transform of that quantity. The transmission factors, A and B , are defined as follows:

$$A = \mathcal{L}^{-1} \{ \bar{X}_p \}$$

$$B = \mathcal{L}^{-1} \{ \bar{Y}_p \}$$

where \mathcal{L}^{-1} denotes the inverse Laplace transform. Finally one has the following:

$$\Psi = A * F$$

$$U = B * F$$

The transmission factors or Green's functions, A and B , are obtained by inspection, after an integral solution of the boundary value problem is brought to the form of the Laplace transform. In the interest of brevity we shall omit the details of the procedure, which are quite involved, used to bring the formula into the desired form for inspection. Use is made of the Sommerfeld formula (Ewing and others, 1957, eq. 1-41), and of a series of changes of variables. The transmission factors are then expressed in terms of a contour integral. The contour of the integral moves with time, and hence is called a moving contour. This integral is finally replaced by an integral over fixed contours. When the transmission factors are thus represented the solution breaks into readily interpreted components, as will now be shown.

The transmission factors, A was analyzed by Cagniard as follows:

$$A(\tau) = A_1(\tau) + A_2(\tau) + A_3(\tau)$$

where (see figure 3),

$$A_1(\tau) = \begin{cases} 0 & , \text{ for } \tau < R S \\ \frac{1}{R} & , \text{ for } \tau > R S \end{cases}$$

where τ denotes time, S , slowness of compressional wave, s , slowness of shear wave. $A_1(\tau)$ represents the classical direct P -wave.

$$A_2(\tau) = \begin{cases} 0 & , \text{ for } \tau < R' S \\ -\frac{1}{R'} & , \text{ for } \tau > R' S \end{cases}$$

$A_2(\tau)$ represents the classical reflected P -wave.

$$A_3(\tau) = \begin{cases} 0 & , \text{ for } \tau < R' S \\ -\frac{i}{\pi} \int_{\Sigma_\tau} \frac{j(u) u du}{\{u^2 r^2 + [\tau - a(h+z)]^2\}^{\frac{1}{2}}} & , \\ & \text{for } \tau > R_1 S + R_2 s \end{cases}$$

$A_3(\tau)$ represents non-classical components and the Rayleigh wave.

$B(\tau)$ is broken down as follows:

$$B(\tau) = \begin{cases} 0, & \text{for } \tau < R_1 S + R_2 s \\ \frac{i}{\pi r} \int_{\Sigma_\tau} \frac{(\tau - ah - bz) f(u) u \, du}{\{u^2 r^2 + [\tau - ah - bz]^2\}^{\frac{1}{2}}}, & \text{for } \tau > R_1 S + R_2 s \end{cases}$$

$B(\tau)$ represent all shear components including the classical P - S conversion and the shear components of Rayleigh wave.

In these equations for $A(\tau)$, and $B(\tau)$, the functions $f(u)$, $j(u)$, $D(u)$, a , and b are defined as follows:

$$f(u) = \frac{u^2 + \frac{s^2}{2}}{D(u)},$$

$$j(u) = \frac{-b u^2}{D(u)},$$

$$D(u) = \left(u^2 + \frac{s^2}{2}\right)^2 - ab u^2,$$

$$a = (u^2 + s^2)^{\frac{1}{2}}$$

and

$$b = (u^2 + s^2)^{\frac{1}{2}}$$

The contour \sum_{τ} is shown in figure 3 (Cagniard, 1939, p. 151).

The integration along the contour \sum_{τ} which moves with time, is replaced by three contours (Γ), (P) and (P'), and (E). The scheme is shown in figure 3. (Γ) is the counterclockwise contour outside all the other contours. (P) and (P') are clockwise contours around the two poles $i S_R$ and $-i S_R$. (E) is the clockwise contour around the branch cuts of $a(u)$ and $b(u)$ on the imaginary axis.

Among other things, the integration along the path Γ yields the remnant effects. The closed form of that integration is obtained through the residue theorem. The transmission factors thus obtained contain terms as function of time, and time squared. Thus these terms give rise to the result that not only $F'(t)$, and $F(t)$, but also the integrals $F^I(t)$, and $F^{II}(t)$ are involved in computing

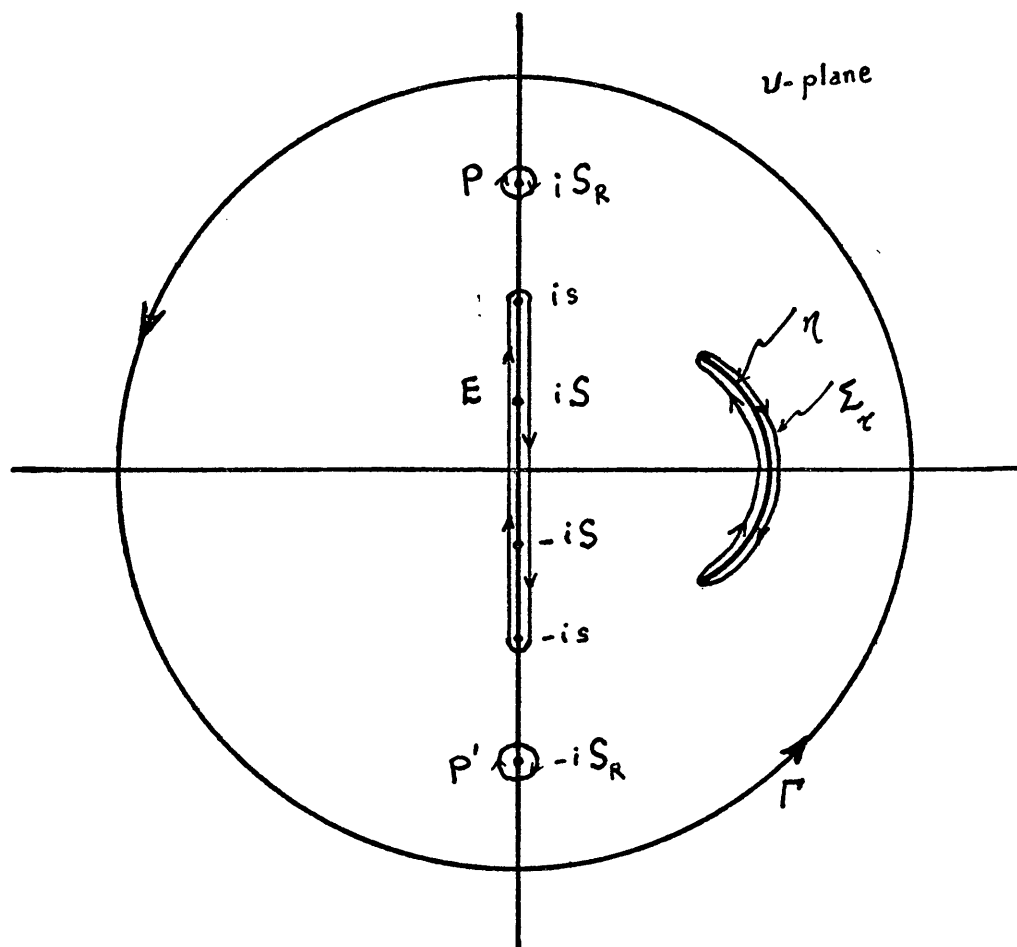


Figure 3. Contours of integration. The contours Σ_r , Γ , ρ and ρ' , and E are shown. S , s , and S_R are slowness of compressional, shear, and Rayleigh wave respectively.

the seismogram.

Here

$$F^I(t) \triangleq \delta^{-1}(t) * F(t),$$

and

$$F^{II}(t) \triangleq \delta^{-2}(t) * F(t)$$

where $\delta^{-1}(t)$ is a unit step, $\delta^{-2}(t)$ is a unit ramp, and \triangleq denotes equal by definition.

The integration around the poles yield the terms corresponding to the Rayleigh wave. It has the characteristics of the classical Rayleigh wave such as the retrograde elliptical particle motion and energy concentration near the free surface. For a surface source and receiver, it has a wave speed which, in the far field, is the classical Rayleigh wave speed. This integration is also carried out through the residue theorem.

The wave corresponding to the integration along the contour (E) around the branch cut on the imaginary axis is called the second surface wave by Cagniard because of some similarities to the Rayleigh wave (see Chao, Fig. 27,

1969). The integration around the branch cut is carried out numerically using Romberg quadrature (Conte, 1965).

In this work only the vertical component of displacement, l_z , is computed. The detailed formulas for l_z , and for the transmission factors are included in the appendix. The program for computing the seismogram permits one to choose arbitrary parameters such as source and receiver positions, elastic properties, and cavity radius.

Figure 4 shows the source-receiver geometry for computing elastic wave forms. The receiver and the center of source cavity are buried at depth of 10 feet from the free surface of the elastic half-space. The radius of source cavity is 5 feet. Five radial distances are chosen to compute the wave forms.

Figure 5 through 14 show the wave forms--the vertical components of displacement computed by means of algorithms based on Cagniard's theory. The vertical component of displacement is composed of body waves, and surface waves. The surface wave, according to Cagniard's formulation, is composed of two parts--the classical Rayleigh wave and the second surface wave.

Figure 5 is a collection of Rayleigh waves at 5 locations with each trace normalized. This collection serves to compare Rayleigh wave as it propagates. Figure 6 is a plot of second surface waves at various locations. Figure 7 is plot of total surface waves, i.e., sum of Rayleigh and second surface wave. It is observed from figure 7 that the second surface wave contributes less at location 1 and 5 than at location 2, 3, and 4. The contribution of second surface wave to the total wave form is more explicitly demonstrated in the figure 10 through 14.

Figure 8 is a collection of body waves--the PP-, and PS-waves at 5 locations. Figure 9 is a plot of vertical components of displacement, which is sum of body wave and total surface wave at 5 locations. It is observed that while body wave is dominant at location 1, the surface wave is dominant at location 5.

Figure 10 through 14 are elastic wave forms at those 5 locations shown in the figure captions. The plot of each location consists of 5 traces, they are from bottom to top the Rayleigh wave, second surface wave, total

surface wave, body wave, and total of the vertical displacement. These traces are scaled to their relative amplitude with respect to the total vertical displacement, which is normalized.

- $r_1 = 12.96 \text{ ft}$
- $r_2 = 64.8 \text{ ft}$
- $r_3 = 129.6 \text{ ft}$
- $r_4 = 194.4 \text{ ft}$
- $r_5 = 259.2 \text{ ft}$

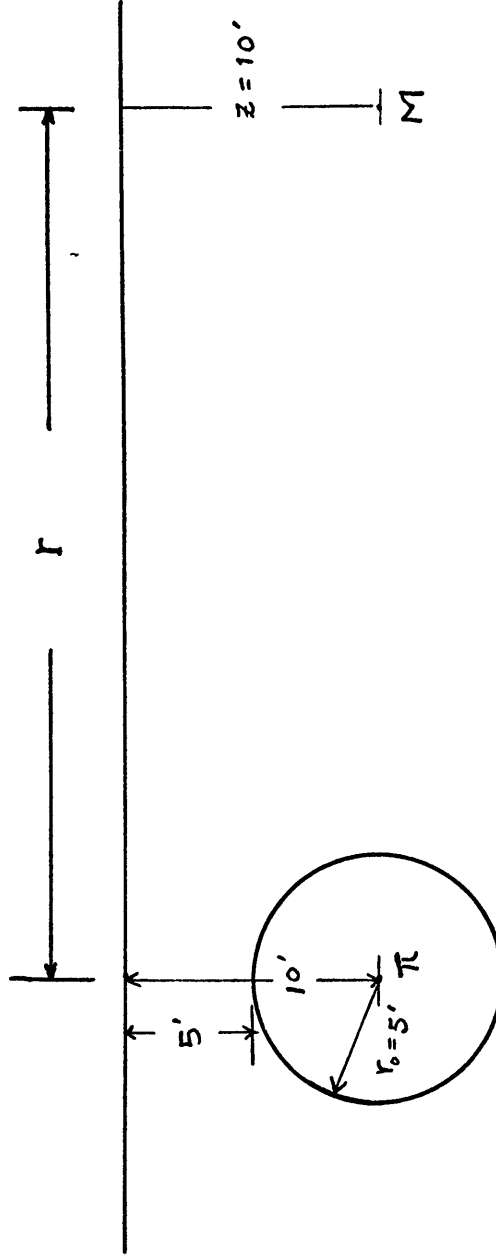


Figure 4. Geometry of source-receiver for half-space problem. The 5 locations used to compute wave forms in this thesis are as shown. All the parameters z , h , r_0 , ρ , V_p , and V_s remain the same throughout 5 locations.

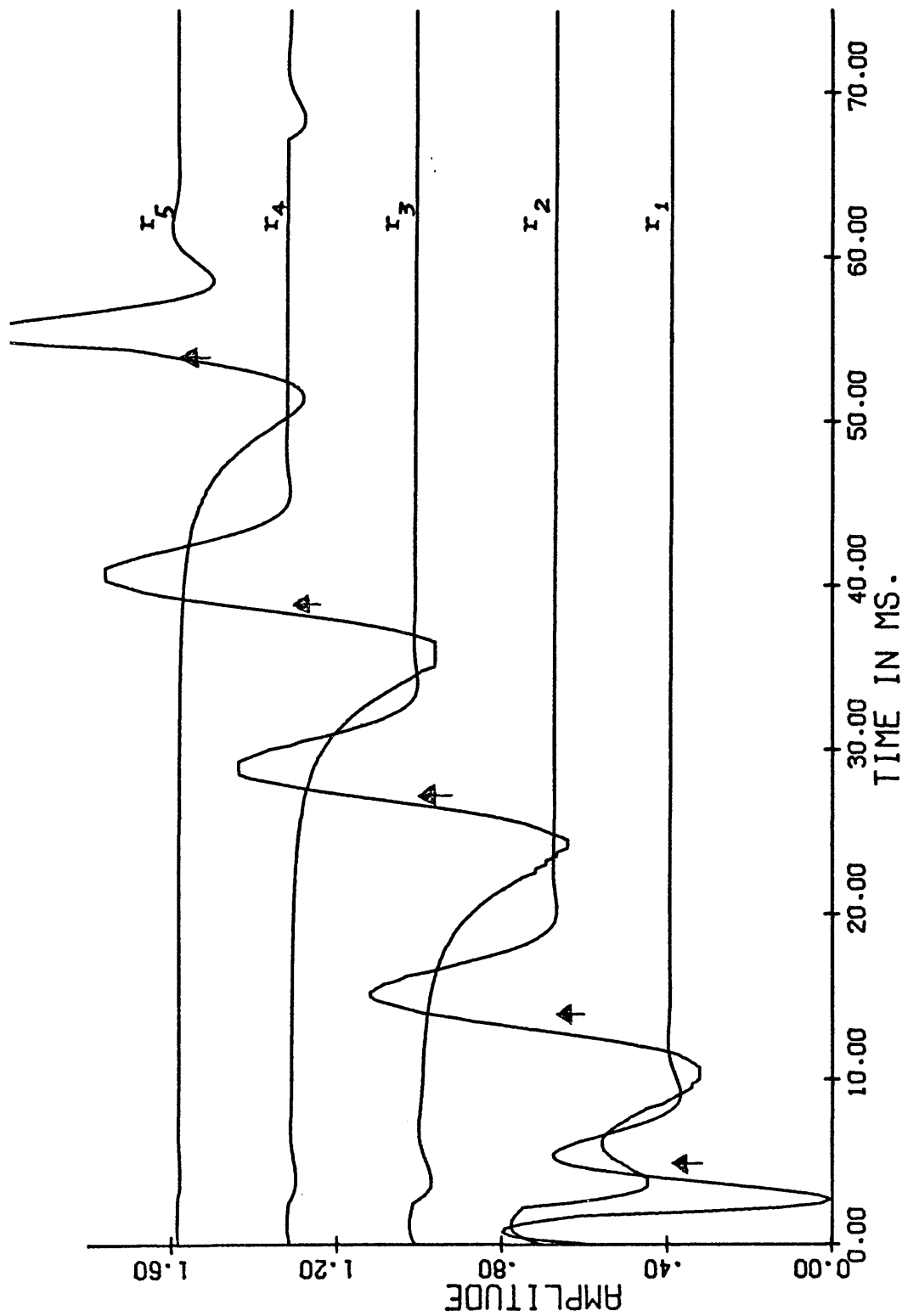


Figure 5. Spherical elastic waves in a half-space--the vertical component of displacement: Rayleigh waves at 5 locations after PP arrival time. The Rayleigh wave arrival times are indicated by the arrows.

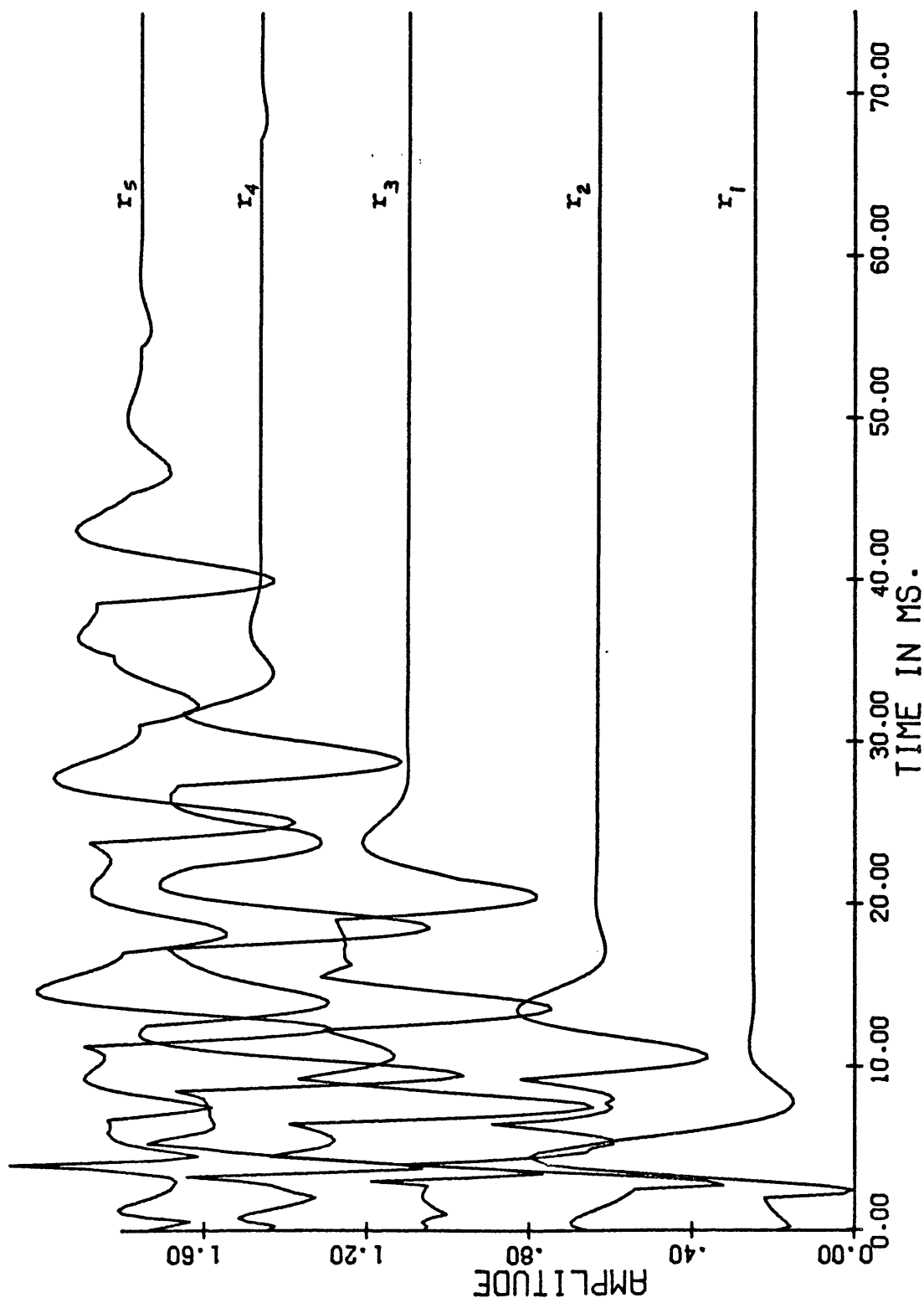


Figure 6. Spherical elastic waves in a half-space--the vertical component of displacement: Second surface waves at 5 locations after PP arrival time.

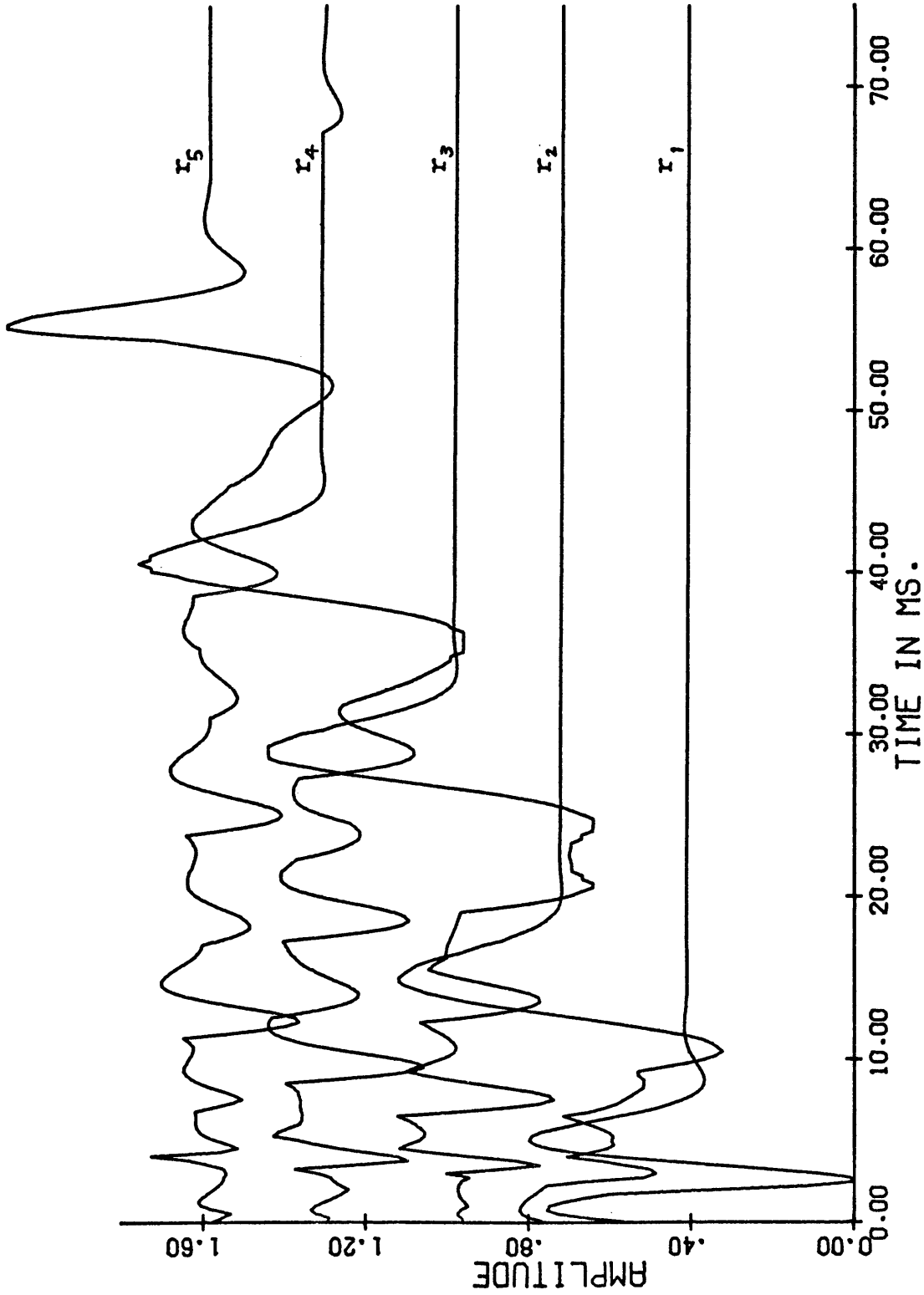


Figure 7. Spherical elastic waves in a half-space--the vertical component of displacement: Total surface waves at 5 locations after PP arrival time. Note that the total surface wave is sum of Rayleigh wave and second surface wave.

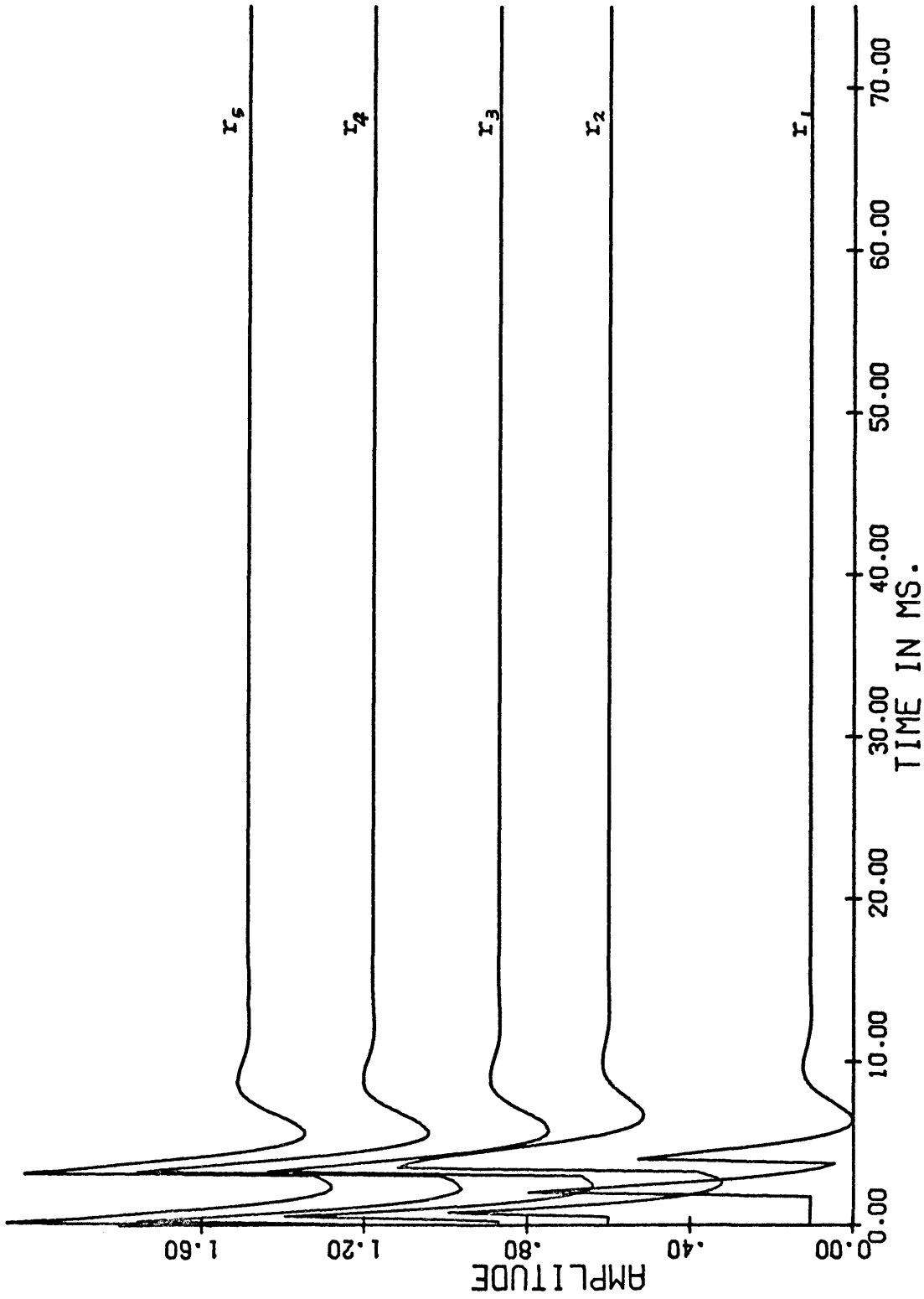


Figure 8. Spherical elastic waves in a half-space--the vertical component of displacement: Reflected body waves at 5 locations after direct wave arrival time. The PP and PS arrival times are as shown.

	PP arrival times (ms)	PS arrival times (ms)
r_5	4.18	6.20
r_4	11.89	14.63
r_3	23.01	25.92
r_2	32.78	35.75
r_1	45.61	48.62

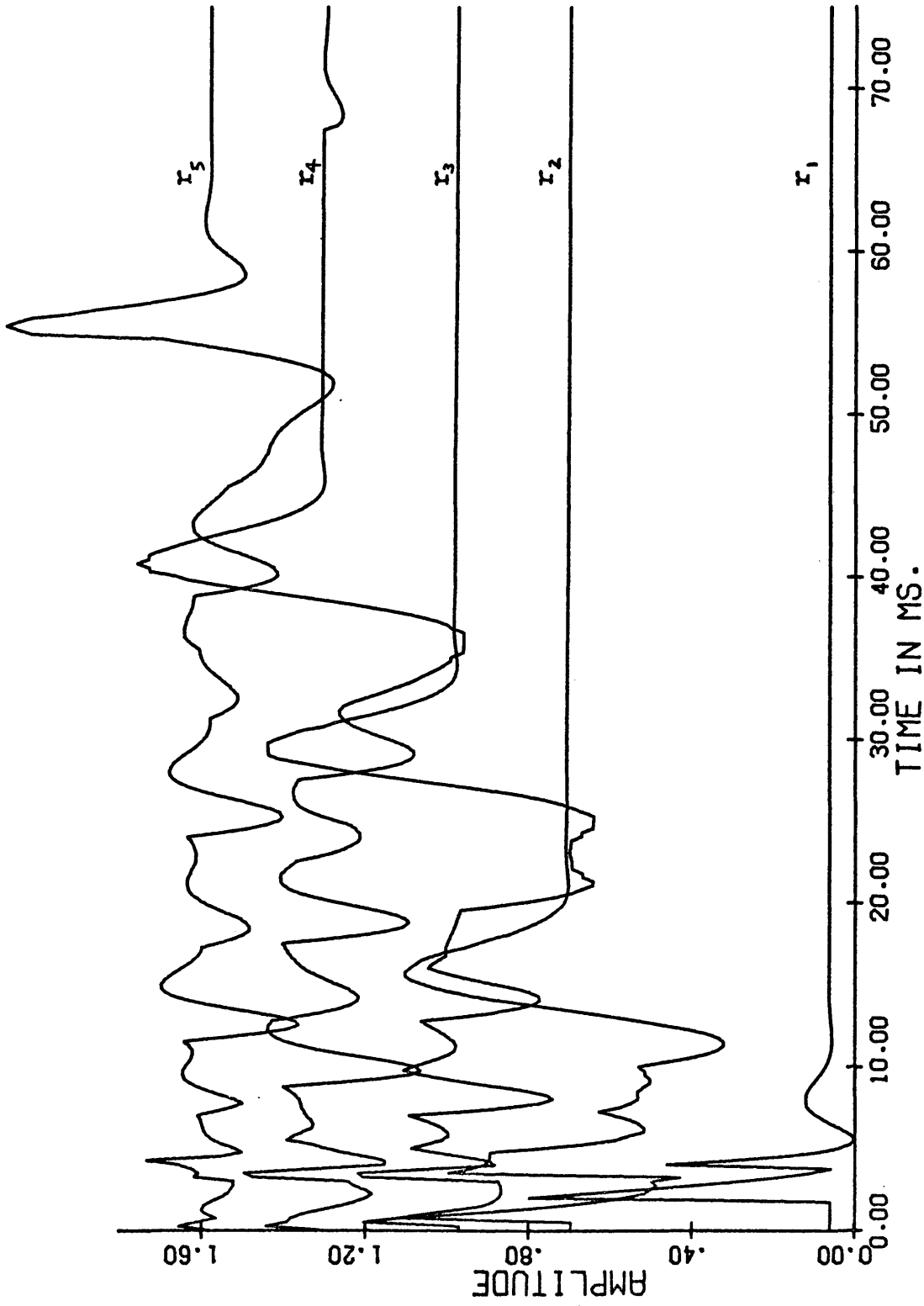


Figure 9. Spherical elastic waves in a half-space--the vertical component of displacement: Total elastic waves at 5 locations after direct wave arrival time. The total elastic wave is the sum of body wave and total surface wave. Note that each trace for each location is normalized.

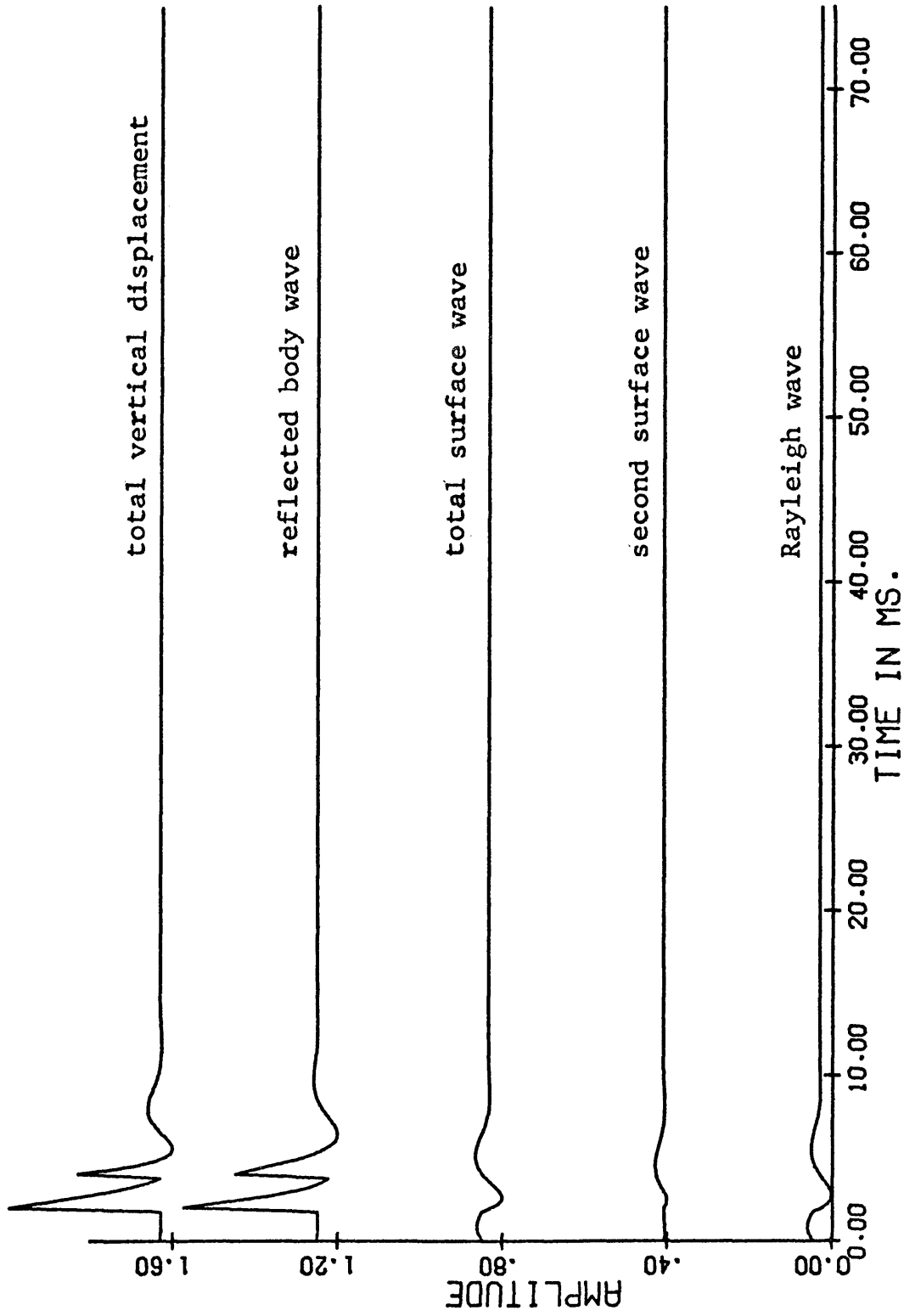


Figure 10. Spherical elastic wave decomposed at location 1. These traces are scaled to their relative amplitude with respect to the total vertical displacement, which is normalized.

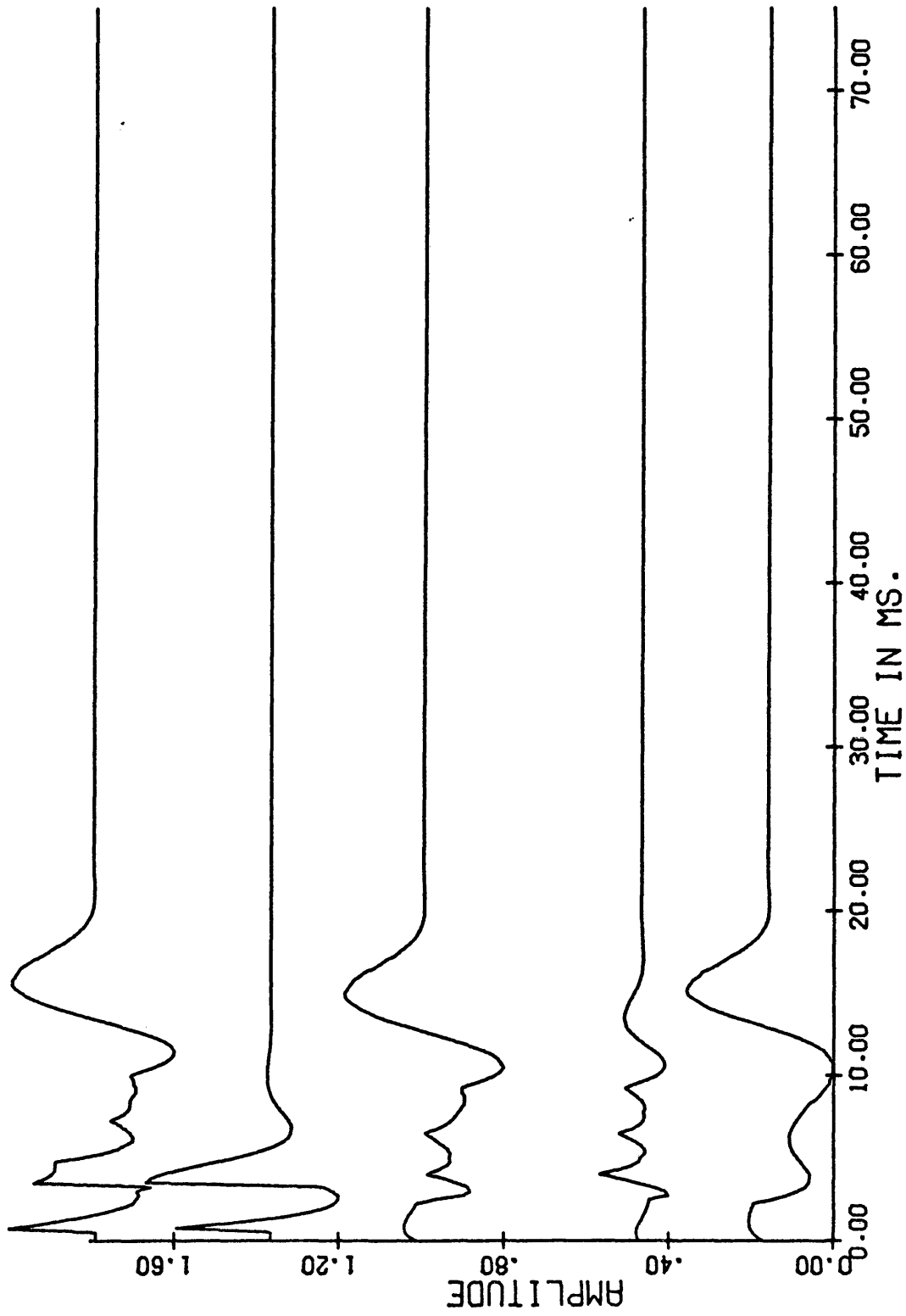


Figure 11. Spherical elastic wave decomposed at location 2. These traces are scaled to their relative amplitude with respect to the total vertical displacement, which is normalized. The arrangement of traces is the same as that of figure 10.

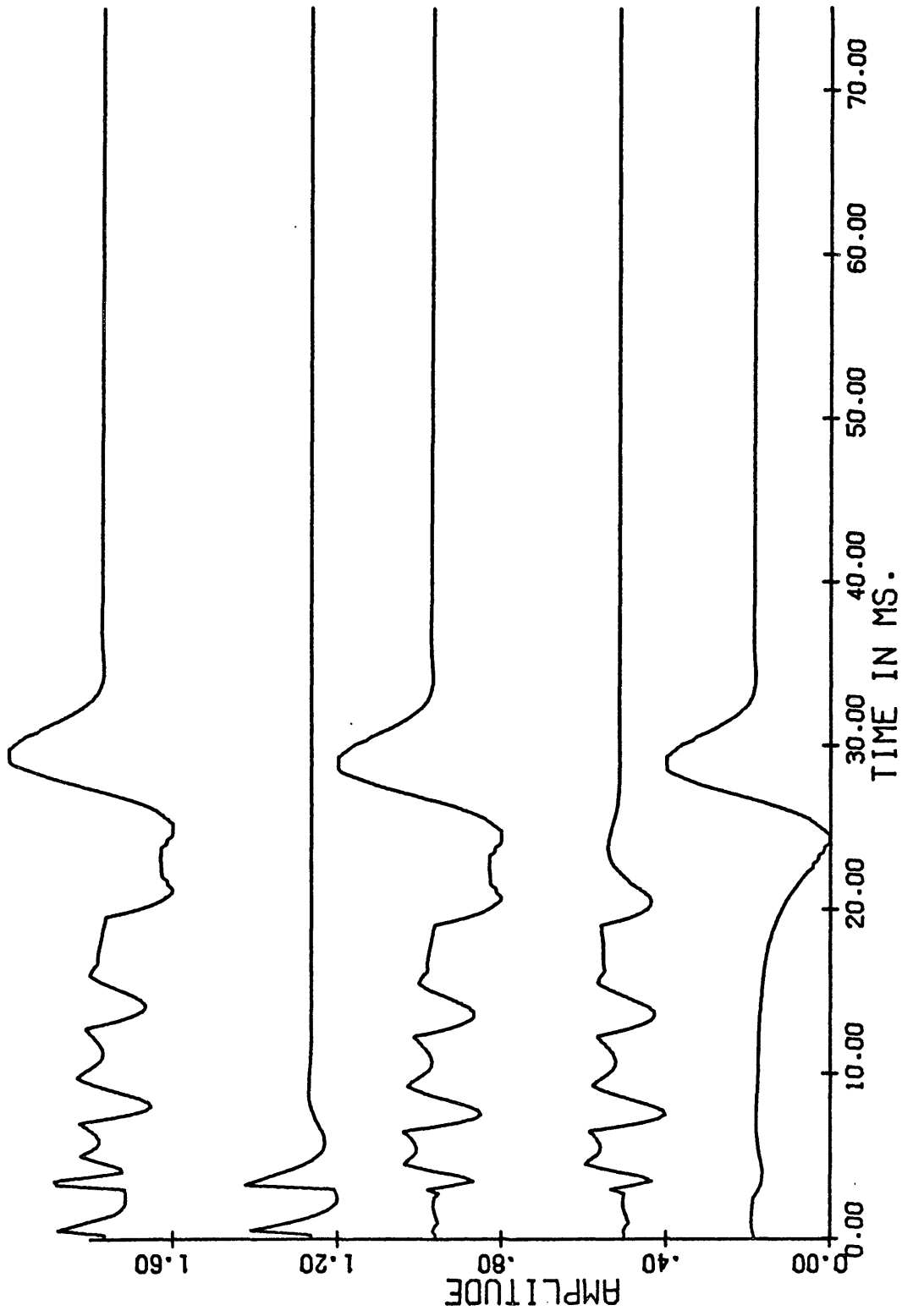


Figure 12. Spherical elastic wave decomposed at location 3. These traces are scaled to their relative amplitude with respect to the total vertical displacement, which is normalized. The arrangement of traces is the same as that of figure 10.

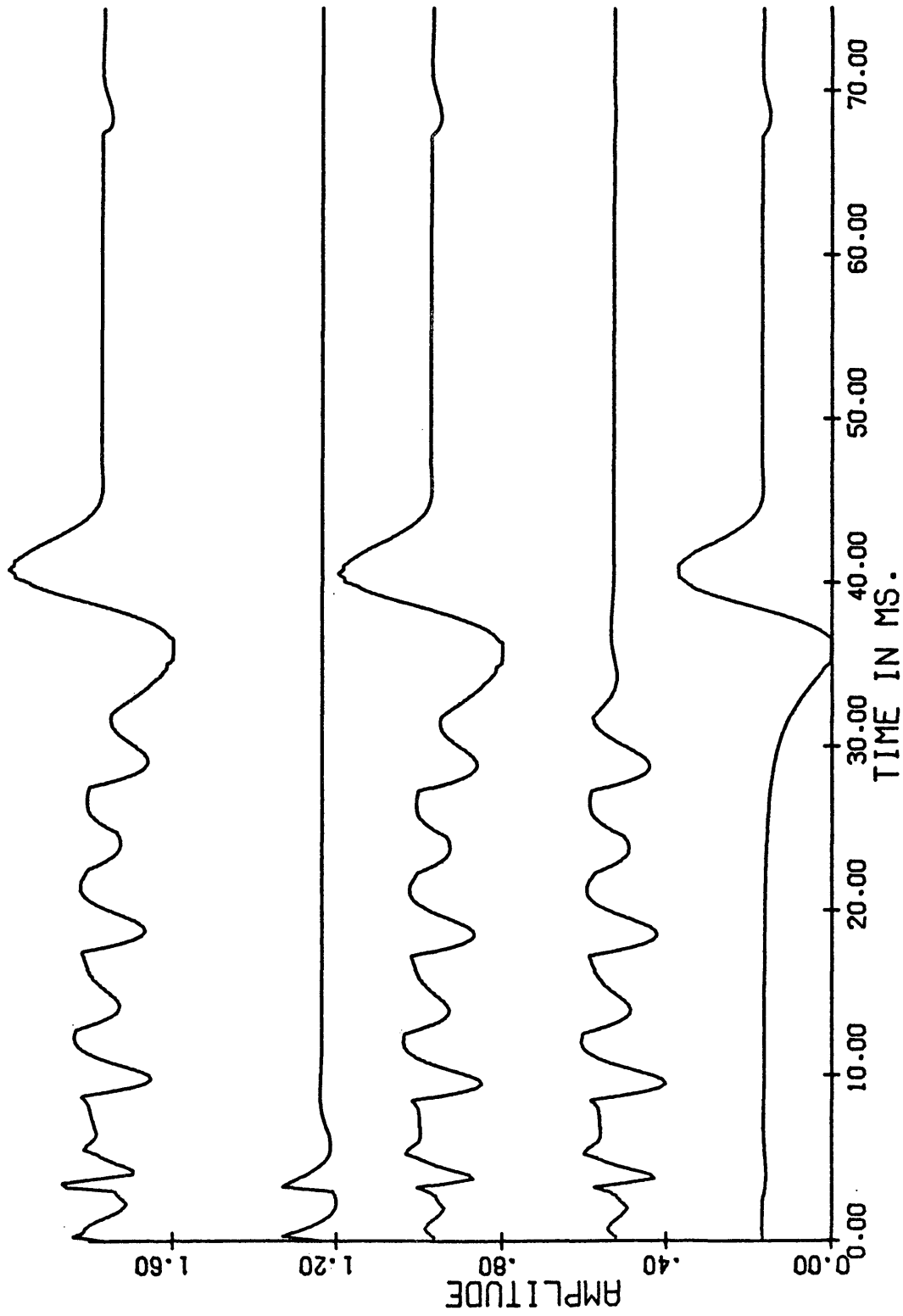


Figure 13. Spherical elastic wave decomposed at location 4. These traces are scaled to their relative amplitude with respect to the total vertical displacement, which is normalized. The arrangement of traces is the same as that of figure 10.

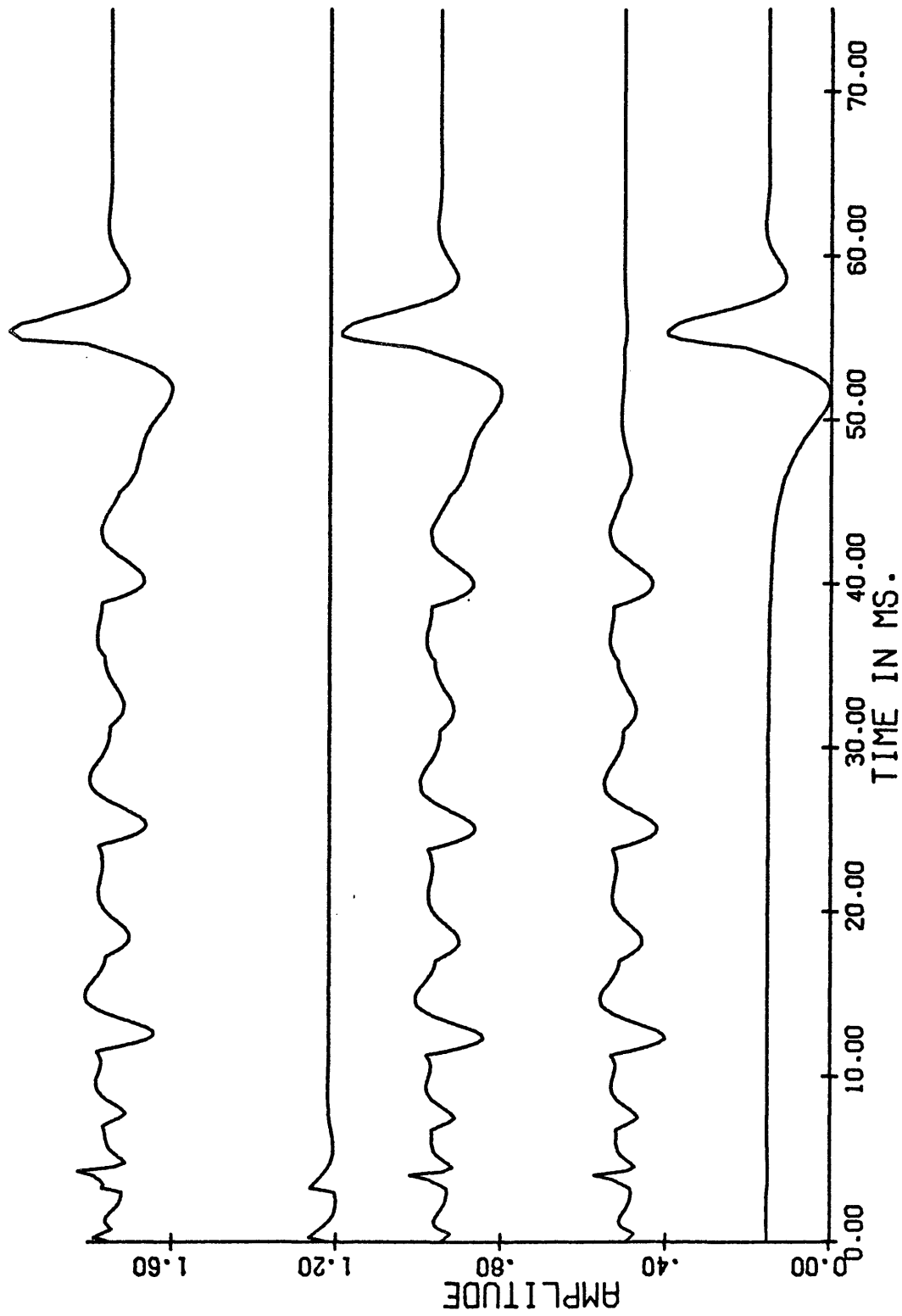


Figure 14. Spherical elastic wave decomposed at location 5. These traces are scaled to their relative amplitude with respect to the total vertical displacement, which is normalized. The arrangement of traces is the same as that of figure 10.

ATTENUATION

INTRODUCTION

In an anelastic medium, the decay of seismic wave forms through propagation is attributed to two effects--spreading and attenuation. The spreading accounts for geometrical spreading of energy and the attenuation accounts for the conversion of coherent elastic energy into incoherent energy. If the inhomogeneities of the medium are atomic in scale then this incoherent energy is heat. In the previous chapter the propagation effects were studied through the elastic wave theory. In this chapter the attenuation effects will be studied by approximating the attenuation by linear systems, one for each receiver position. Thus the input into the approximate attenuation system is the unattenuated elastic wave, and the output is an approximation to the attenuated seismic wave.

In the description of attenuation in terms of linear systems, an attenuation amplitude characteristic is assumed over a frequency range which is generally finite. It is assumed that the source provides negligible energy

outside of this range. Another assumption on this system is that it is causal and has the minimum-phase characteristic (Papoulis, 1962).

The linear attenuator is represented by its system function

$$H(\omega, x) = e^{-d(\omega, x)} e^{-i\phi(\omega, x)}$$

where $d(\omega, x)$ is called the attenuation of the propagation path of length x , $e^{-d(\omega, x)}$ is the amplitude response of the system, and $\phi(\omega, x)$ is the phase lag of the system.

The attenuation of waves in the earth has been extensively studied. The earth acts as a low pass filter for the propagation of earthquake waves (Gutenberg, 1959). The attenuation of seismic waves has been measured from explosive sources in the field (McDonal and others, 1958).

Besides the measurements of attenuations, there have been theoretical studies of possible physical mechanisms of attenuation of seismic waves (Kolsky, 1953; White, 1965). The relative importance of these mechanisms depends on the frequency range of the waves, and on the temperature,

pressure, and constituents of the medium (Knopoff and McDonald, 1960; Jackson and Anderson, 1970).

There are two types of attenuations have been extensively studied--the Voigt solid, and the "constant Q" solid (Ricker, 1943; Futterman, 1962). Several methods, such as the Laplace transform method (Collins, 1960; Jaramillo and Colvin, 1970), the contour integration method (Mattice and Lieber, 1954), and the finite difference method (Balch and Smolka, 1970), have been applied to solve the associated boundary value problems.

Before going into detail on the attenuation filter, a brief review of the measurements and proposed mechanisms of several authors will be given.

MECHANISMS AND MEASUREMENTS OF ATTENUATION

In this section some mechanisms proposed by various authors, and some field and laboratory measurements of attenuation will be reviewed briefly. Some characteristics of attenuation drawn from these studies will be used in the specification of the attenuation filter.

Loss Mechanisms

Mechanisms which convert coherent energy into incoherent energy are termed loss mechanisms. The mechanisms whereby elastic energy is dissipated into the medium by converting it into heat are collectively termed internal friction. Kolsky (1953) gave a quite extensive summary on this subject. Also Knopoff and McDonald (1960), and Jackson and Anderson (1970) gave both macroscopic and microscopic models of loss mechanisms.

Viscous Loss

If the wave energy loss of a medium is well predicted by terms proportional to stress rate or strain rate, then it is called viscous loss. There are two types of viscous loss in solids--Maxwell and Voigt.

For the Voigt solid the stress is the sum of two terms, one proportional to the strain the other to the strain rate. This solid yields a frequency-dependent attenuation function and is dispersive (Ricker, 1953). Ricker's studies in this field are well noted. In the lower frequency range, say below 60 hz, which is less than a quarter of Ricker's transition frequency, the attenuation is proportional to the second power of frequency, while the phase velocity is almost equal to that of a perfectly elastic medium.

The Maxwell solid and Voigt solid behave in opposite ways, i.e., with stress and strain playing opposite roles.

Thermal Loss

For compressional waves the solid has a temperature difference between the compressed and rarefied parts. Hence there exists a heat flux, and the mechanical energy is transformed into thermal energy and dissipated.

For very low frequencies, where the heat transfer takes place isothermally, the thermal loss yields an attenuation proportional to frequency squared (Treitel, 1959; Knopoff, 1960). Thermal loss is important in the ultra-high-frequency range above 10^7 to 10^8 hz. Thus it

is relatively unimportant in seismology.

Scattering Loss

This is the loss due to inhomogeneities of the media not deterministically considered in the formulation of the boundary value problem. The attenuation increases monotonically as the frequency increases. This type of attenuation is proportional to the fourth power of frequency for the high frequency range (Miles, 1960; Hadsell, 1961).

Ferromagnetic and Ferroelectric Loss

If the solid is ferromagnetic or ferroelectric, the elastic energy can be transformed into magnetic or electric energy, and finally into heat. It is unlikely that these losses are important in seismic wave attenuation (Knopoff and McDonald, 1960).

Coulomb Frictional Loss

Knopoff and McDonald (1960) proposed that microscopic sliding may be an important loss mechanism. This type of internal friction, called Coulomb friction, yields a model with Q dependent on frequency, and hence attenuation which is not proportional to frequency. For a lucid discussion of Q see White (1965).

Variable Solid Friction Loss

This model is an extension of the above. The solid friction force increases linearly with distance from the equilibrium position. This model, proposed by Knopoff and McDonald (1960), yields a constant Q , i.e., attenuation as a linear function of frequency. This mechanism has been supported by the observations that the Q of a material increases with pressure. Knopoff and McDonald have compared this mechanism to dislocation theory in crystals.

Static Friction Loss

In addition to the previous works by Knopoff and McDonald (1960), which attribute all the loss to the sliding friction, White (1966) extends the model of solid friction by incorporating the static friction. This model yields constant Q .

Jackson and Anderson (1970) very extensively reviewed the theoretical and experimental evidence concerning mechanisms of attenuation of seismic waves. They emphasized the microscopic models and the conditions likely to be prevailing in the mantle of the earth. Many mechanisms yield a strongly frequency dependent Q ; however, for rock,

the observed Q is likely to result from a superposition of several mechanisms, and hence a more complicated frequency dependence than any single mechanism.

Measurements of Attenuation

White (1965) gave an extensive review of the measurements of attenuation both from the earth material in the laboratory and from the field. The methods of measurement in laboratory fall into three main groups: (1) pulses in rock specimens, which are generally limited to ultrasonic pulses; (2) resonant bar methods, which are generally limited to frequencies less than 30 k hz; and (3) the slow stress torsion pendulum method, which is generally limited to frequencies less than 100 hz (White, 1965).

The measurements of attenuation in the field from an explosive seismic source have been carried out by many authors (Ricker, 1953; McDonal and others, 1958). More recently field measurements of attenuation were carried out by De Bremaecker and others (1966) on lava flows, unconsolidated cinders, and compacted limestone, and by O'Brien (1969) on clay and sandstone.

ATTENUATION, DISPERSION, AND FREQUENCY DEPENDENCE

Dispersion is a necessary consequence of attenuation in the linear theory of wave propagation. Lamb (1962), and Futterman (1962) derived the Kramer-Kronig dispersion relations for attenuation proportional to the square root of frequency. The assumption that the dispersion of seismic body waves may be largely ignored is consistent with their calculations.

Although the dispersion of seismic body waves is quite likely to be undetectable, it is important in the linear theory of waves because the absence of accompanying dispersion implies noncausal seismic propagation. By imposing causality on the attenuation filter, one will get a frequency dependent phase velocity, i.e., dispersion.

The attenuation function α , and the phase velocity v , of a Voigt solid (Ricker, 1953) and of a constant Q solid (Futterman, 1962) are given below:

Voigt Solid

$$\alpha(\omega, x) = \frac{x \omega_0}{V_p} \frac{1}{\sqrt{2}} \left[\frac{\omega_0 (\omega_0^2 + \omega^2)^{\frac{1}{2}} - \omega_0^2}{\omega^2 + \omega_0^2} \right]^{\frac{1}{2}}$$

$$v(\omega, x) = \sqrt{2} V_p \left[\frac{\omega^2 + \omega_0^2}{\omega_0 (\omega_0^2 + \omega^2)^{\frac{1}{2}} + \omega_0^2} \right]^{\frac{1}{2}},$$

for $\omega > 0$

For the limiting case of low frequency range these become

$$\alpha(\omega, x) = \frac{x}{2 V_p \omega_0} \omega^2$$

$$v(\omega) = V_p$$

where $\alpha(\omega, x)$ is the attenuation, $v(\omega)$ is the phase velocity, ω_0 is the transition frequency, and V_p is the wave velocity in a perfectly elastic medium.

Constant Q Solid

$$\alpha(\omega, x) = \frac{x}{2 V_p Q} \omega$$

$$v(\omega, x) = V_p \left[1 - \frac{\ln \left(\gamma \frac{\omega}{\omega_0} \right)}{\pi Q} \right]^{-1}, \text{ for } \omega > 0$$

where $\alpha(\omega, x)$ is the attenuation, $v(\omega, x)$ is the phase

velocity, V_p is the wave velocity in perfectly elastic media, and $\gamma = 0.5772156649\dots$, is Euler's constant.

In the next section of this thesis, these functions will be used to specify the attenuation filters. The methods developed in this thesis will be applicable to other types of attenuation.

LINEAR ATTENUATION FILTER

The models of mechanisms of attenuation proposed by various authors are far from conclusive. Each model fits the observed data well only in a certain range of frequencies. This suggests a phenomenological approach to the study of attenuation of seismic wave forms.

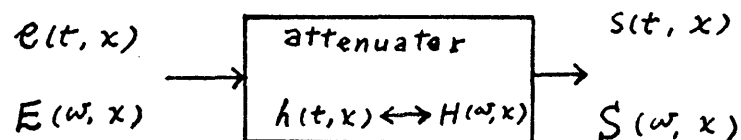
To calculate the attenuated plane seismic wave from an impulse, Carpenter (1966) used a linear attenuation function and Futterman's (1962) phase velocity with the wave equation. Thus the effect of attenuation was incorporated into the solution and was mixed with the propagation effects.

In this thesis it is assumed that the propagation effects and the source characteristics can be separated from the attenuation effects. If this is so then attenuation can be applied to various wave components and sources, such as plane waves, spherical waves in an infinite medium, and the waves in a half-space due to a spherically symmetrical dilatational source.

The linear attenuator is constructed according to the following procedures based upon previously mentioned

assumptions. First, an attenuation function, $\alpha(\omega, x)$, is chosen arbitrarily; then the assumption is made that the system has minimum-phase characteristics. The Paley-Wiener causality condition is checked, and the Hilbert transform is applied to produce the phase response of the attenuation system. Finally, the impulse response is obtained by inverse Fourier transforming the system function.

The linear attenuation filter is defined as shown below:



$$s(t, x) = e(t, x) * h(t, x),$$

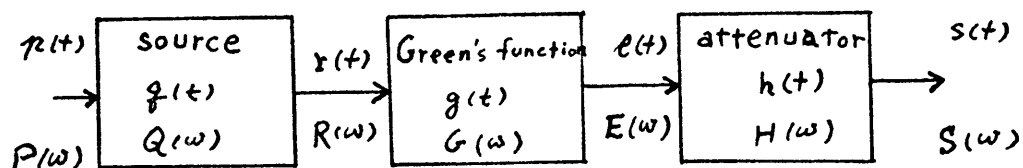
$$S(\omega, x) = E(\omega, x) H(\omega, x),$$

$$H(\omega, x) = e^{-\alpha(\omega, x)} e^{-i\phi(\omega, x)}$$

where $H(\omega, x)$ is the system function of the linear attenuator, $h(t, x)$ is the impulse response of the system, $\alpha(\omega, x)$ is the attenuation, and $\phi(\omega, x)$ is the phase lag of the system.

The input into this system is the unattenuated elastic wave at any point, and the output is the attenuated seismic

wave at the same point. The following diagram shows the whole scheme of the propagation of seismic waves, of which the attenuator is a part:



In the above figure spacial dependence is not shown. Here $p(t)$ is the input to the source, $r(t)$ is the output of the source region, which provides the source characteristics, $e(t)$ is the output of the propagation operator and also the input to the attenuator, and $s(t)$ is the final output--the seismic wave.

Causality

The necessary and sufficient condition, called the Paley-Wiener condition, (Papoulis, 1962) for a square-integrable function $|H(\omega)|$ to be the modulus of the Fourier transform of a causal time function is the convergence of the following integral:

$$\int_{-\infty}^{\infty} \frac{|\ln |H(\omega)| |}{1 + \omega^2} d\omega$$

Some remarks on the Paley-Wiener condition are in order:

- (1). If the amplitude of a function satisfies the Paley-Wiener condition, it does not follow that it has a causal inverse. Rather, it follows that to such a function, a suitable phase can be associated so that the resulting function has a causal inverse. A method of associating the phase is the Hilbert transform, which requires that a minimum phase characteristic be assumed.
- (2). If the function $|H(\omega)|$ is not square-integrable, then the Paley-Wiener condition is neither necessary nor sufficient.

Minimum Phase and the Hilbert Transform

If the function $H(\omega, x)$ is minimum-phase, then the attenuation $\alpha(\omega, x)$, and the phase $\phi(\omega, x)$ of $H(\omega, x)$;

$H(\omega, x) = e^{-d(\omega, x)} e^{-i\phi(\omega, x)}$ are related by the Hilbert transform (Papoulis, 1962):

$$\phi(\Omega, x) = \frac{\Omega}{\pi} \mathcal{P} \left\{ \int_{-\infty}^{\infty} \frac{d(\omega, x)}{\omega^2 - \Omega^2} d\omega \right\}$$

Here $\mathcal{P} \left\{ \right\}$ represents the Cauchy principal value. Thus the phase $\phi(\omega, x)$ can be uniquely determined from the attenuation $d(\omega, x)$.

The System Function

After the attenuation function has been chosen and the phase response is obtained through the Hilbert transform, the system function is known. With the system function, the linear attenuation filter is defined.

IMPULSE RESPONSES OF VOIGT AND CONSTANT Q SOLIDS

The impulse response, which characterizes the system in the time domain, is obtained by inverse Fourier transforming the system function. In this section, two models of attenuation are studied: The low-frequency approximation of the Voigt solid and the constant Q solid. The Paley-Wiener condition is checked, the phase response is obtained, and the impulse response is computed for these two models.

Voigt Solid

The Voigt solid is one of the models of viscoelasticity. The stress of the Voigt solid is proportional to the strain and the strain rate. Hence, the wave equation for compressional waves in the Voigt solid is

$$\nabla^2 \left(\Phi + \frac{1}{\omega_0} \frac{\partial}{\partial t} \Phi \right) = \frac{1}{V_p^2} \frac{\partial^2 \Phi}{\partial t^2}$$

where Φ is the displacement potential and ω_0 , a property of the solid, is called the transition frequency

(Ricker, 1953). Ricker has solved the plane wave equation and obtained the attenuation as follows:

$$d(\omega, x) = \frac{\omega x}{\sqrt{2} V_p} \left[\frac{\omega_0 (\omega_0^2 + \omega^2)^{\frac{1}{2}} - \omega_0^2}{\omega_0^2 + \omega^2} \right]^{\frac{1}{2}}$$

where ω_0 is estimated by Ricker as $2\pi(280)$ for shale, and V_p is the velocity of the wave in perfectly elastic medium.

In a low frequency range, say $\frac{\omega}{\omega_0} < 0.25$, the attenuation $d(\omega, x)$ has the familiar second-power frequency dependence:

$$d(\omega, x) = \frac{x}{2 V_p \omega_0} \omega^2$$

The Paley-Wiener condition requires that there be a high end cut-off frequency. Since the integral

$$\int_{-\infty}^{\infty} \frac{|\ln |H(\omega)| |}{1 + \omega^2} d\omega$$

does not converge, the Paley-Wiener condition requires

that there be a high end cut-off frequency ω_c .

So the attenuation of the low frequency range Voigt solid is specified as follows:

$$d(\omega, \alpha) = \begin{cases} \frac{\alpha}{2 V_p \omega_0} \omega^2 & , \text{ for } \omega < \omega_c \\ 0 & , \text{ for } \omega \geq \omega_c \end{cases}$$

The phase response for the low frequency range of the Voigt solid is obtained from the Hilbert transform as follows:

$$\begin{aligned} \phi(\Omega) &= \frac{\Omega}{\pi} P \left\{ \int_{-\infty}^{\infty} \frac{d(\omega, \alpha)}{\omega^2 - \Omega^2} d\omega \right\} \\ \phi(\omega) &= \frac{2\omega}{\pi} P \left\{ \int_0^{\omega_c} \frac{\frac{\alpha \eta^2}{2 V_p \omega_0}}{\eta^2 - \omega} d\eta \right\} \\ &= \frac{\alpha \omega_c}{\pi V_p \omega_0} \omega + \frac{\alpha}{2\pi V_p \omega_0} \omega^2 \ln \left| \frac{\omega_c - \omega}{\omega_c + \omega} \right| \end{aligned}$$

With $d(\omega, \alpha)$, and $\phi(\omega, \alpha)$ so defined, the impulse

response for the attenuation filter is found as follows:

$$h(t, x) = \frac{1}{2\pi} \int_{-\infty}^{\infty} e^{-\frac{x \omega^2}{2v_p \omega_0}} \cos[\omega t - \phi(x, \omega)] d\omega$$

This integration is carried out numerically after $H(\omega, x)$ and $\phi(\omega, x)$ are expanded in Maclaurin's series.

$$h(t, x) \cong \frac{1}{\pi} \sum_{n=1}^N \int_{\omega_n}^{\omega_{n+1}} (A_n + \beta_n \omega) \cos[(t - \gamma_n)\omega - \phi_n] d\omega$$

case 1

For $t \neq \gamma_n$

$$h(t, x) = \frac{1}{\pi} \sum_{n=1}^N \left\{ A_n \frac{1}{t - \gamma_n} \sin((t - \gamma_n)\omega - \phi_n) + \beta_n \left[\frac{1}{(t - \gamma_n)^2} \cos((t - \gamma_n)\omega - \phi_n) + \frac{\omega}{t - \gamma_n} \sin((t - \gamma_n)\omega - \phi_n) \right] \right\} \Bigg|_{\omega_n}^{\omega_{n+1}}$$

case 2

For $t = \gamma_n$

$$h(t, x) = \frac{1}{\pi} \sum_{n=1}^N \left\{ A_n [(\omega_{n+1} - \omega_n) \cos \phi_n] + \beta_n \frac{\omega_{n+1}^2 - \omega_n^2}{2} \cos \phi_n \right\}$$

where

$$A_n = e^{-\frac{x \omega_n^2}{2 V_p \omega_0}}$$

$$\beta_n = \frac{A_{n+1} - A_n}{\omega_{n+1} - \omega_n}$$

$$\phi_n = \frac{x \omega_c \omega_n}{\pi V_p \omega_0} + \frac{x \omega_n^2}{2 \pi V_p \omega_0} \ln \left| \frac{\omega_c - \omega_n}{\omega_c + \omega_n} \right|$$

$$\gamma_n = \frac{\phi_{n+1} - \phi_n}{\omega_{n+1} - \omega_n}$$

Figure 15 shows some results of this computation. Each trace is normalized. The horizontal line associated with each trace represents the zero amplitude for that trace.

Figure 16 gives a plot comparing the plane Voigt wave and the plane low-frequency-approximated Voigt wave. The solid line represents the plane Voigt wave from Collins (1960), and Balch and Smolka (1970), and the broken line, the low-frequency-approximated plane Voigt wave computed by means of the algorithms based on the above formulation. The difference observed is explained by the fact that

the operator of this thesis transmits more of the high frequencies.

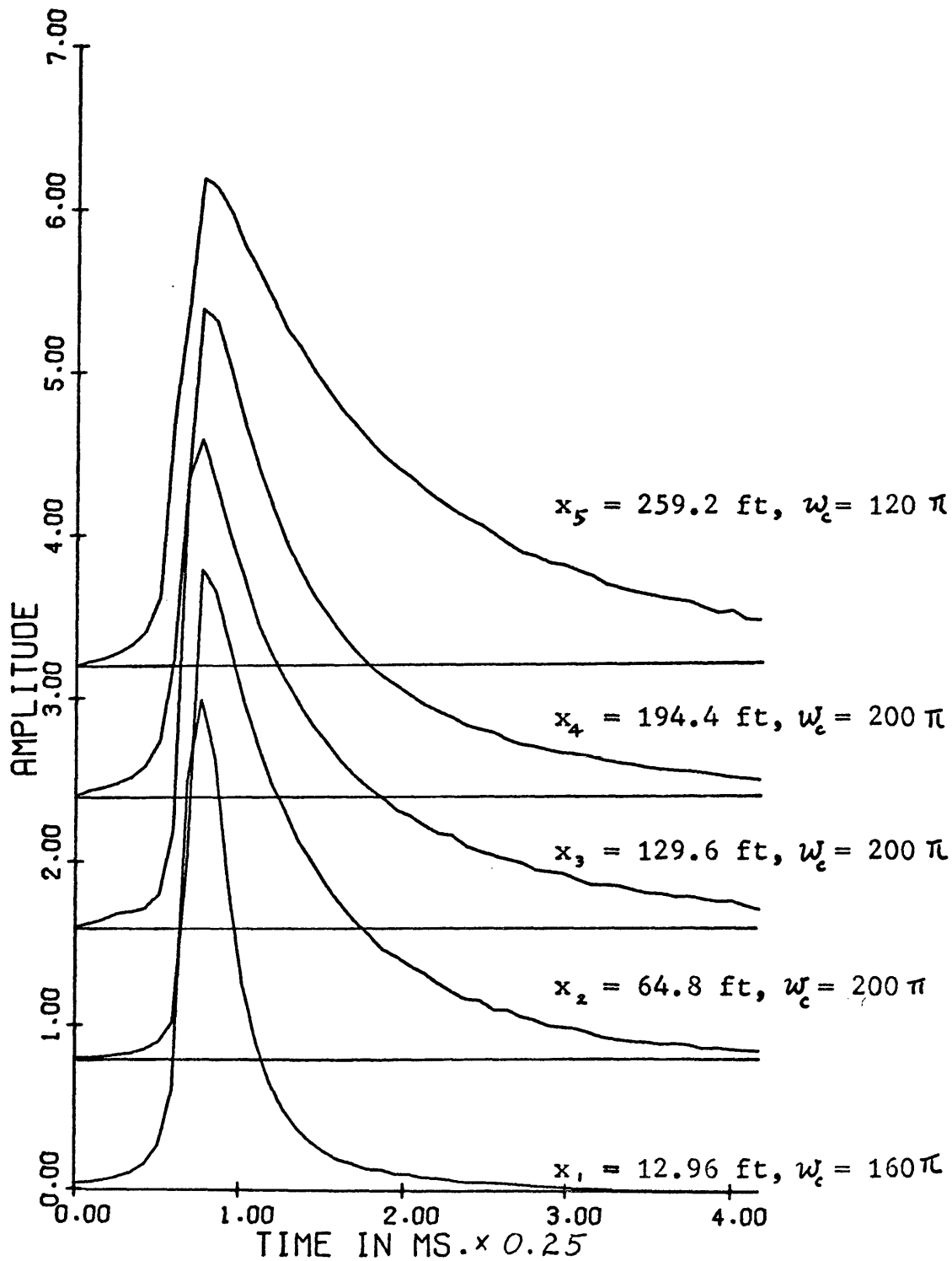


Figure 15. Impulse responses of attenuators of low-frequency-approximated Voigt solid at 5 locations. $V_p = 5700$ ft/sec, $\omega_0 = 560 \pi$ rad/sec, and ω_c are as shown.

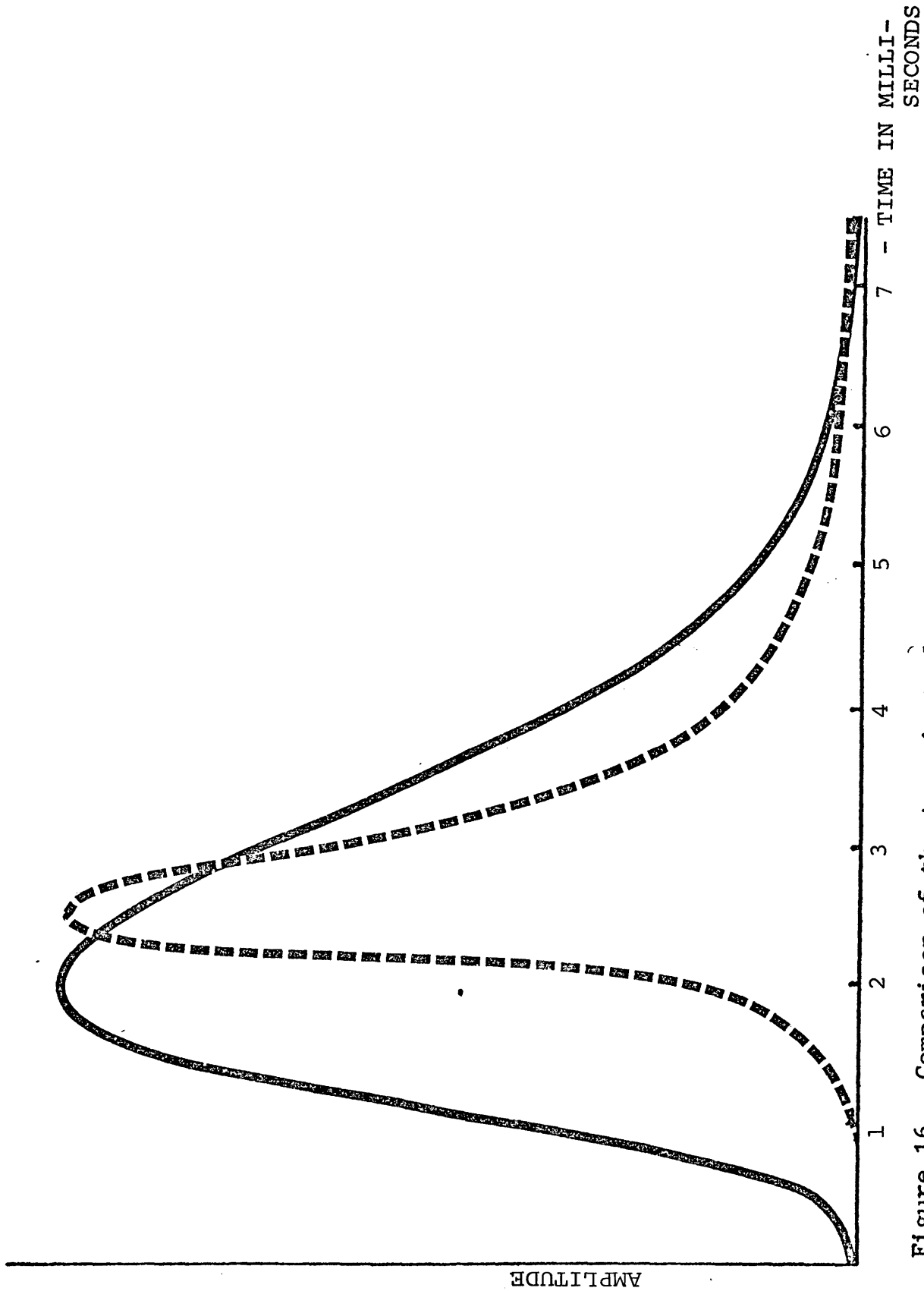


Figure 16. Comparison of the transient plane Voigt waves. The solid line is from Collins (1960), and Balch and Smolka (1970); and the broken line is the low-frequency-approximated Voigt model. Parameters for broken line are: $\omega_f = 5700$ ft/sec, $\omega_c = 560 \pi$ rad/sec, $\omega_c = 160 \pi$, and $x = 12.96$ ft.

Constant Q Solid

The constant Q model yields attenuation proportional to the first power of frequency.

The constant Q solid is causal if its attenuation is defined as follows:

$$d(\omega, x) = \begin{cases} \frac{x}{2V_p Q} |\omega| & , \text{ for } |\omega| < \omega_c \\ 0 & , \text{ for } |\omega| \geq \omega_c \end{cases}$$

where ω_c is the high cut-off frequency. The integral of the Paley-Wiener condition is convergent, for

$$\begin{aligned} I &= 2 \int_0^{\omega_c} \frac{x|\omega| / (2V_p Q)}{1 + \omega^2} d\omega \\ &= \frac{x}{2V_p Q} \ln(1 + \omega_c^2) < \infty \end{aligned}$$

The phase response for the constant Q solid is obtained from the Hilbert transform as follows:

$$\phi(\omega, x) = \frac{\omega}{\pi} \frac{x}{2V_p Q} \ln \left| \frac{\omega_c^2}{\omega^2} - 1 \right|$$

With $\alpha(\omega, x)$, and $\phi(\omega, x)$ so defined, the impulse response for the attenuation filter is:

$$h(x, t) = \frac{1}{\pi} \int_0^{\infty} e^{-\frac{\omega x}{V_p Q}} \cos \left[\omega t + \frac{\ln \left| \frac{\omega_c^2}{\omega^2} - 1 \right|}{2\pi V_p Q} \right] d\omega$$

This integration is numerically carried out as before according to

$$h(x, t) \cong \frac{1}{\pi} \sum_{n=1}^N \int_{\omega_n}^{\omega_{n+1}} (A_n + \beta_n \omega) \cos[(t - \gamma_n)\omega - \phi_n] d\omega$$

case 1 For $t \neq \gamma_n$

$$h(x, t) = \frac{1}{\pi} \sum_{n=1}^N \left\{ A_n \frac{1}{t - \gamma_n} \sin((t - \gamma_n)\omega - \phi_n) \right. \\ \left. + \beta_n \left[\frac{1}{(t - \gamma_n)^2} \cos((t - \gamma_n)\omega - \phi_n) \right. \right. \\ \left. \left. + \frac{\omega}{t - \gamma_n} \sin((t - \gamma_n)\omega - \phi_n) \right] \right\} \Bigg|_{\omega_n}^{\omega_{n+1}}$$

case 2 For $t = Y_n$

$$h(x, t) = \frac{1}{\pi} \sum_{n=1}^N \left\{ A_n (\omega_{n+1} - \omega_n) \cos \phi_n + \beta_n \frac{\omega_{n+1}^2 - \omega_n^2}{2} \cos \phi_n \right\}$$

where

$$A_n = e^{-\frac{x \omega_n}{v_p Q}}$$

$$\beta_n = \frac{A_{n+1} - A_n}{\omega_{n+1} - \omega_n}$$

$$Y_n = \frac{\phi_{n+1} - \phi_n}{\omega_{n+1} - \omega_n}$$

$$\phi_n = \frac{\omega_n}{\pi} \frac{x}{2 \pi Q} \ln \left| \frac{\omega_c^2}{\omega_n^2} - 1 \right|$$

Figure 17 shows some results of this computation. Each trace is normalized in this plot. The horizontal line associated with each trace represents the zero amplitude for that trace.

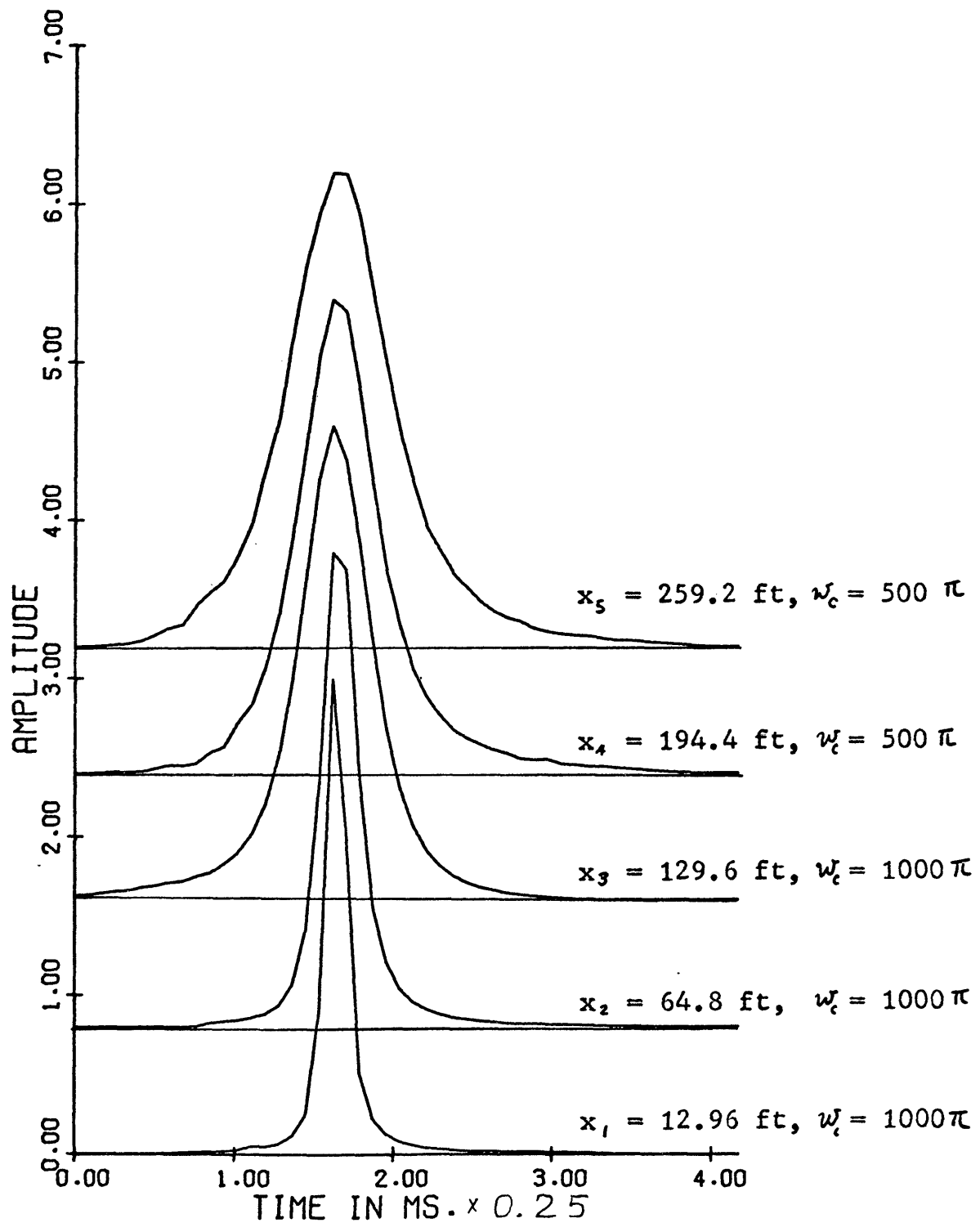


Figure 17. Impulse responses of attenuators of constant Q solid at 5 locations. $V_p = 5700$ ft/sec, $Q = 20$, and ω_c are as shown.

SEISMIC WAVES

PLANE COMPRESSIONAL SEISMIC WAVES

IN AN INFINITE MEDIUM

The displacement of plane compressional seismic waves for a doublet pressure source has the same form as the impulse response of the attenuator, because the input to the attenuator, the elastic wave, is a spike. The plane compressional seismic wave for a pressure spike has the wave form of the impulse response of the attenuator integrated, because the input to the attenuator, the elastic wave, is a unit step.

SPHERICAL COMPRESSIONAL SEISMIC WAVES
IN AN INFINITE MEDIUM

The spherical compressional elastic waves were calculated using the computer program library of the Department of Geophysics. The following figures show the seismic wave forms at various distances for the two attenuation models studied.

Figure 18 and 19 are collections of the seismic waves in an infinite medium for the low-frequency-approximated Voigt and the constant Q model. The 5 traces from bottom of the plot toward the top corresponds to the attenuated seismic wave from near field traveling outward. Each trace is normalized, and the horizontal line associated with each trace represents the zero amplitude for that trace.

In Figure 18, the effect of truncating the impulse response of the attenuator is observed. This effect demonstrates itself most conspicuously in the top trace. This is because the operator corresponding to that location has a very long tail end. Because the farther the location

is, the longer the tail end of the impulse response of the attenuator lasts, it is expected that the truncation effect will be more conspicuous in the traces corresponding to longer propagation paths. The truncation effect does not appear in Figure 19 because the impulse responses of the attenuators generating these traces are not severely truncated.

It is interesting to compare Figures 18 and 19. Note that the seismic waves of both models broaden during propagation. Note also that the absolute values of the amplitudes of the peak and trough approach equality as the wave propagates through the constant Q medium. It is observed that the constant Q model yields a slower rate of broadening than low-frequency-approximated Voigt model.

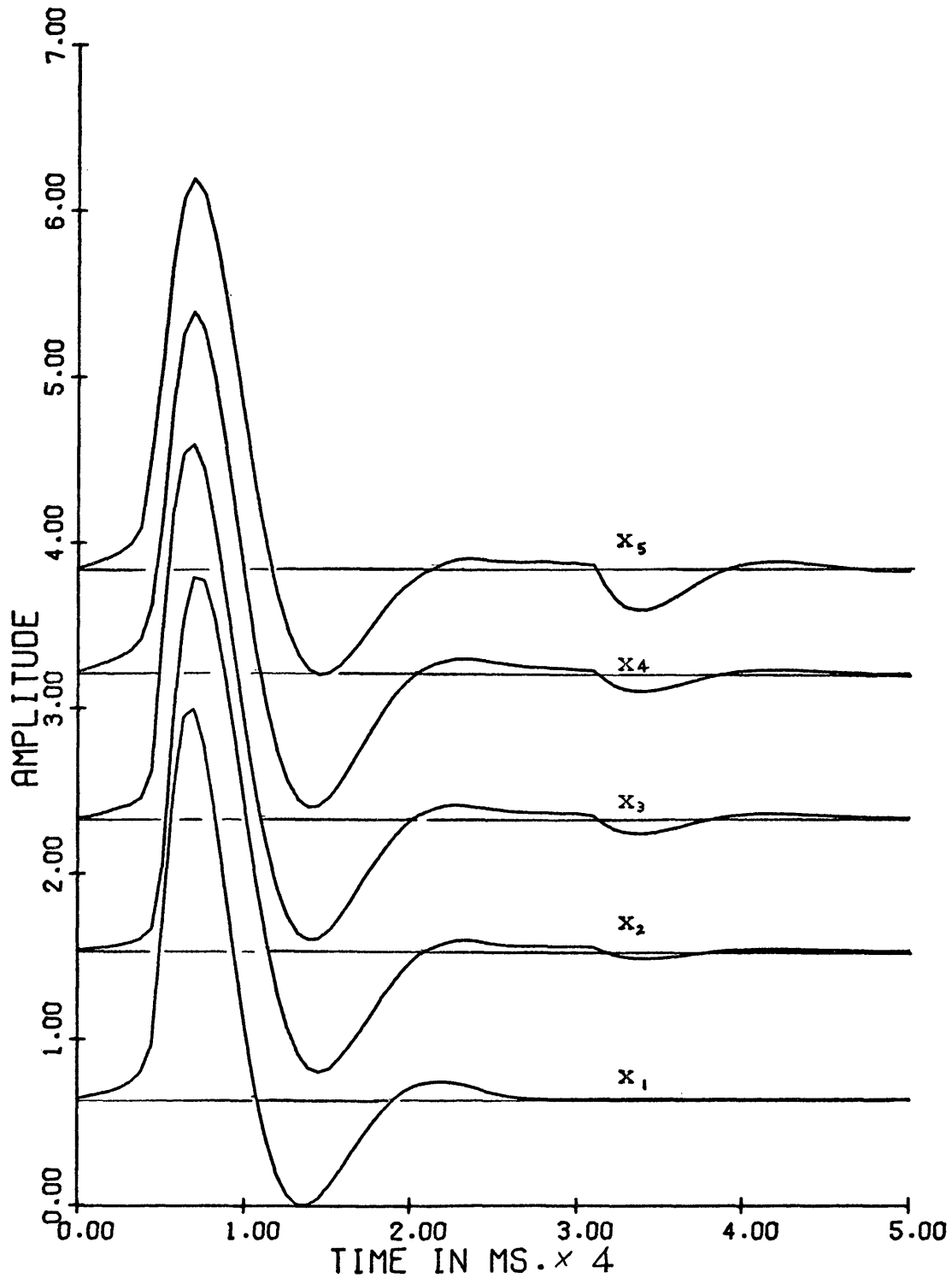


Figure 18. Spherical compressional seismic waves in an infinite low-frequency-approximated Voigt solid: radial displacement at 5 locations from an impulsive pressure. $\sqrt{\rho} = 5700$ ft/sec, $\omega_0 = 560 \pi$ rad/sec, and x'_i are as shown.

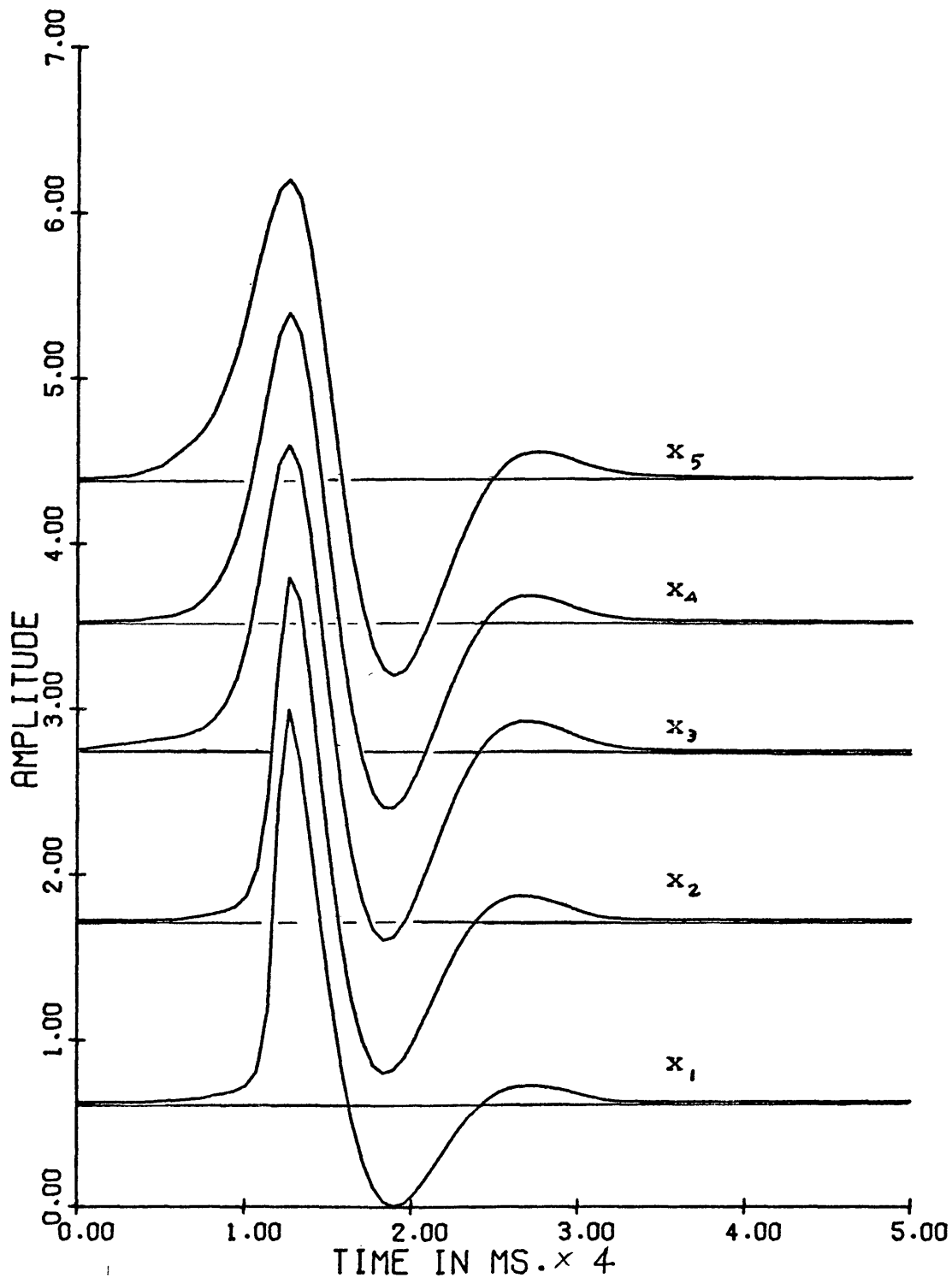


Figure 19. Spherical compressional seismic waves in an infinite constant Q solid: radial displacement at 5 locations from an impulsive pressure. $V_p = 5700$ ft/sec, $Q = 20$, and χ 's are as shown.

SPHERICAL COMPRESSIONAL SEISMIC WAVES
IN A HALF-SPACE

The spherical seismic wave forms are obtained by convolving the elastic wave forms with the impulse responses of the attenuators corresponding to the length of the classical ray path. The seismic wave forms for the two models investigated in this thesis are shown in figure 20 through 39. Figure 20 through 29 are for the low-frequency-approximated Voigt model, and figure 30 through 39 for the constant Q model.

The sequence of layout of these plots for seismic wave forms in figure 20 through 29, and for 30 through 39 follows that for the elastic wave forms in figure 5 through 14. The sequence is as follows: (1) Rayleigh waves, (2) second surface waves, (3) total surface waves, (4) body waves, and (5) total vertical component of displacement. Each trace in figure 20 through 24, and in figure 30 through 34 is normalized. The traces in figure 25 through 30, and in figure 35 through 39 are scaled to show the relative amplitude of the

components to the amplitude of the total vertical displacement. These schemes again follow those in the chapter of elastic wave forms. The normalized plots are intended to show the changes of wave forms of each component at various locations. The scaled relative amplitude plots are intended to present, at a glance, the relative contribution of each component to the total at various locations.

It is observed that both models have the effect of broadening and smoothing the elastic wave forms. This is most conspicuously seen in the body waves where there are sharp, "brick-wall" arrivals in elastic wave forms (see Figure 8). It is also noted that the approximated Voigt model tends to merge the PP- and PS-waves slightly more than the constant Q model. (see Figures 8, 23, and 33). The same attenuator is used with body waves and both types of surface waves. Thus the following assumptions are implied:

1. The medium has same effect of attenuation on compressional waves, shear waves, Rayleigh waves, and second surface waves.

2. The differences in path lengths of the PP-wave, PS-wave, surface waves, and the direct wave are neglected.

These assumptions were made because it takes more than 10 times more computer central processing time to compute an operator than it does to compute the elastic waves at a location. The approximated Fourier transform (Sato, 1955) is used to compute the operator. To eliminate these two assumptions one should specify different transition frequencies, ω_0 , and Q for each wave component (Press and Healy, 1957).

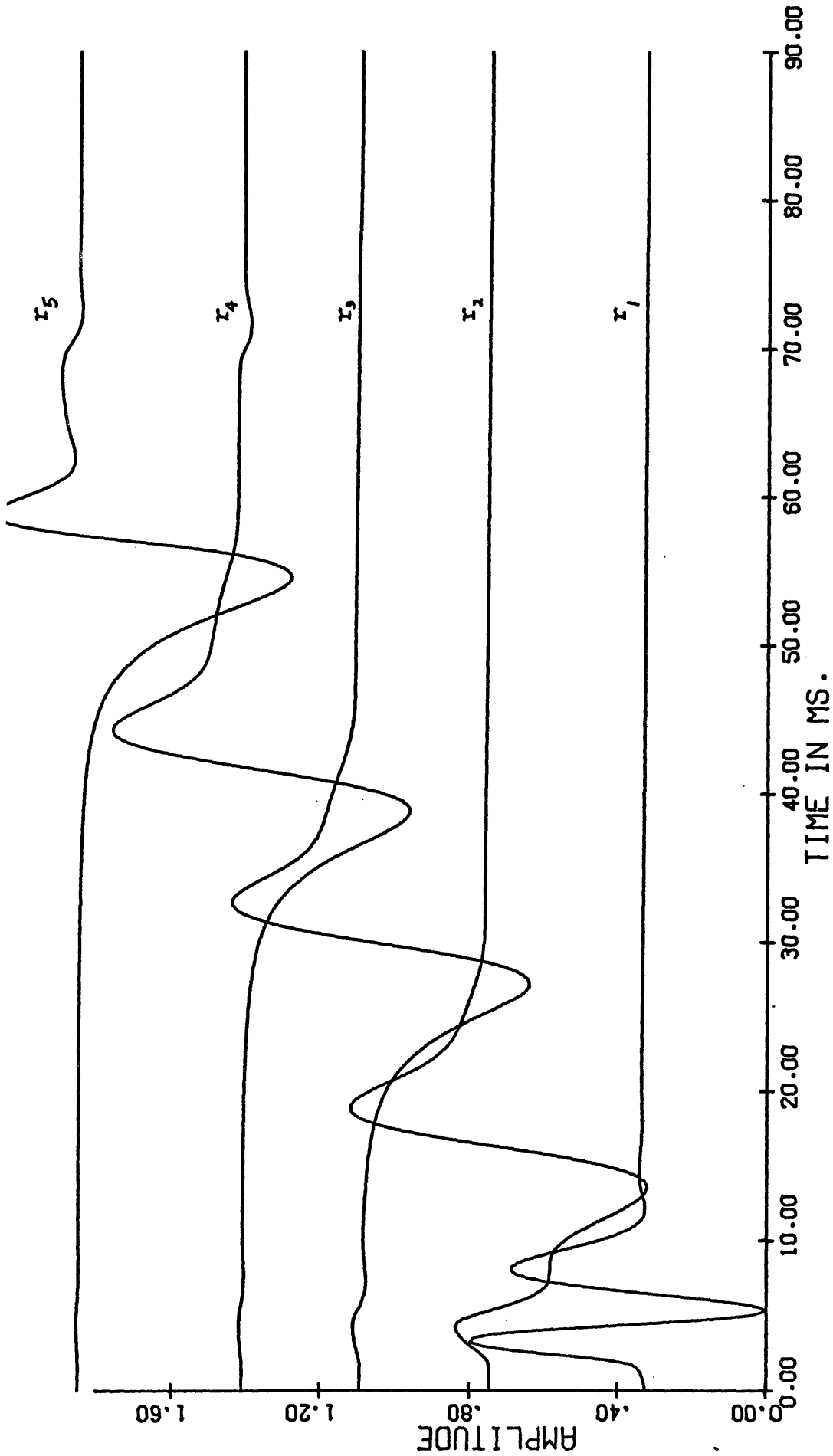


Figure 20. Spherical seismic waves in a low-frequency-approximated Voigt half-space--- the vertical component of displacement: Rayleigh waves at 5 locations after PP arrival time.

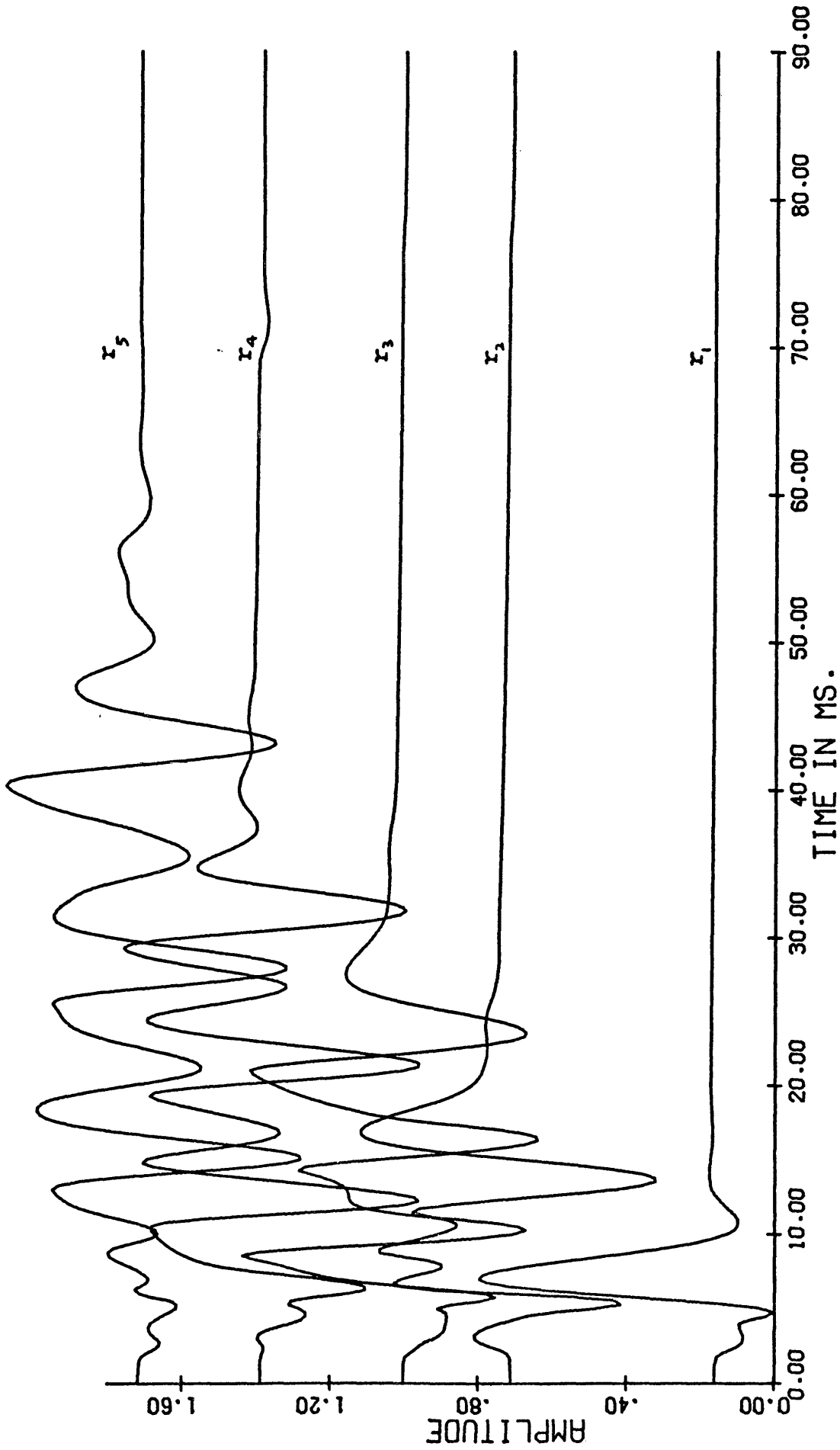


Figure 21. Spherical seismic waves in a low-frequency approximated Voigt half-space--- the vertical component of displacement: Second surface waves at 5 locations after PP arrival time.

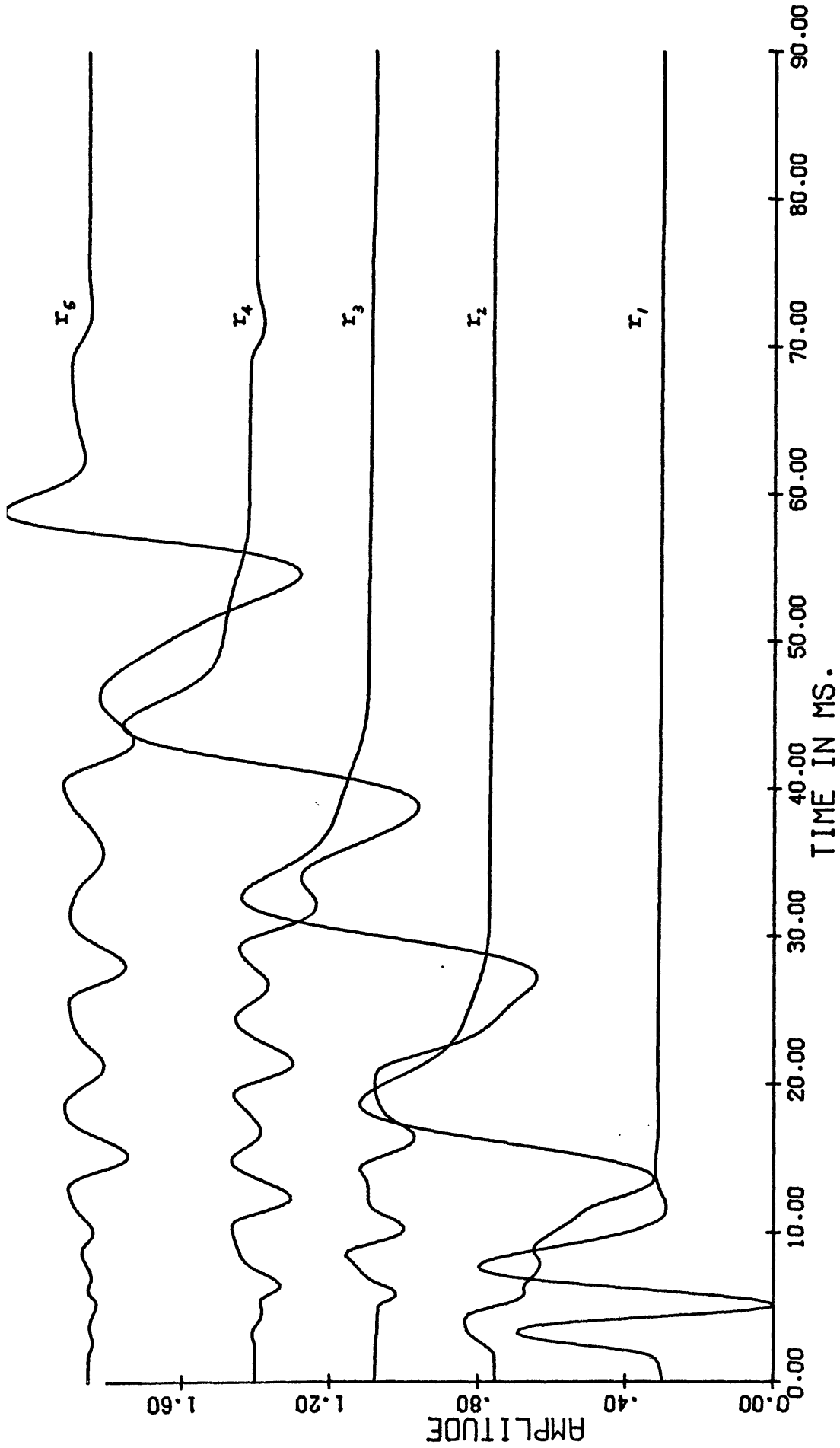


Figure 22. Spherical seismic waves in a low-frequency-approximated Vogit half-space--- the vertical component of displacement: Total surface waves at 5 location after PP arrival time.

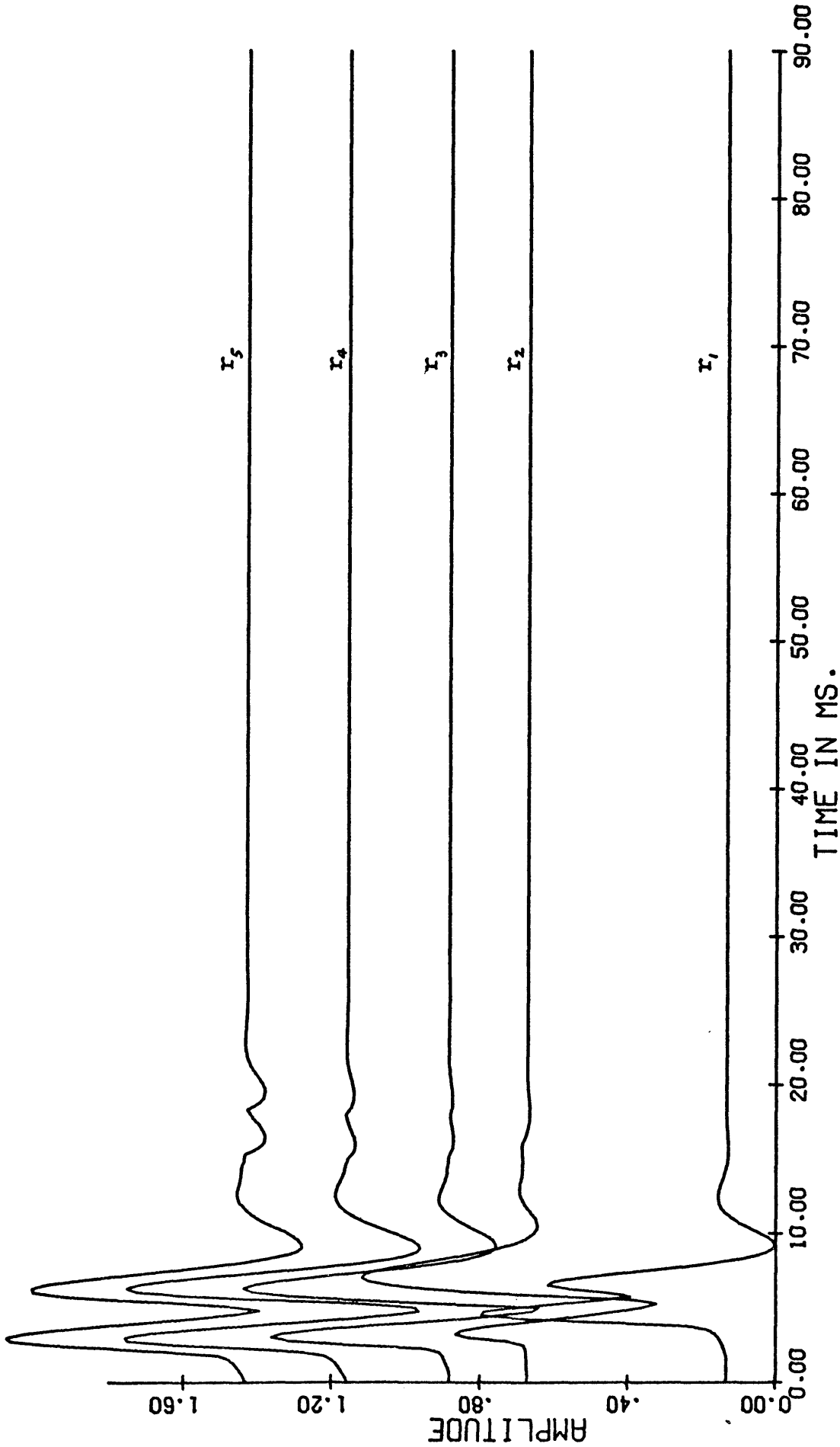


Figure 23. Spherical seismic waves in a low-frequency-approximated Voigt half-space-- the vertical component of displacement: Reflected body waves at 5 locations after direct wave arrival time.

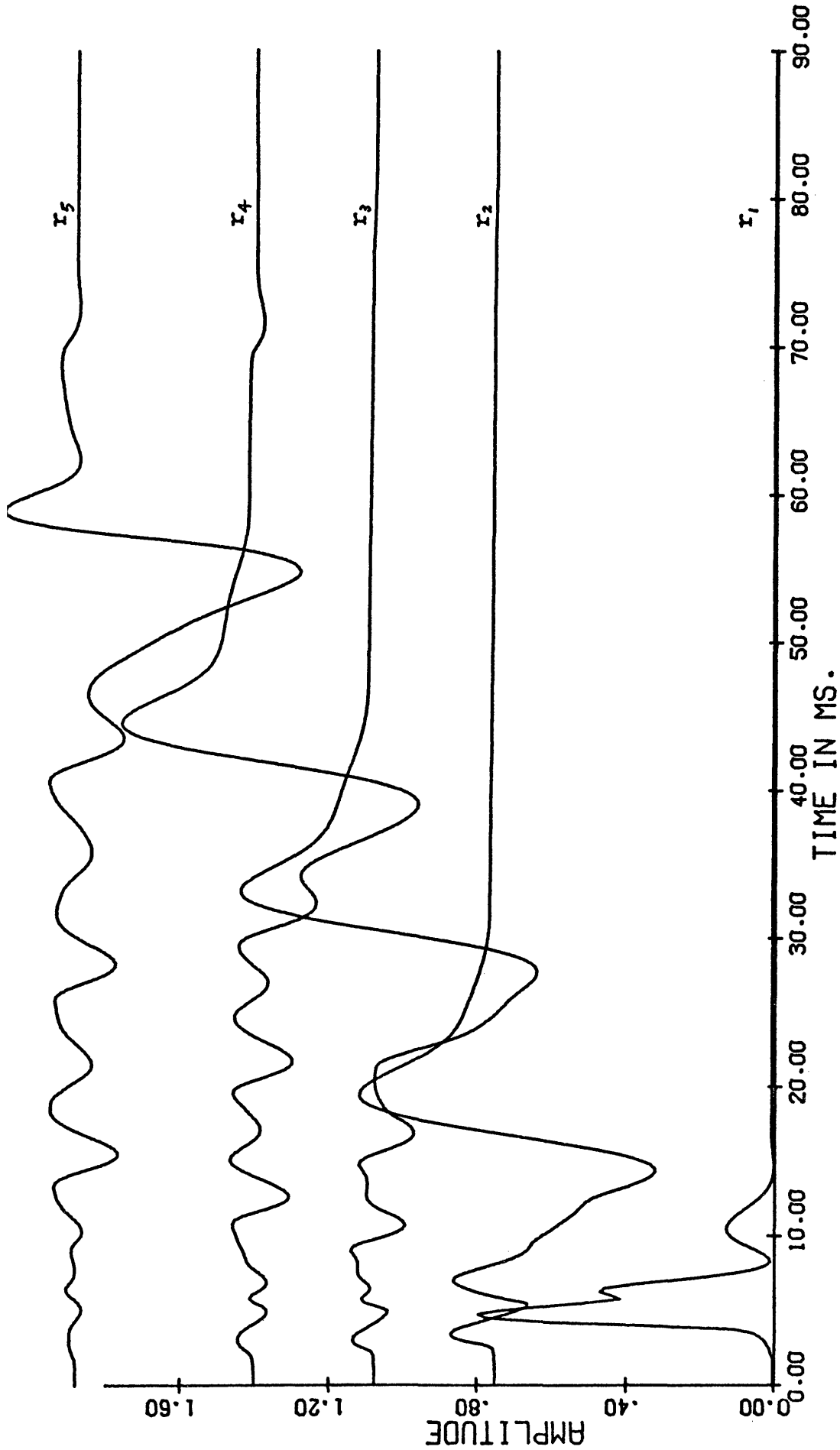


Figure 24. Spherical seismic waves in a low-frequency-approximated Voigt half-space--- the vertical component of displacement: Total seismic waves at 5 locations after direct wave arrival time.

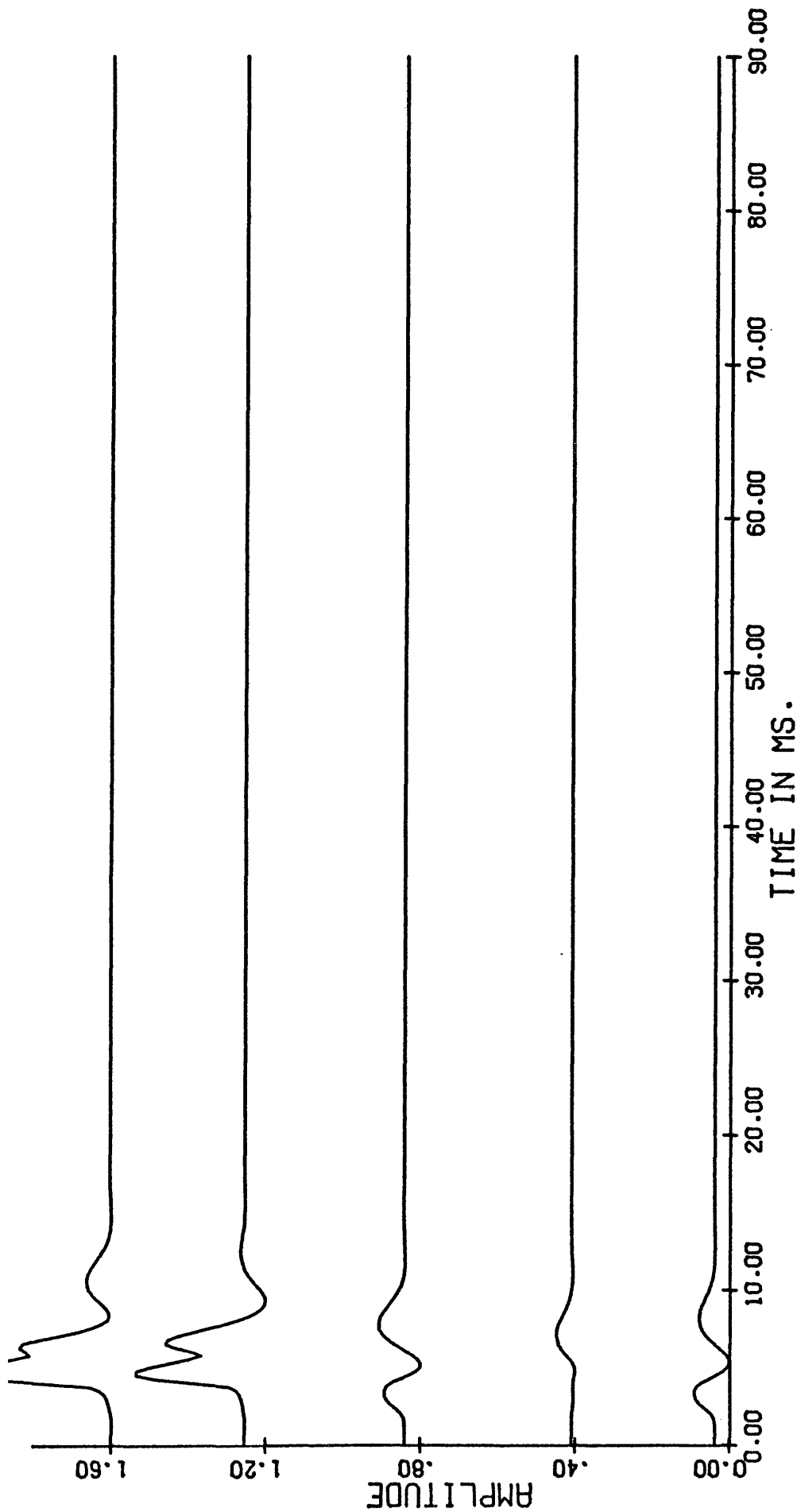


Figure 25. Spherical seismic waves in a low-frequency-approximated Voigt half-space decomposed at location 1. These traces are scaled to their relative amplitude with respect to the total vertical displacement, which is normalized. The arrangement of traces is the same as that of figure 10.

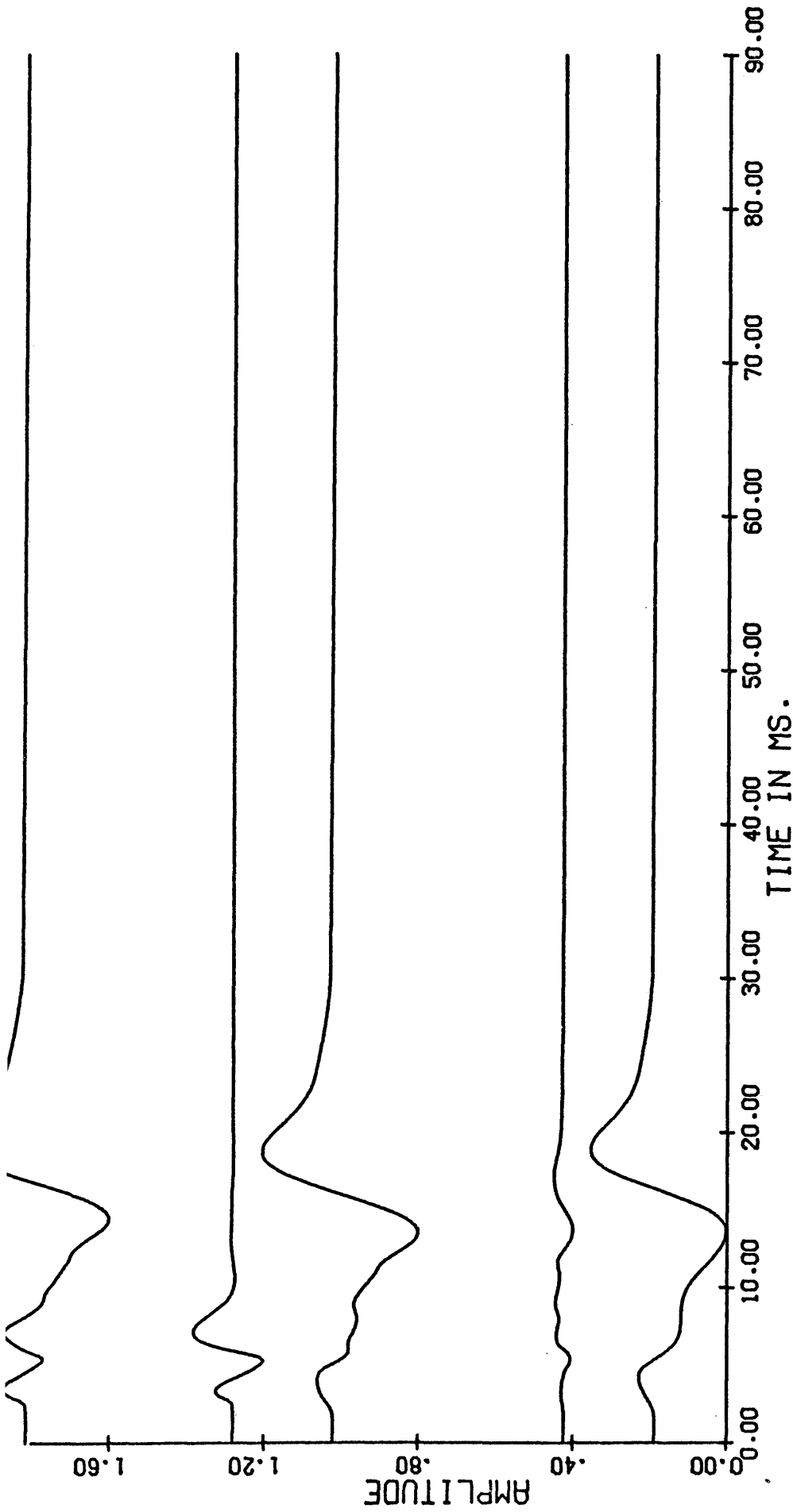


Figure 26. Spherical seismic waves in a low-frequency-approximated Voigt half-space decomposed at location 2. These traces are scaled to their relative amplitude with respect to the total vertical displacement, which is normalized. The arrangement of traces is the same as that of figure 10.

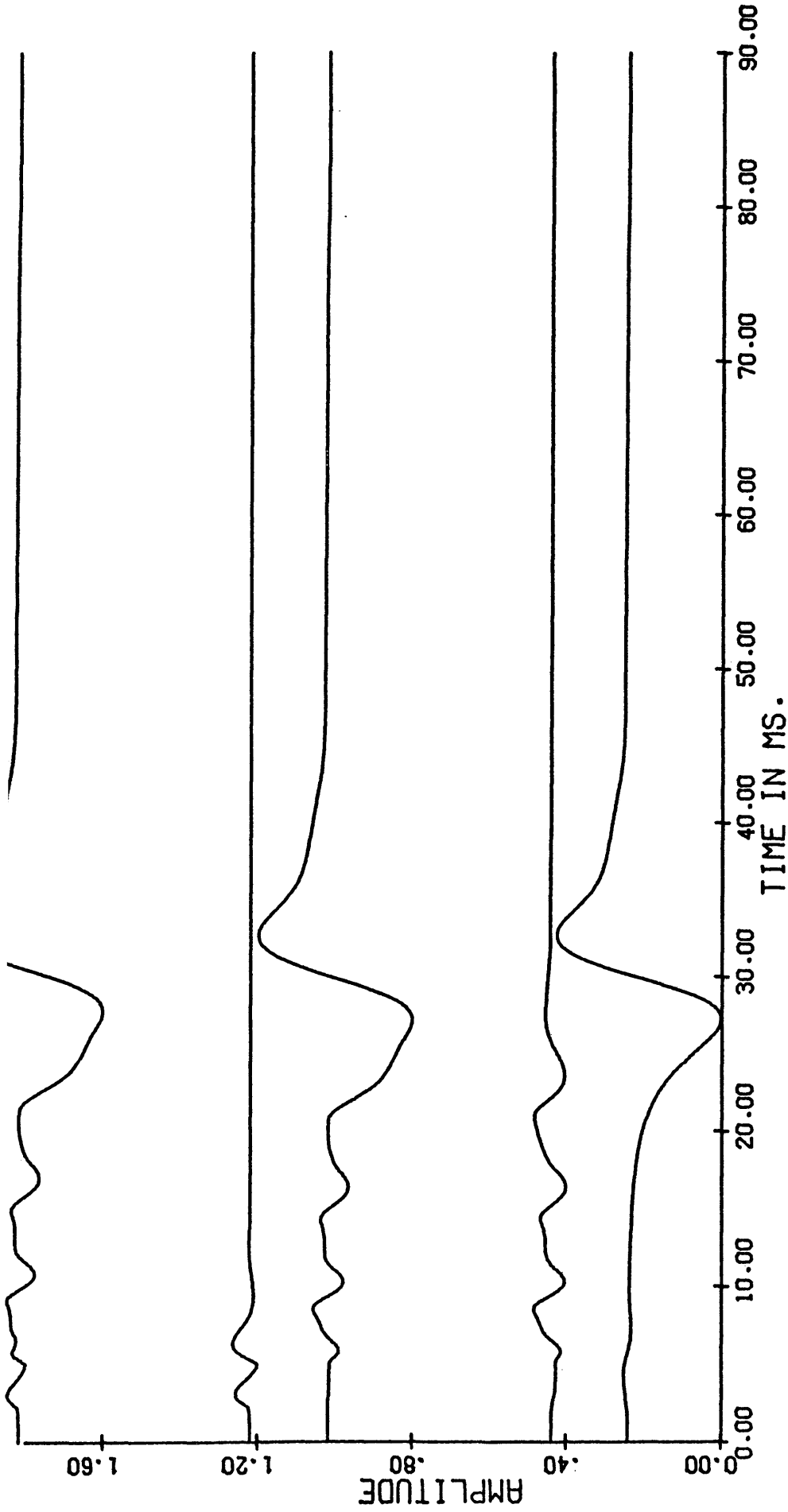


Figure 27. Spherical seismic waves in a low-frequency-approximated Voigt half-space decomposed at location 3. These traces are scaled to their relative amplitude with respect to the total vertical displacement, which is normalized. The arrangement of traces is the same as that of figure 10.

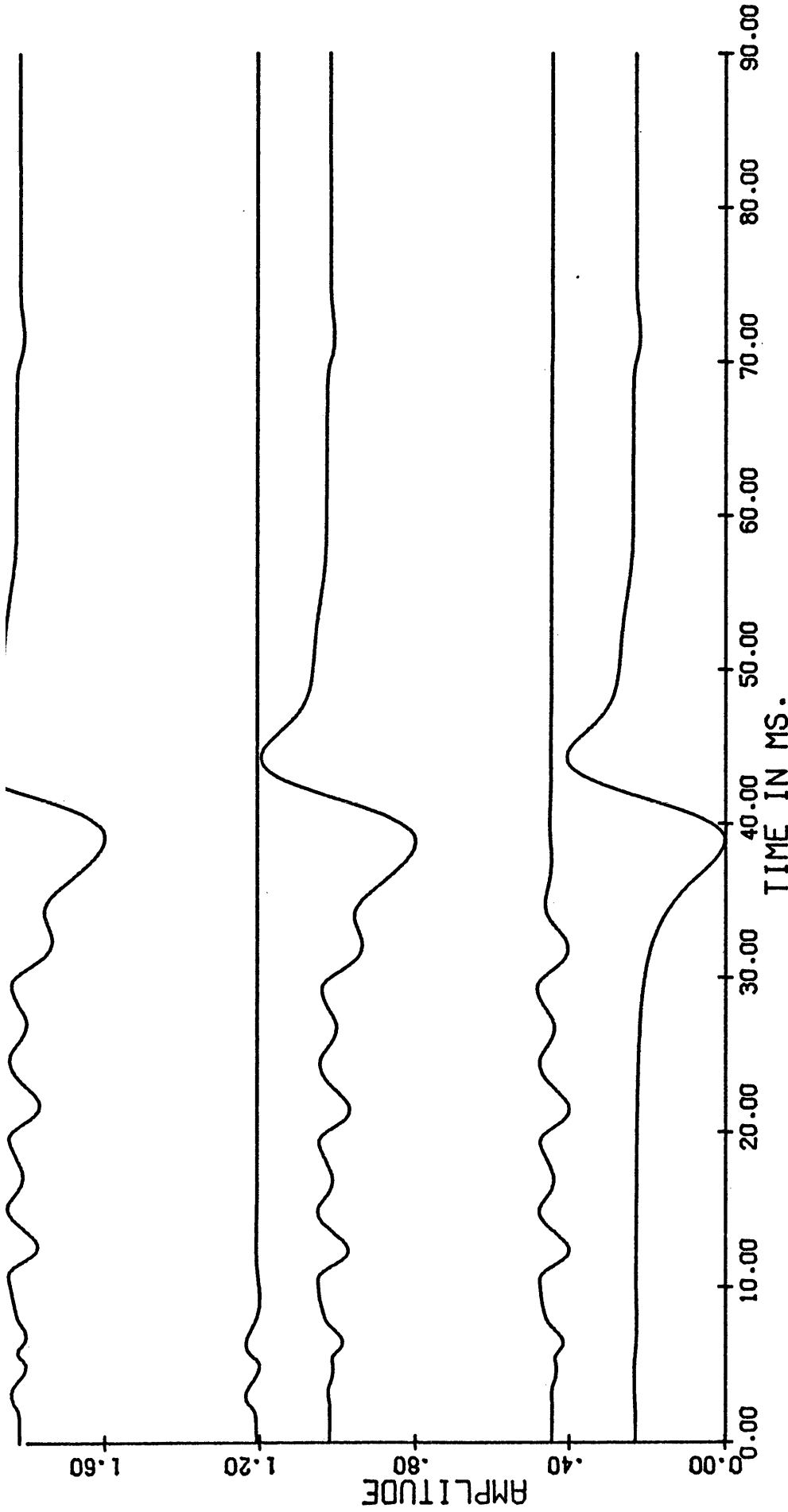


Figure 28. Spherical seismic waves in a low-frequency-approximated Voigt half-space decomposed at location 4. These traces are scaled to their relative amplitude with respect to the total vertical displacement, which is normalized. The arrangement of traces is the same as that of figure 10.

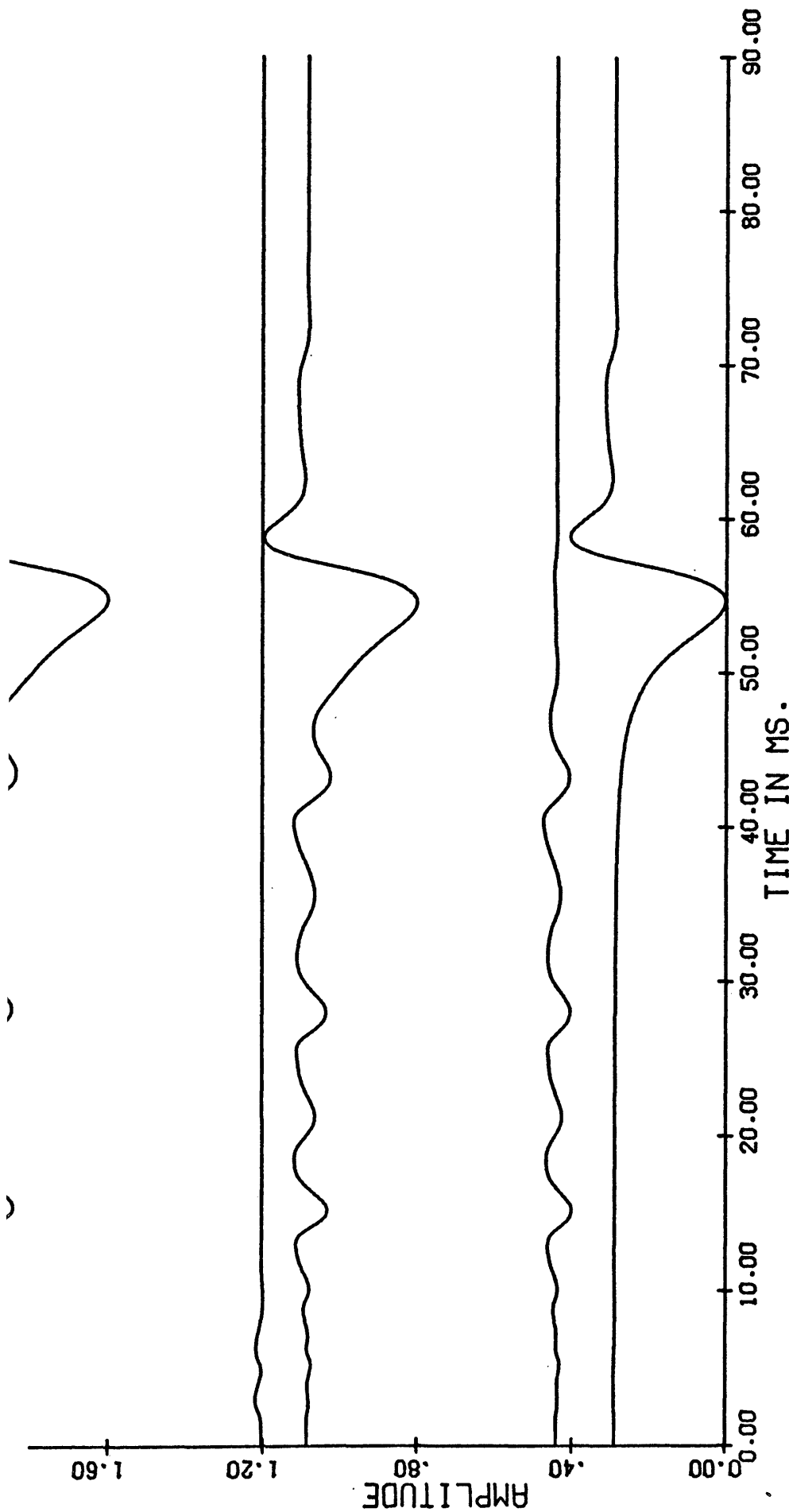


Figure 29. Spherical seismic waves in a low-frequency-approximated Voigt half-space decomposed at location 5. These traces are scaled to their relative amplitude with respect to the total vertical displacement, which is normalized. The arrangement of traces is the same as that of figure 10.

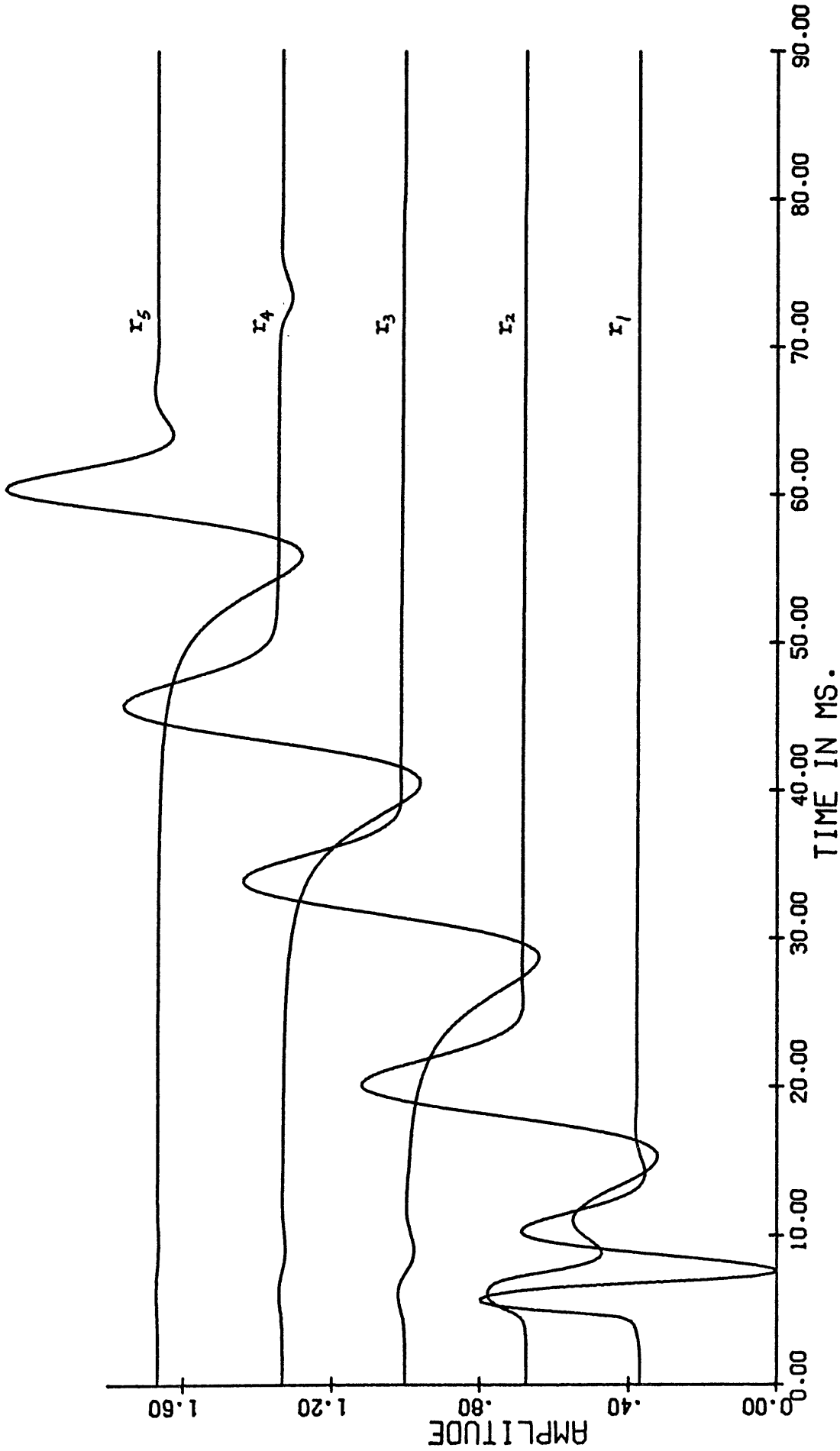


Figure 30. Spherical seismic waves in a constant Q half-space--the vertical component of displacement: Rayleigh waves at 5 locations after PP arrival time.

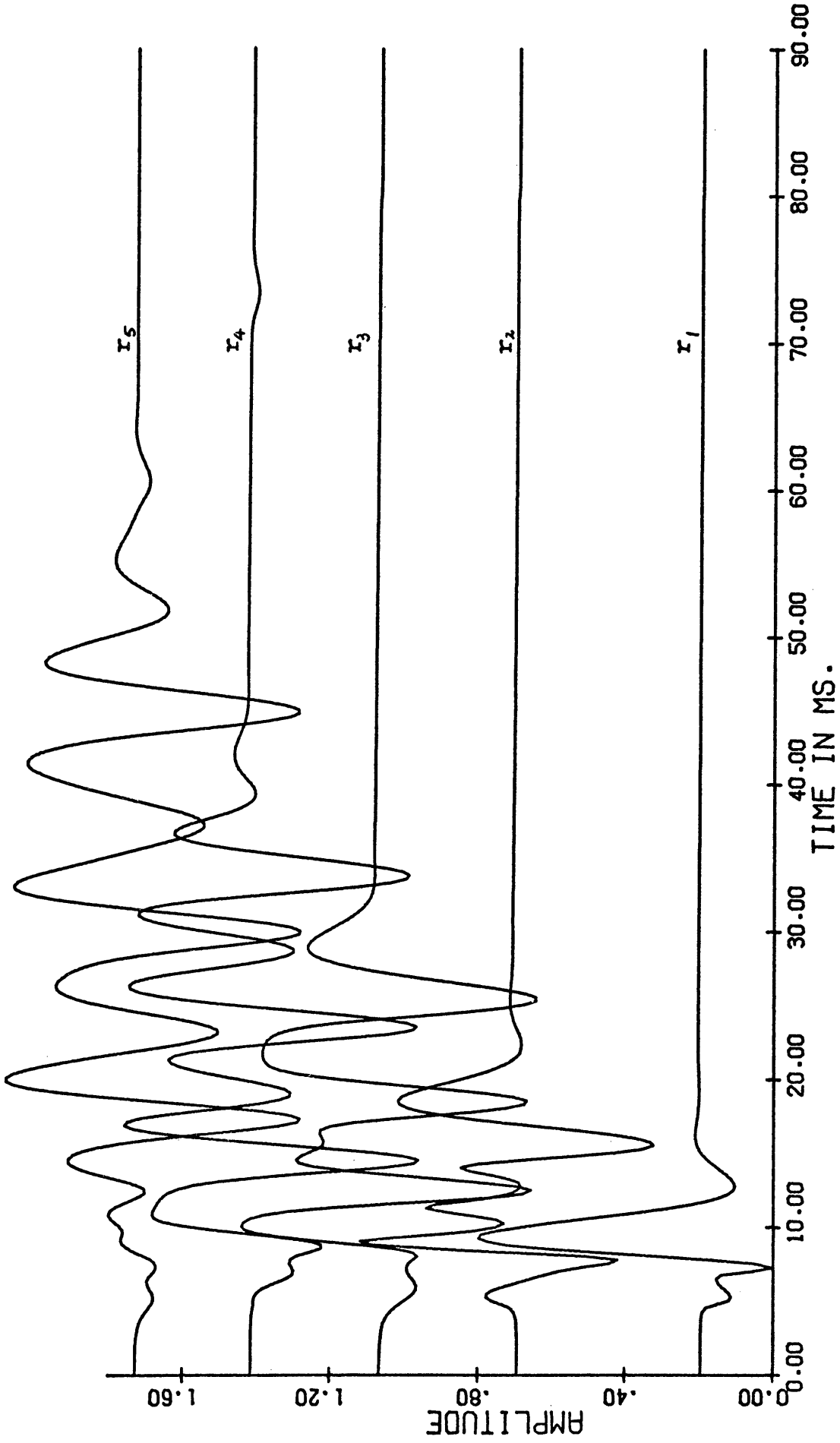


Figure 31. Spherical seismic waves in a constant Q half-space--the vertical component of displacement: Second surface waves at 5 locations after PP arrival time.

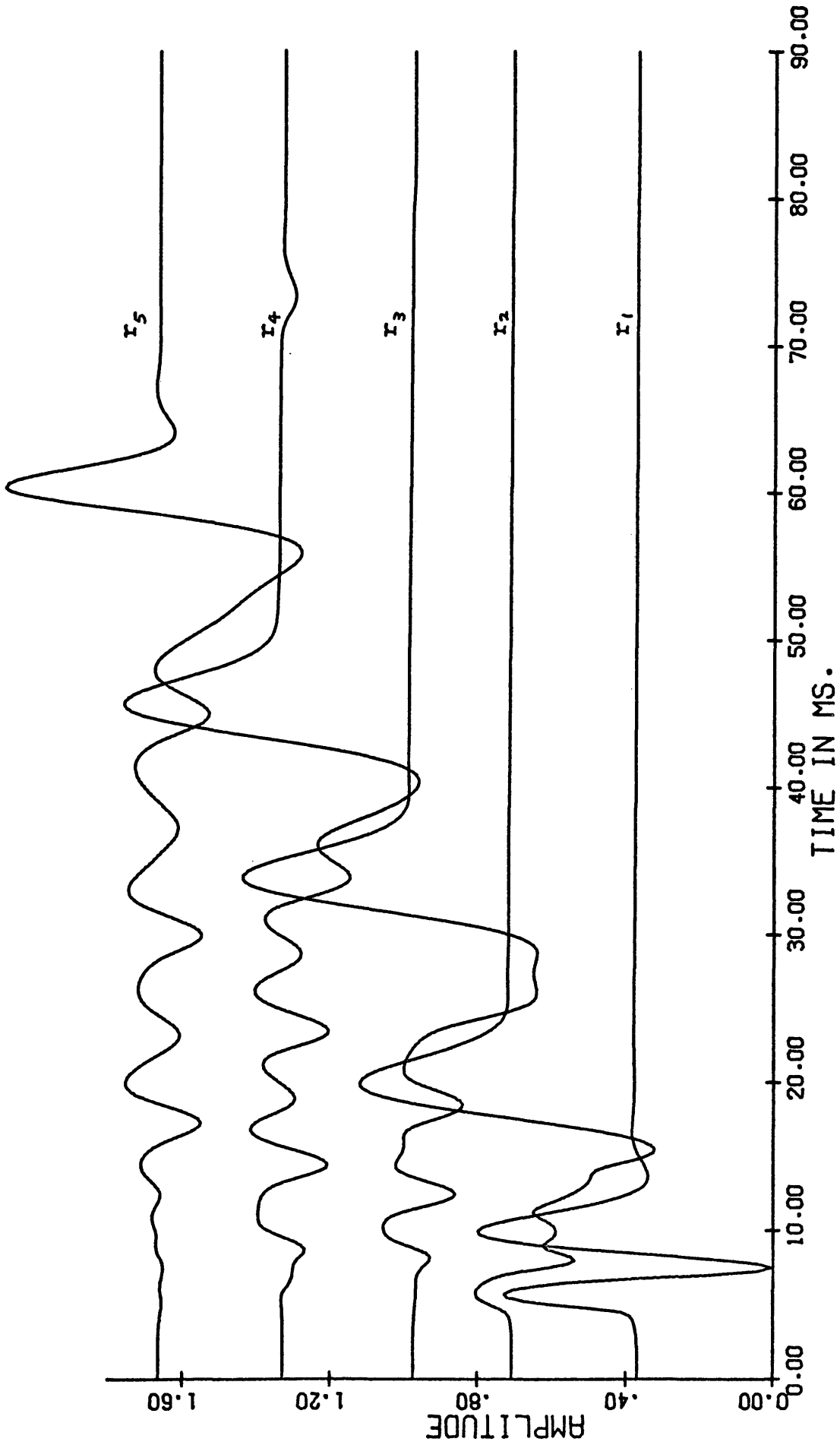


Figure 32. Spherical seismic waves in a constant Q half-space--the vertical component of displacement: Total surface waves at 5 locations after PP arrival time.

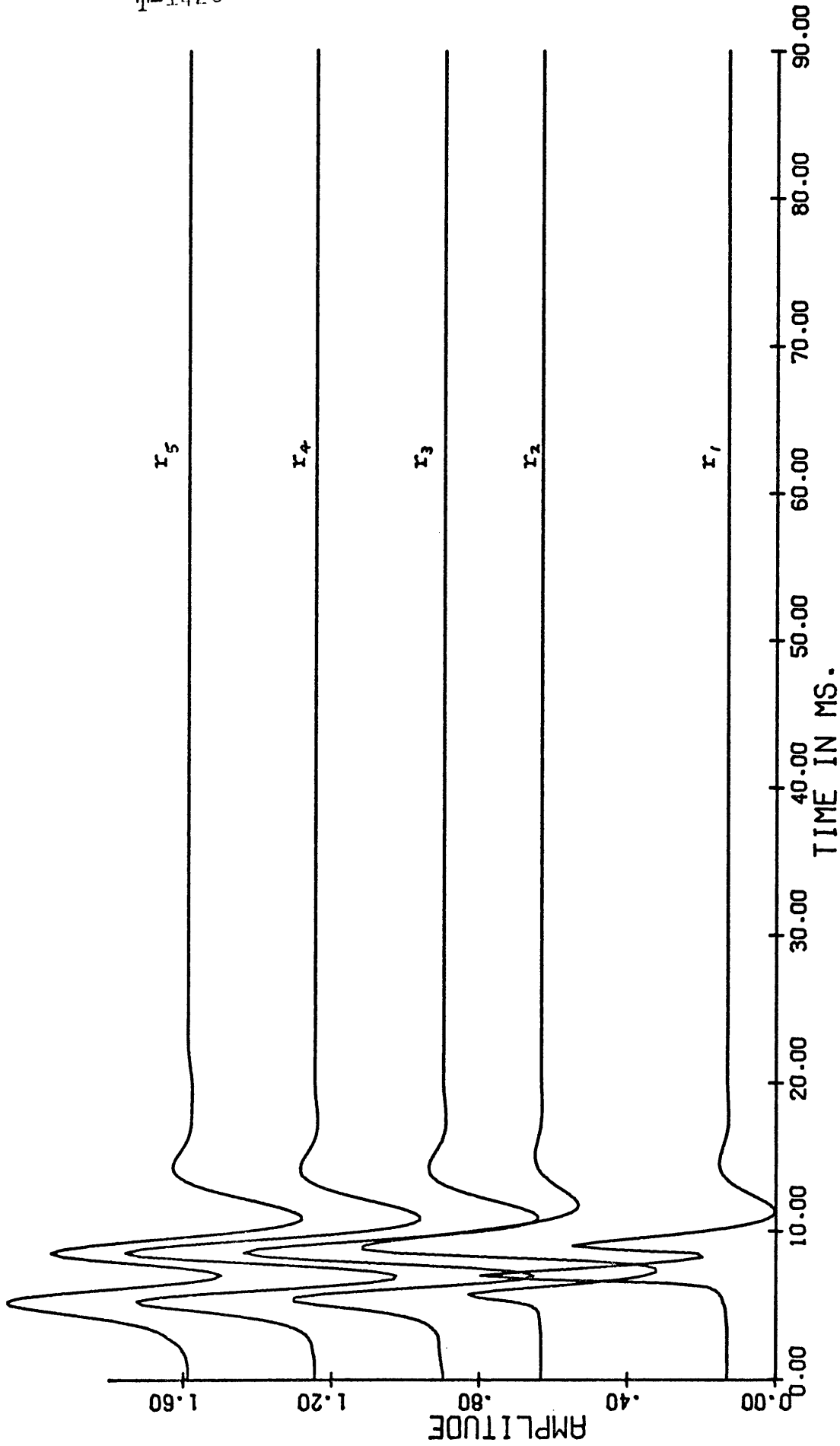


Figure 33. Spherical seismic waves in a constant Q half-space--the vertical component of displacement: Reflected body waves at 5 locations after direct wave arrival time.

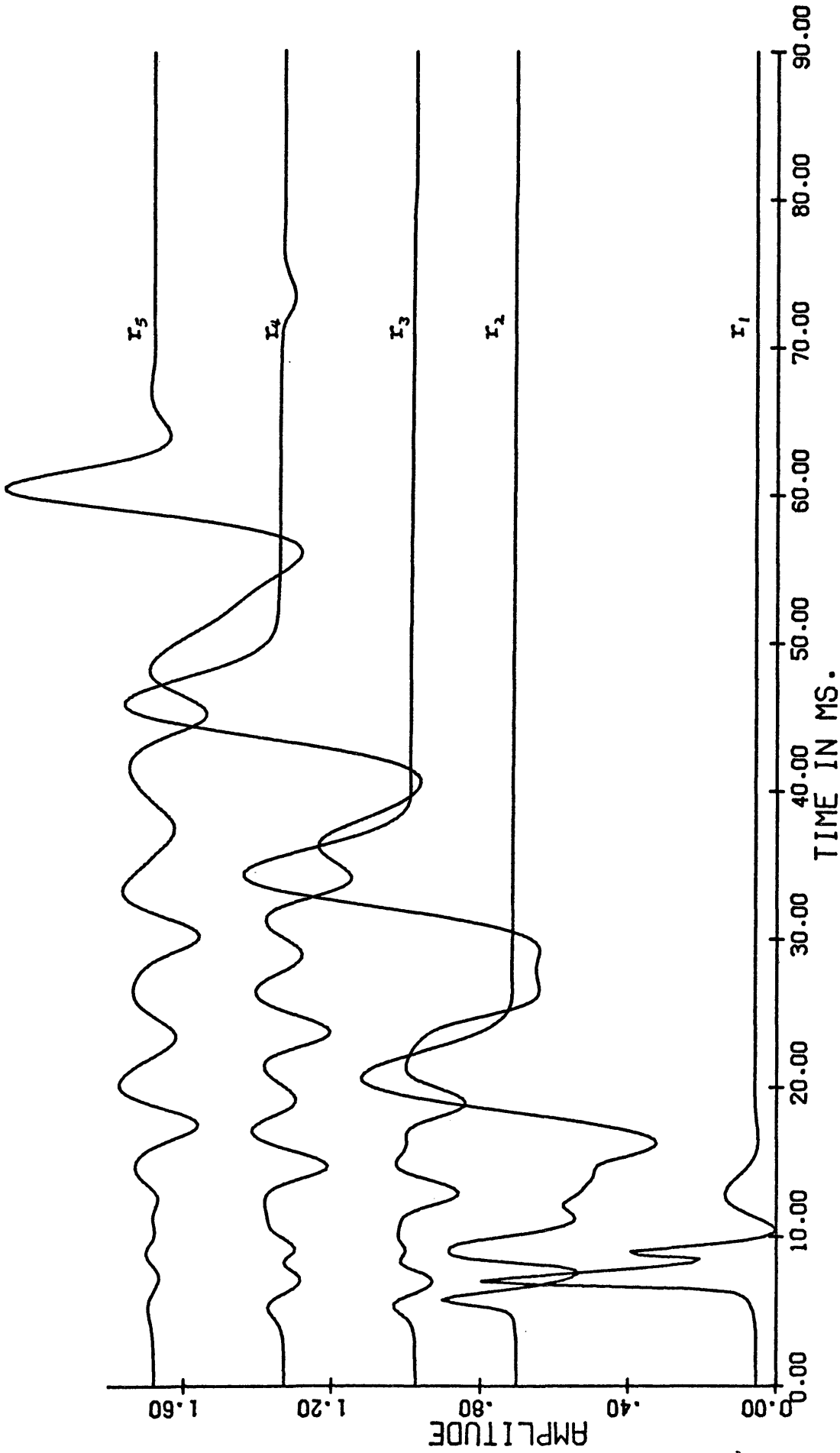


Figure 34. Spherical seismic waves in a constant Q half-space--the vertical component of displacement: Total seismic waves at 5 locations after direct wave arrival time.

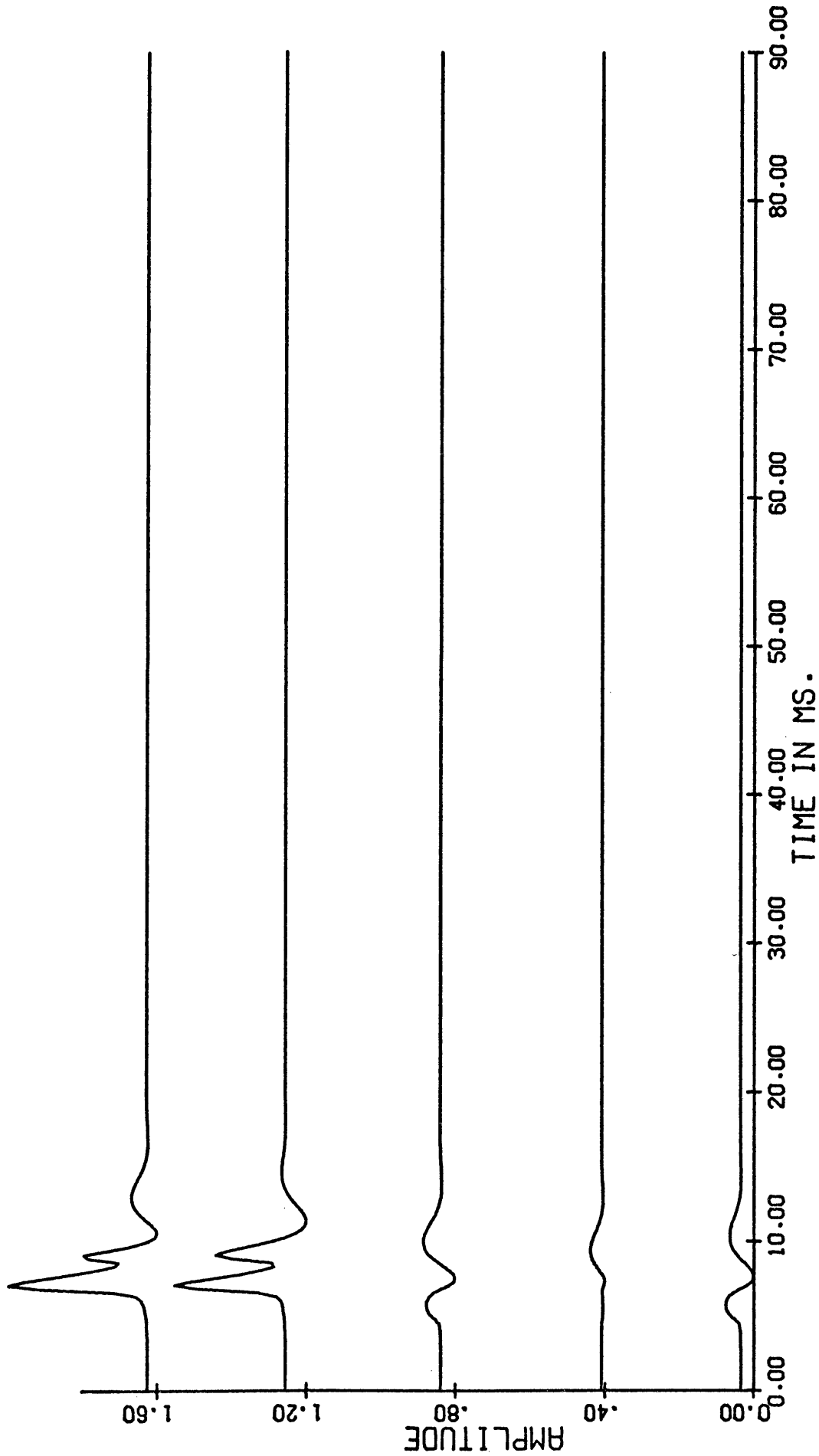


Figure 35. Spherical seismic waves in a constant Q half-space decomposed at location 1. These traces are scaled to their relative amplitude with respect to the total vertical displacement, which is normalized. The arrangement of traces is the same as that of figure 10.

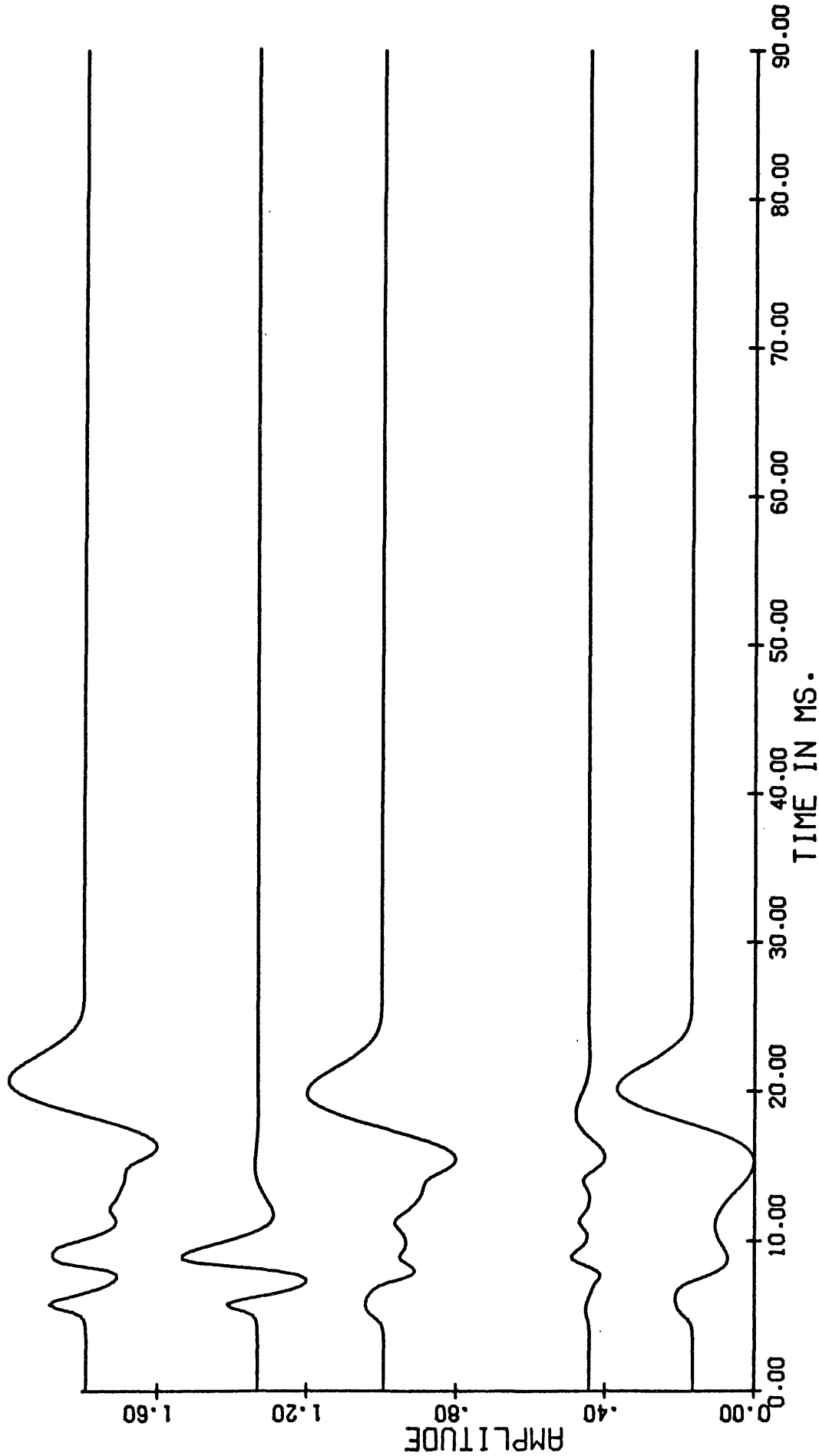


Figure 36. Spherical seismic waves in a constant Q half-space decomposed at location 2. These traces are scaled to their relative amplitude with respect to the total vertical displacement, which is normalized. The arrangement of traces is the same as that of figure 10.

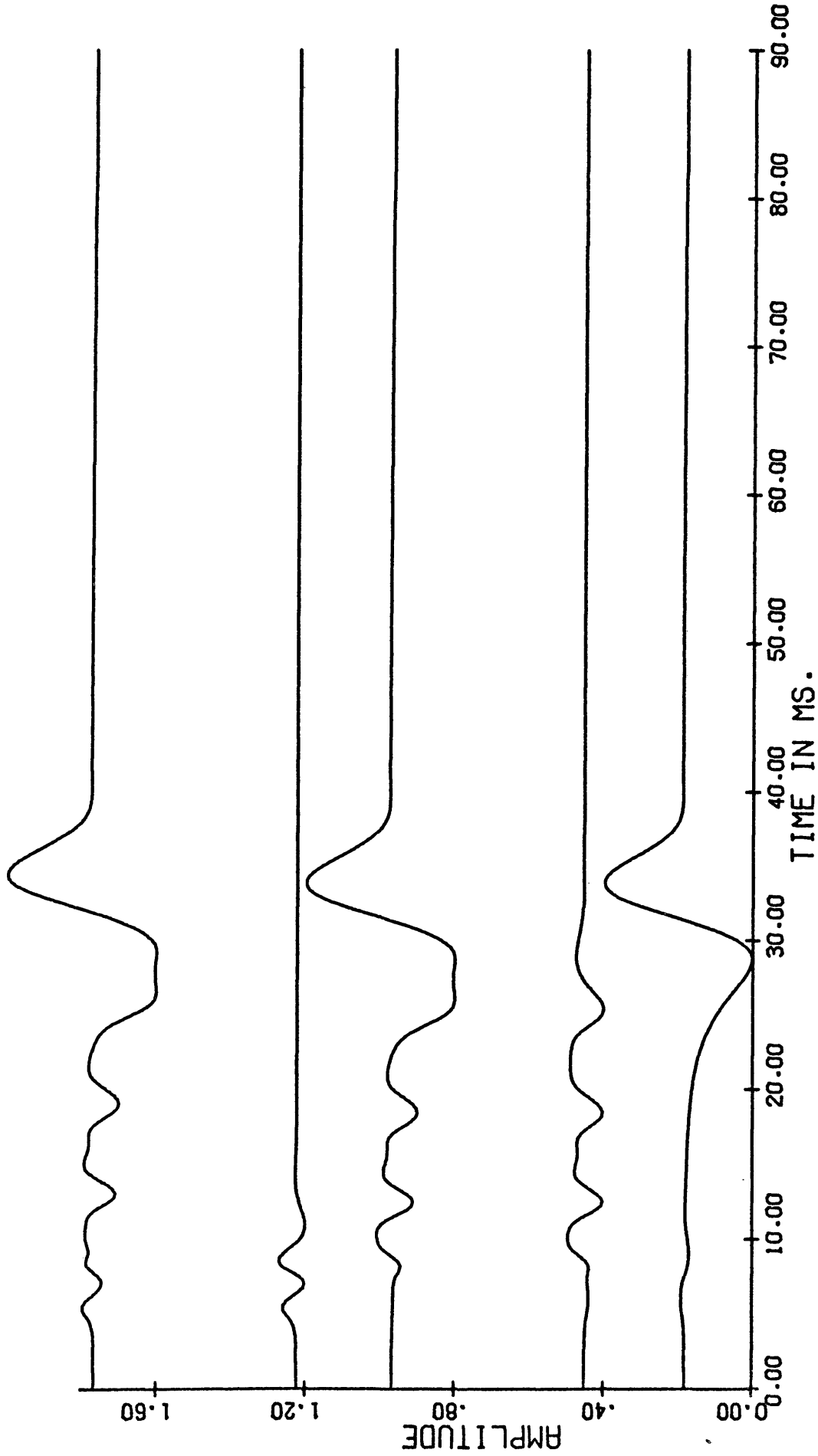


Figure 37. Spherical seismic waves in a constant Q half-space decomposed at location 3. These traces are scaled to their relative amplitude with respect to the total vertical displacement, which is normalized. The arrangement of traces is the same as that of figure 10.

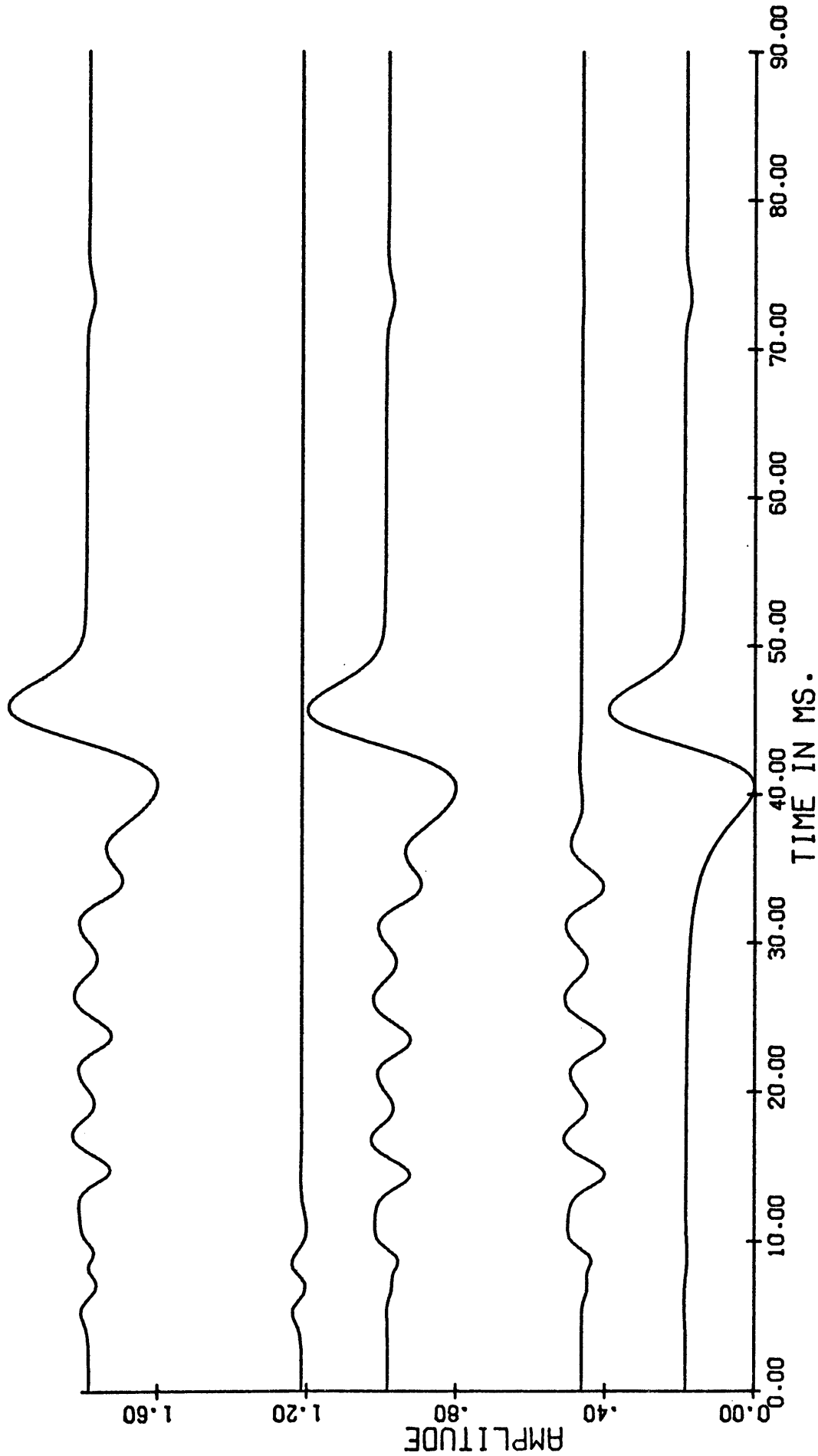


Figure 38. Spherical seismic waves in a constant Q half-space decomposed at location 4. These traces are scaled to their relative amplitude with respect to the total vertical displacement, which is normalized. The arrangement of traces is the same as that of figure 10.

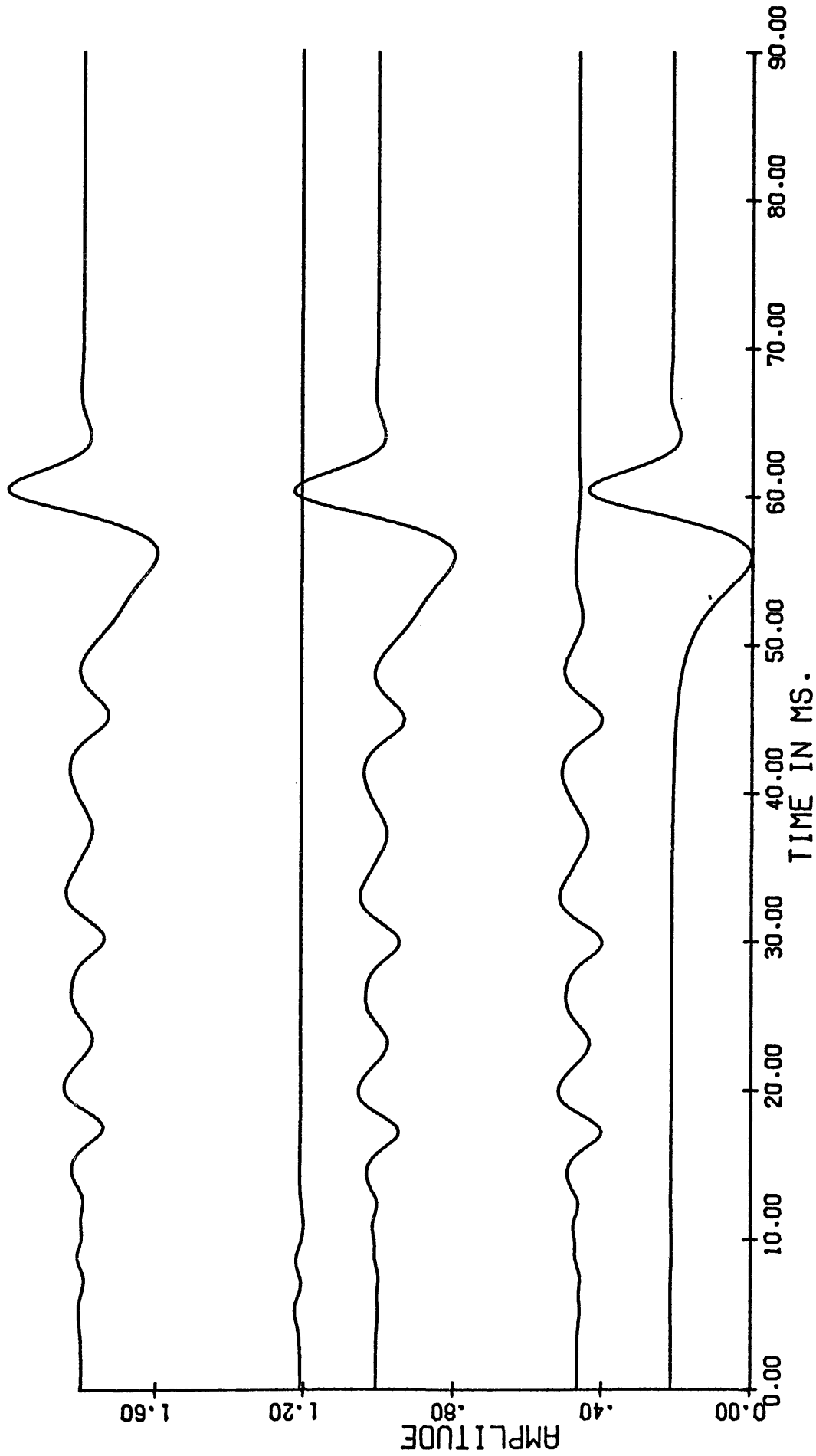


Figure 39. Spherical seismic waves in a constant Q half-space decomposed at location 5. These traces are scaled to their relative amplitude with respect to the total vertical displacement, which is normalized. The arrangement of traces is the same as that of figure 10.

CONCLUSIONS AND RECOMMENDATIONS

This phenomenological theory of attenuation is, like so many other theories, a linear approximation to reality. The attenuation system is also assumed to be a minimum phase system whose amplitude response satisfies the Paley-Wiener condition. Given a finite band of frequencies of interest the Paley-Wiener condition can always be satisfied if the given attenuation is multiplied by a suitable truncation function.

To supply input to the attenuator, one must compute the elastic waves for various boundaries of interest. Cagniard's method is applied to compute spherical waves in a half-space. The second surface wave (Cagniard, 1939) component of the elastic wave consumes the most computer time. Its contribution to the total elastic wave depends on the source-receiver geometry, but it is usually small compared to the classical body or surface waves.

Numerical calculations of the inverse Fourier transform take more computer time than calculations of the elastic waves. The digital convolution of the elastic wave input and the attenuator impulse response is relatively fast.

The seismic waves obtained in this thesis show dispersion. The spherical seismic waves in the infinite low-frequency-approximated Voigt medium broaden faster than in the constant Q medium.

This theory of seismic waves has the advantage that it is not necessary to incorporate the loss mechanisms into the boundary value problems, which are already very complicated. However, one sacrifices any opportunity of gaining insight to the processes and causes of attenuation. The derivation of the phase response through the Hilbert transform is difficult if the amplitude response is complicated. The numerical inverse Fourier transform is also a burden of this approach.

For further pursuit of studies in related fields, it is recommended that z -transform methods be considered or that more sophisticated and/or more efficient inverse Fourier transforms be used. It is also recommended that additional field studies and laboratory experiments be conducted to match attenuation functions and rock types.

BIBLIOGRAPHY

- Attewell, P. B., and Ramana, Y. V., 1966, Wave attenuation and internal friction as functions of frequency in rocks: *Geophysics*, v. 31, no. 6, p. 1049-1056.
- Balch, A. H., and Smolka, F. R., 1970, Plane and spherical transient Voigt wave: *Geophysics*, v. 35, no. 5, p. 745-761.
- Blake, F. G., 1952, Spherical wave propagation in solid media: *Acoust. Soc. Am. Jour.*, v. 24, p. 211-215.
- Bracewell, R., 1965, *The Fourier transform and its application*: New York, McGraw-Hill Book Co., Inc.
- Cagniard, L., 1939, *Reflexion et refraction des ondes progressive seismiques*: Paris, Gauthier-Villars.
(Transl. by Flinn, E. A., and Dix, C. H., 1962, N. Y., McGraw-Hill Book Co., Inc.)
- Carpenter, E. W., 1966, Absorption of elastic wave--an operator for a constant Q mechanism: Atomic Weapons Research Establishment, AWRE Report O-43/66.
- Chao, T. K., 1970, Quantitative analysis of elastic near fields in a half-space: Colorado School of Mines Doctoral Thesis.
- Clark, G. B., and Rupert G. B., 1966, Plane and spherical waves in a Voigt medium: *Jour. of Geophys. Res.*, v. 71, p. 2047-2053.
- Collins, F., 1960, Plane compressional Voigt waves: *Geophysics*, v. 25, no. 2, p. 483-504.

- Conte, S. D., 1965, Elementary numerical analysis: New York, McGraw-Hill Book Co., Inc.
- Corinaldesi, E., 1959, An introduction to dispersion relations: Supplemento al volume XIV, serie X del Nuovo Cimento, no. 2, p. 1801-1816.
- Debremaecker, J. CL., Godson, R. H., and Watkins, J. S., 1966, Attenuation measurements in the field: Geophysics, v. 31, no. 3, p. 562-569.
- Donato, R. J., O'Brien, P. N. S., and Usher, M. J., 1962, Absorption and dispersion of elastic energy in rocks: Nature, v. 193, p. 764-765.
- Ewing, M. W., Jardetzky, W. S., and Press, F., 1957, Elastic waves in layered media: New York, McGraw-Hill Book Co., Inc.
- Futterman, W. I., 1962, Dispersive body waves: Jour. of Geophys. Res., v. 67, no. 13, p. 5279-5291.
- Gray, R. L., 1968, Numerical investigation of reflection and transmission of spherical compressional waves: Colorado School of Mines Doctoral Thesis.
- Jackson, D. D., and Anderson, D. L., 1970, Physical mechanisms of seismic wave attenuation: Review of Geophysics and Space Physics, v. 8, no. 1.
- Jaramillo, E. E., and Colvin, J. D., 1970, Transient waves in a Voigt medium: Jour. of Geophys. Res., v. 75, no. 29, p. 5767-5773.
- Knopoff, L., 1956, The attenuation of compression waves in lossy media: Bull. Seismol. Soc. Amer., v. 46, p. 47-56.
-
- 1956, The seismic pulse in materials possessing solid friction, 1: Plane waves: Bull. Seismol. Soc. Amer., v. 46, p. 175-183.

- Knopoff, L., 1960, Models for acoustic loss in solids: Jour. of Geophys. Res., v. 65, no. 7, p. 2191-2197.
- Knopoff, L., and McDonald, J. F., 1958, Attenuation of small amplitude stress waves in solids: Review of Modern Physics, v. 30, no. 4, p. 1178-1192.
- Kolsky, H., 1953, Stress waves in solids: Oxford, Britain, Clarendon Press.
- _____ 1956, The propagation of stress pulses in visco-elastic solids: Philosophical Magazine, series 8, v. 1, no. 8, p. 693-710.
- Lamb, G. L. Jr., 1962, The attenuation of waves in a dispersive medium: Jour. of Geophys. Res., v. 67, no. 13, p. 5273-5277.
- Leitinger, H., 1969, Investigation of displacement steps in a layered half-space by the finite difference method: Colorado School of Mines Doctoral Thesis.
- Mattice, H. D., and Lieber, P., 1954, On attenuation of waves produced in visco-elastic materials: Amer. Geophys. Union Trans., v. 35, no. 4, p. 613-624.
- McDonal, F. A., Angona, F. A., Mills, R. L., Sengbush, R. L., Van Nostrand, R. G., and White, J. E., 1958, Attenuation of shear and compressional waves in Pierre shale: Geophysics, v. 23, no. 3, p. 421-439.
- O'Brien, P. N. S., 1969, Some experiments concerning the primary seismic pulse: Geophys. Prospecting, v. 17, no. 4, p. 511-547.
- Papoulis, A., 1962, The Fourier integral and its application: New York, McGraw-Hill Book Co., Inc.
- Pekeris, C. L., 1940, A pathological case in the numerical solution of integral equation: U. S. Natl. Acad. Sci. Proc., v. 26, p. 433-437.

- Pekeris, C. L., 1948, Theory of propagation of explosive sound in shallow water: Geol. Soc. Amer. Mem. 27.
- Press, F., and Healy, J., 1957, Absorption of Rayleigh waves in low-loss media: Jour. of Appl. Physics, v. 28, no. 11, p. 1323-1325.
- Ricker, N., 1943, Further developments in the wavelet theory of seismogram structure: Bull. Seismol. Soc. Amer., v. 33, no. 3, p. 197-228.
- _____ 1953, The forms and laws of propagation of seismic wavelets: Geophysics, v. 18, no. 1, p. 10-40.
- Sato, Y., 1955, Analysis of dispersed surface waves by means of Fourier transform: Earthquake Research Institute, Bull., Tokyo Univ., v. 33, p. 33-48.
- Savage, J. C., and Hasegawa, H., 1967, Evidence for a linear attenuation mechanism: Geophysics, v. 32, no. 6, p. 1003-1014.
- Sharpe, J. A., 1942a, The production of elastic waves by explosion pressure, Part 1: Theory and empirical field observations: Geophysics, v. 7, no. 2, p. 144-154.
- _____ 1942b, The production of elastic waves by explosion pressures, Part II: Results of observations near an exploding charge: Geophysics, v. 7, no. 3, p. 311-321.
- Sherwood, J. W. C., and Trorey, A. W., 1965, Minimum phase and related properties of the response of a horizontally stratified absorptive earth to plane acoustic wave: Geophysics, v. 30, no. 2, p. 191-197.
- Sobolev, S., 1933, Sur les vibration d'un demiplan et d'une couce a conditions initiaees arbitraires: Sbornik Mat. (Moscow), v. 40.

- Spencer, T. W., 1960, The method of generalized reflection and transmission coefficients: *Geophysics*, v. 25, no. 3, p. 625-641.
- _____ 1965, Long-time response predicted by exact ray theory: *Geophysics*, v. 30, no. 3, p. 363-368.
- Strick, E., 1970, A predicted pedestal effect for pulse propagation in constant-Q solids: *Geophysics*, v. 35, no. 3, p. 387-403.
- Toll, J. S., 1956, Causality and the dispersion relation: Logical foundations: *Phys. Review*, v. 104, no. 6, p. 1760-1770.
- Treitel, S., 1959, On the attenuation of small amplitude plane stress waves in a thermo-elastic solid: *Jour. of Geophys. Res.*, v. 64, no. 6, p. 661-665.
- Trorey, A. W., 1962, Theoretical seismogram with frequency and depth dependent absorption: *Geophysics*, v. 27, no. 6, p. 766-785.
- Van de Waerden, B. L., 1947, Reflection and refraction of seismic waves: Reprinted by Shell Development Co. in 1957.
- Walsh, J. B., 1966, Seismic wave attenuation in rock due to friction: *Jour. of Geophys. Res.*, v. 71, no. 10, p. 2591-2599.
- White, J. E., 1965, Seismic waves: radiation, transmission, and attenuation: New York, McGraw-Hill Book Co., Inc.
- _____ 1966, Static friction as a source of seismic attenuation: *Geophysics*, v. 31, no. 2, p. 333-339.
- Wuenschel, P. C., 1965, Dispersive body waves--an experimental study: *Geophysics*, v. 30, p. 539-557.

Wyllie, W. R. J., Gardner, G. H. F., and Gregory, A. R.,
1962, Study of elastic wave attenuation in porous
media: Geophysics, v. 27, no. 5, p. 569-589.

APPENDIXEXPRESSION FOR h_z ,

THE VERTICAL COMPONENT OF DISPLACEMENT

$$\begin{aligned}
h_z &= 0 \quad , \quad \text{for } t < R'S \\
&= \cos I \left[\frac{S}{R} F'(t-R'S) + \frac{1}{R^2} F(t-R'S) \right], \quad \text{for } R'S < t < R'S \\
&= \cos I \left[\frac{S}{R} F'(t-R'S) + \frac{1}{R^2} F(t-R'S) \right] + \cos I' \left[\frac{S}{R'} F'(t-R'S) \right. \\
&\quad \left. + \frac{1}{R'^2} F(t-R'S) - S \cos I' A_3 (R'S + 0) F'(t-R'S) \right. \\
&\quad \left. - F'(t) * M_z(t) \right], \quad \text{for } R'S < t < R_1'S + R_2'S
\end{aligned}$$

$$= \cos I \left[\frac{S}{R} F'(t-R'S) + \frac{1}{R^2} F(t-R'S) \right] + \cos I' \left[\frac{S}{R'} \cdot$$

$$F'(t-R'S) + \frac{1}{R'^2} F(t-R'S)$$

$$\begin{aligned}
& - S \cos I' A_3 (R'S + 0) F'(t - R's) \\
& - F'(t) * M_z(t) - s \sin I_2 B(R_1 S + R_2 s + 0) \\
& F'[t - (R_1 S + R_2 s)] \\
& + F'(t) * N_r(t) \quad , \\
& \text{for } t > R_1 S + R_2 s
\end{aligned}$$

where $F(t)$ is the source function, A_3 and B are transmission factors as previously defined in the context, and M_z and N_r are the spacial derivatives of the transmission factors. They are expressed in closed form as follows:

$$A_3 (R'S + 0) = \frac{2}{R'} \left\{ 1 + \frac{\left[\frac{g^2}{2} - \sin^2 I' \right]^2}{\sin^2 I' \cos I' (g^2 - \sin^2 I')^{\frac{1}{2}}} \right\}^{-1}$$

$$B(R_1 S + R_2 S + 0) = - \frac{4 \sin^2 I_1 \cos^2 I_2}{g^2 \cos^2 2I_2 + \sin 2I_2 \sin 2I_1}$$

$$r^{-\frac{1}{2}} \left(\frac{h \sin I_1}{\cos^3 I_1} + \frac{z \sin I_2}{\cos^2 I_2} \right)^{-\frac{1}{2}}$$

$$M_z = - \frac{i}{\pi} \frac{\partial}{\partial z} \left(\int_{\Sigma_r} \frac{j(u) u \, du}{\{u^2 r^2 + [\tau - a(h+z)]^2\}^{\frac{1}{2}}} \right)$$

$$= M_z^r + M_z^E + M_z^P$$

$$N_r = \frac{i}{\pi r} \frac{\partial}{\partial r} \left(\int_{\Sigma_r} \frac{(\tau - ah - bz) f(u) u \, du}{\{u^2 r^2 + (\tau - ah - bz)^2\}^{\frac{1}{2}}} \right)$$

$$= N_r^r + N_r^E + N_r^P$$

where Γ , E , and P denote the contours of integration as shown in Figure 3.

The symbol $*$ denotes convolution.

The closed forms of M_z^{Γ} , M_z^P , N_r^{Γ} , and N_r^P are given as follows:

$$M_z^{\Gamma} = - \frac{2 \cos I'}{(g^2-1)R'^2} \left[3 \cos^2 I' + \frac{g^4 - 4g^2 + 5}{2(g^2-1)} \right] \\ + \frac{6\tau^2 \cos I' (5 \cos^2 I' - 3)}{(g^2-1)R'^4 S^2}$$

$$N_r^{\Gamma} = - \frac{3h}{R'^3} \sin 2I' + \frac{g^2 \sin I'}{(g^2-1)R'^2} \\ \left[6 \cos^2 I' + \frac{2g^2 + 1 - g^4}{g^2(g^2-1)} \right] \\ - \frac{6\tau^2}{(g^2-1)R'^4 S^2} \sin I' (5 \cos^2 I' - 1)$$

$$M_z^P = \frac{-2\delta \left[m^2 - \frac{g^2}{2} \right]^2}{R'^2} M_1^{-\frac{3}{4}} M_2^{\frac{1}{2}} \cos \left(\theta_2 - \frac{3}{2} \theta_1 \right)$$

$$N_{\Gamma}^P = \frac{-2 \delta m^2 \left[m^2 - \frac{g^2}{2} \right] (m^2 - g^2)^{\frac{1}{2}}}{R'^2}.$$

$$N_1^{-\frac{3}{4}} \sin \frac{3\varphi_1}{2} \sin I'$$

where m , δ , M_1 , M_2 , N_1 , θ_1 , θ_2 , and φ_1 are defined as follows:

$$m = \frac{S_R}{S} = \frac{V_P}{V_R}$$

$$\delta = \frac{2 \left[m^2 - \frac{g^2}{2} \right]^2}{3 m^4 (g^2 - 1) - m^2 g^2 (3 g^2 - 2) + \frac{g^6}{2}}$$

$$M_1 = \frac{(\gamma_*^2 - m^2 + \cos^2 I')^2 + 4 \gamma_*^2 \cos^2 I'}{(m^2 - 1)}$$

$$M_2 = \gamma_*^2 + (m^2 - 1) \cos^2 I'$$

$$N_1 = \left(\tau_*^2 - m^2 \sin^2 I' - \left\{ \frac{h}{R'} \right. \right.$$

$$\left. \left[(m^2 - 1)^{\frac{1}{2}} - (m^2 - g^2)^{\frac{1}{2}} \right] + \cos I' \right.$$

$$\left. (m^2 - g^2)^{\frac{1}{2}} \right\}^2 + 4 \tau_*^2 \left\{ \frac{h}{R'} \right.$$

$$\left. \left[(m^2 - 1)^{\frac{1}{2}} - (m^2 - g^2)^{\frac{1}{2}} \right] \right.$$

$$\left. + \cos I' (m^2 - g^2)^{\frac{1}{2}} \right\}^2$$

$$\tau_* = \frac{\tau}{R S} \Big|_{r=0}$$

$$\varphi_1 = \tan^{-1} \frac{2 \tau_* \left\{ \frac{h}{R'} \left[(m^2 - 1)^{\frac{1}{2}} - (m^2 - g^2)^{\frac{1}{2}} \right] \right.}{\tau_*^2 - m^2 \sin^2 I' - \left\{ \frac{h}{R'} \left[(m^2 - 1)^{\frac{1}{2}} \right. \right.$$

$$\left. \left. + \cos I' (m^2 - g^2)^{\frac{1}{2}} \right\} \right.}$$

$$\left. \left. - (m^2 - g^2)^{\frac{1}{2}} \right] + \cos I' (m^2 - g^2)^{\frac{1}{2}} \right\}^{\frac{1}{2}}$$

$$0 < \varphi_1 < \pi$$

$$\theta_2 = \tan^{-1} \left[(m^2 - 1)^{\frac{1}{2}} \frac{\cos I'}{\tau_*} \right] ,$$

$$0 < \theta_2 < \frac{\pi}{2}$$

$$\theta_1 = \tan^{-1} \left[\frac{2\tau_* \cos I' (m^2 - 1)^{\frac{1}{2}}}{\tau_*^2 - m^2 + \cos^2 I'} \right]$$

$$0 < \theta_1 < \pi$$

$$g^2 = \frac{s^2}{s'^2}$$